Sensitivity of Past, Present, and Future Fire Regimes to Climate and Vegetation Variability in Boreal Forest and Tundra Ecosystems

A Dissertation

Presented in Partial Fulfillment of the Requirements for the
Degree of Doctorate of Philosophy
with a
Major in Natural Resources
in the
College of Graduate Studies
University of Idaho
by
Adam M. Young

Major Professors: Philip E. Higuera, Ph.D.; Luigi Boschetti, Ph.D.
Committee Members: John Abatzoglou, Ph.D.; Paul A. Duffy, Ph.D.; Feng Sheng Hu, Ph.D.
Department Administrator: P. Charles Goebel, Ph.D.

May 2018

Authorization to Submit Dissertation

This dissertation of Adam M. Young, submitted for the degree of Doctorate of Philosophy with a Major in Natural Resources and titled "Sensitivity of Past, Present, and Future Fire Regimes to Climate and Vegetation Variability in Boreal Forest and Tundra Ecosystems," has been reviewed in final form. Permission, as indicated by the signatures and dates below, is now granted to submit final copies to the College of Graduate Studies for approval.

Major Professors: _____ Date: _____

Philip E. Higuera, Ph.D.

_____ Date: _____

Luigi Boschetti, Ph.D.

Committee Members: _____ Date: _____

John Abatzoglou, Ph.D.

_____ Date: _____

Paul A. Duffy, Ph.D.

_____ Date: _____

Feng Sheng Hu, Ph.D.

Department Administrator: _____ Date: _____

P. Charles Goebel, Ph.D.

Abstract

Wildfire activity in North American boreal forest and tundra ecosystems is strongly controlled by climate, indicating the potential for widespread fire-regime shifts in response to ongoing and future climate change. This dissertation focuses on understanding how fire regimes in boreal forest and tundra ecosystems respond to variability in past, present, and future climate.

Chapter 1 addresses how climate, vegetation, and topography control the spatial distribution of fire occurrence in Alaskan boreal forest and tundra ecosystems. Through statistical modelling, I found that climate was the primary control of historical fire activity. Informing these statistical models with 21st-century climate projections suggests tundra and forest-tundra ecosystems will be particularly vulnerable to fire-regime shifts, due to increasing summer temperatures. In some areas, fire may become four times more likely to occur by 2100, relative to the past 6,000-35,000 years.

In Chapter 2, I studied the importance of vegetation as a control of fire activity across North American boreal forests, using continental-scale fire and vegetation datasets spanning the past several decades. After climate, fire activity was most strongly linked to landscape tree cover (%). The likelihood of burning was also not independent of past fire, suggesting negative fire-vegetation feedbacks exist across North American boreal forests. These feedbacks are estimated to have reduced total area burned by ≈ 2.7-3.6 $\times 10^6$ ha (4-5%) from 1981-2016, relative to expectations if there were no feedbacks. While these negative fire-vegetation feedbacks may offset climatically driven increases in fire activity for several

decades, continued warming and increasing aridity will likely overwhelm the mediating effects of vegetation by the mid- to late-21st century.

In Chapter 3, I evaluate the ability of the statistical models from Chapter 1 to project fire regimes outside of the observational period (i.e., 1950-2009 CE). I informed these models with GCM data from 850-1850 CE, and compared these paleo-projections to independent fire histories derived from lake-sediment records. The accuracy of the paleo-projections varied regionally, with uncertainty highest in regions close to an observed temperature threshold to burning. These results highlight how threshold relationships can cause significant uncertainty in anticipating the timing, location, and magnitude of future ecosystem change.

Acknowledgements

First and foremost, I would like to thank and acknowledge my major advisor, Dr. Philip Higuera. It is because of his encouragement, knowledge, and patience that I have been able to challenge myself and reach this milestone. I want to thank and acknowledge each of my committee members: Drs. John Abatzoglou, Luigi Boschetti, Paul Duffy, and Feng Sheng Hu. Their advice, help, and knowledge has been essential to my development as a Ph.D. scientist.

I would like to acknowledge and thank the faculty and staff at the University of Idaho who provided resources and support, particularly members in the College of Natural Resources, College of Science, and College of Graduate Studies. I would also like to thank the W.A. Franke College of Forestry and Conservation at the University of Montana for providing critical support to me over the past three years.

Finally, but not least, I would like to acknowledge the funding agencies that supported my research through the following awards: a National Science Foundation (NSF) Arctic System Science Award (Grant# ARC-1023669 to Dr. Higuera), an NSF GK12 Fellowship awarded through the Water Resources Program at the University of Idaho, a BLM Joint Fire Science Program (JFSP) Graduate Research and Innovation Award (#14-3-01-7), and a NASA Earth and Space Science Fellowship (#NNX14AK86H).

Dedication

This is for my mother and father, who provided the upbringing, freedom, and love needed to find this calling.

This is also for my best friend and wife, Nicole, whose joyfulness, support, and love kept me going. It would have been impossible to do this without you.

And last, but not least, this is dedicated to our two pups, Molly and Dug, who kept me company and smiling as I worked from home the past three years.

Table of Contents

List of Figures

List of Tables

Introduction

Wildfire in the context of global change

Climate change is altering the structure and function of ecosystems worldwide (Walther et al. 2002, Grimm et al. 2013), including changes to global patterns of fire activity (Moritz et al. 2012). Climate has a strong and pervasive influence over wildfires, directly and indirectly controlling fire activity through pathways that span multiple spatial-temporal scales (Macias Fauria et al. 2011). At multi-decadal timescales, patterns in temperature and precipitation influence biomass production, and thus broad-scale patterns in fuel type and fuel loading (Pausas et al. 2004, Krawchuk and Moritz 2011). At finer temporal scales, weather and climate drive intra- to inter-annual variability in fuel moisture, and fine-fuel production through the growth of annual grasses (Littell et al. 2009). Within a fire season, temperature, precipitation, and wind patterns, from hour to weeks, determine the probability of ignition and subsequent rates of fire spread and area burned (Rothermel 1972, Johnson 1992). Fire-related changes in vegetation can also increase or decrease subsequent probabilities of burning, generating positive or negative feedbacks with fire (Tepley et al. 2018).

In addition to being highly sensitive to climate variability, fire also plays a key role in shaping terrestrial ecosystem dynamics across a range of spatial and temporal scales (Cochrane et al. 1999, Westerling et al. 2006, Bonan 2008, Bowman et al. 2009, Krawchuk et al. 2009, Moritz et al. 2012, Marlon et al. 2013, Parisien et al. 2014). The ecological role of fire is significant and wide ranging, including impacts on biogeochemical cycling (e.g., Hicke et al. 2003, Bond-Lamberty et al. 2007), radiative forcing (e.g., Beck et al. 2011, Rogers et al. 2013), human health and livelihood (e.g., Aditama 2000), and wildlife (e.g., Joly et al. 2012).

Furthermore, the effects of fire are potentially long lasting, as succession can last from years to decades (Baker 2009), and in some instances, fire may catalyze ecosystem state changes (e.g., Crausbay et al. 2017). Fire also has significant impacts on the broader Earth system, through its effects on greenhouse gas emissions (i.e., CO_2 and CH_4) and radiative forcing (Bowman et al. 2009). For example, global biomass burning from 1997-2016 is estimated to have emitted approximately 2.2 Pg C yr^{-1} to the atmosphere, through combustion and post-fire decomposition of nonliving vegetation, with net emissions ≈ 6% of total annual anthropogenic fossil-fuel emissions in 2014 (van der Werf et al. 2017).

In boreal forest and Arctic tundra biomes, the climate is warming at a rate approximately twice that of the global average (ACIA 2004, Chapin et al. 2005, Serreze and Barry 2011, Hinzman et al. 2013). The impacts of such rapid changes in northern high latitudes can be particularly important, due to the vast quantities of carbon stored in permafrost and peatland soils (McGuire et al. 2009, Tarnocai et al. 2009). Because fire plays a key role in influencing global scale greenhouse-gas emissions, fire will also likely play a major role in determining future trajectories of carbon cycling in these ecosystems. For example, the 2007 Anaktuvuk River Fire burned ≈ 1000 km^2 of Alaskan tundra, and released an estimated 2.1 Tg C to the atmosphere, comparable to the entire annual carbon sink of the Arctic tundra biome (Mack et al. 2011). Increasing fire frequency in response to climate change may ultimately shift some tundra ecosystems to a net carbon source (Hu et al. 2015). Boreal forest ecosystems also have the potential to shift from a net carbon sink to a net carbon source (Pan et al. 2011), due to increased combustion and fire-related emissions (Bond-Lamberty et al. 2007, Balshi et al. 2009a, Kelly et al. 2016). Overall, such findings illustrate

the importance of fire as an Earth system process, particularly in boreal forest and tundra ecosystems, and thus the need to understand the climatic controls of fire to anticipate the impacts of 21st-century climate change.

Fire regimes in North American boreal forest and tundra ecosystems

Fire regimes, the characteristic patterns in the frequency, size, intensity, and seasonality of fire events in an ecosystem, have been extensively studied in North American boreal forests (Kasischke et al. 2002, Stocks et al. 2002, Wooster and Zhang 2004, Higuera et al. 2009, Kasischke et al. 2010, Kelly et al. 2013, Rogers et al. 2015). Late-successional North American boreal forest ecosystems are dominated by coniferous taxa, including black spruce (*Picea mariana*), white spruce (*Picea glauca*), and jack pine (*Pinus banksiana*). Generally, fire regimes in these ecosystems are characterized by large, high intensity crown fires (Johnson 1992), with mean fire return intervals ranging from ≈ 50-250 yr (Carcaillet et al. 2001, Higuera et al. 2009, Ali et al. 2012, Barrett et al. 2013, Kelly et al. 2013).

The primary driver of fire activity in the boreal forest is seasonal to annual climate, which drives the confluence of hot, dry, and windy conditions that promote low fuel moisture, lightning ignition, and fire spread (Bessie and Johnson 1995, Duffy et al. 2005, Macias Fauria and Johnson 2006, 2008, Veraverbeke et al. 2017). The spatial-temporal variability in the co-occurrence of these warm and dry conditions, which form over days to months, are commonly driven by ocean-atmosphere teleconnections that vary at inter-annual to multi-decadal scales (e.g., El Niño-Southern Oscillation, Pacific Decadal Oscillation, Arctic Oscillation; Duffy et al. 2005, Macias Fauria and Johnson 2006). For example, interactions between the Pacific Decadal Oscillation and El Niño-Southern Oscillation influence the frequency of mid-

tropospheric blocking highs over western North America (Macias Fauria and Johnson 2008), named so because they create an atmospheric ridge that "blocks" the flow of wetter air masses from the Pacific Ocean. These conditions lead to multi-week periods of warm, dry conditions that decrease fuel moisture, creating the conditions necessary for large forest fires to occur. When frontal passage ultimately occurs, lightning-ignited fires can spread rapidly through abundant dry fuels.

While climatic variability is the primary control of fire in North American boreal forest ecosystems, vegetation also plays a key role in influencing the probability of burning in boreal forest landscapes (Kelly et al. 2013, Héon et al. 2014, Dash et al. 2016, Erni et al. 2017). Specifically, post-fire succession includes years to decades of young forest stands (Héon et al. 2014) and/or a high deciduous dominance (Cumming 2001, Krawchuk et al. 2006), both which reduce the probability of burning by reducing fuel loading and/or increasing fuel moisture, respectively. Overall, these fire-vegetation interactions suggest the presence of a significant negative fire-vegetation feedback in North American boreal forest ecosystems. Understanding the existence and impact of such a feedback remains a key question in boreal forest ecology, with implications for understanding how fire regimes may shift over the course of the current century.

While the climatic controls of boreal forest fire regimes have been well studied, our understanding of similar linkages in tundra ecosystems is less developed. Nonetheless, recent studies have demonstrated a tight linkage between climate and fire activity across a range of scales in the tundra biome. At the biome scale and a decadal timescale, evidence suggests that some tundra fire regimes may be limited by fuel availability (Moritz et al. 2012, Pausas and

Ribeiro 2013), rather than low-fuel moisture, with this limitation most likely occurring in high-Arctic and/or barren tundra ecosystems (Walker et al. 2005). However, recent work in Alaska, in some of the most productive tundra ecosystems within the biome, highlight that annual summer temperature and precipitation can explain significant inter-annual variability in area burned from 1950-2009 (Hu et al. 2010, Hu et al. 2015). While this annual-scale linkage highlights variability in fuel moisture as a key driver of Alaskan tundra fire regimes, these specific studies are inherently unable to examine the climatic drivers underlying high spatial variability in these regions. Specifically, these studies summarize area burned across all of Alaskan tundra for each year, thus masking out any spatial variability in fire activity (Higuera et al. 2011, Chipman et al. 2015). Spatial variability in Alaskan tundra fire regimes is quite significant, with mean fire return intervals ranging from ≈150-350 yr in the Noatak River Watershed to >4500 yr on the Alaskan North Slope (Hu et al. 2010, Higuera et al. 2011, Chipman et al. 2015). Understanding the drivers of such regional variability is critical for anticipating spatial variations in potential tundra fire-regime shifts under future climate change. Prior to my dissertation, little work had been done explicitly linking spatial variability in tundra fire activity to different climatic drivers (although, see Rocha et al. 2012, Chipman et al. 2015).

Fire-regime projections in North American boreal forest and tundra ecosystems, driven using output from global climate models (GCM), overwhelmingly suggest that future climate conditions will become more conducive to burning, relative to historical periods (Flannigan et al. 2013, Flannigan et al. 2016). For example, in North American boreal forest ecosystems, area burned is projected to increase from 50-300% by the end of the 21st century

(Flannigan et al. 2005, Balshi et al. 2009b, Wotton et al. 2010, Boulanger et al. 2013). While such projections provide valuable information regarding the potential magnitude and timing of increased fire activity, these projections also come with important limitations. In particular, the statistical models used to drive these projections are generally calibrated on datasets of fire and climate that only span a relatively short amount of time (e.g., 1950-2009 in Alaska). Thus, these statistical models are characterizing fire-climate relationships under a narrow range of climatic variability, relative to the full range of conditions expected under future climate change (Williams et al. 2007). Evaluating the ability of statistical models to project fire-regime behavior outside the observational record is thus key to understanding the strengths and weaknesses associated with such projections.

Goals and objectives

My dissertation broadly focuses on understanding and quantifying the importance and nature of fire-regime controls in northern high-latitude ecosystems, with a particular focus on how climate and vegetation variability drive spatial and temporal patterns in wildfire activity. The findings from this research have implications and applications for anticipating how fire regimes may respond to 21st-century climate change, not only in boreal forest and tundra ecosystems, but in fire-prone ecosystems worldwide.

In Chapter 1, I evaluate and quantify the importance and nature of spatial relationships between fire and different environmental variables across Alaskan boreal forest and tundra ecosystems, including summer temperature, moisture availability, vegetation, and topography. Specifically, I developed statistical models quantifying the controls of fire in Alaska over the observational record (i.e., 1950-2009), and I then informed these models with downscaled

21st-century GCM projections of climate change. Overall, this chapter provides key information on fire-climate relationships in Alaska, particularly in tundra ecosystems, along with a depiction of how fire regimes may shift spatially over the remainder of the current century.

In my second dissertation chapter, I investigated the strength of vegetation, relative to climate, as a control of area burned across North American boreal forest ecosystems. Specifically, this work evaluated evidence for negative fire-vegetation feedbacks in these ecosystems, and then quantified the overall impact of these feedbacks on total area burned. I used historical fire records, remote sensing estimates of tree cover, and various climate data to test the null hypothesis that burning in boreal forest landscapes is independent of past fire activity. This chapter presents quantitative evidence for negative fire-vegetation feedbacks across North American boreal forests, and an estimate of the extent to which these negative feedbacks offset the direct impacts of climate on boreal forest fire activity.

Finally, in my third dissertation chapter, I build off of the work from Chapter 1 to test the ability of the statistical models to project fire regime variability outside of the observational record. I conducted paleodata-model comparisons in Alaskan boreal forest and tundra ecosystems. Specifically, I informed the statistical models from Chapter 1 with downscaled GCM paleoclimate data spanning 850-1850 CE, and compared past projections to independent fire histories derived from charcoal in lake-sediment records. This work provides a unique look and evaluation of the strengths and weaknesses that accompany statistically derived projections outside the observational record, with implications for interpreting future projections of fire activity.

References

ACIA. 2004. Impacts of a Warming Arctic: Arctic Climate Impact Assessment. Cambridge University Press, Cambridge.

Aditama, T. Y. 2000. Impact of haze from forest fire to respiratory health: Indonesian experience. Respirology **5**:169-174.

Ali, A. A., O. Blarquez, M. P. Girardin, C. Hely, F. Tinquaut, A. El Guellab, V. Valsecchi, A. Terrier, L. Bremond, A. Genries, S. Gauthier, and Y. Bergeron. 2012. Control of the multimillennial wildfire size in boreal North America by spring climatic conditions. Proceedings of the National Academy of Sciences of the United States of America **109**:20966-20970.

Baker, W. L. 2009. Fire Ecology in Rocky Mountain Landscapes. Island Press.

Balshi, M. S., A. D. McGuire, P. Duffy, M. Flannigan, D. W. Kicklighter, and J. Melillo. 2009a. Vulnerability of carbon storage in North American boreal forests to wildfires during the 21st century. Global Change Biology **15**:1491-1510.

Balshi, M. S., A. D. McGuire, P. Duffy, M. Flannigan, J. Walsh, and J. Melillo. 2009b. Assessing the response of area burned to changing climate in western boreal North America using a Multivariate Adaptive Regression Splines (MARS) approach. Global Change Biology **15**:578-600.

Barrett, C. M., R. Kelly, P. E. Higuera, and F. S. Hu. 2013. Climatic and land cover influences on the spatiotemporal dynamics of Holocene boreal fire regimes. Ecology **94**:389-402.

Beck, P. S. A., S. J. Goetz, M. C. Mack, H. D. Alexander, Y. F. Jin, J. T. Randerson, and M. M. Loranty. 2011. The impacts and implications of an intensifying fire regime on Alaskan boreal forest composition and albedo. Global Change Biology **17**:2853-2866.

Bessie, W. C. and E. A. Johnson. 1995. The Relative importance of fuels and weather on fire behavior in sub-alpine forests. Ecology **76**:747-762.

Bonan, G. B. 2008. Forests and climate change: Forcings, feedbacks, and the climate benefits of forests. Science **320**:1444-1449.

Bond-Lamberty, B., S. D. Peckham, D. E. Ahl, and S. T. Gower. 2007. Fire as the dominant driver of central Canadian boreal forest carbon balance. Nature **450**:89-92.

Boulanger, Y., S. Gauthier, D. R. Gray, H. Le Goff, P. Lefort, and J. Morissette. 2013. Fire regime zonation under current and future climate over eastern Canada. Ecological Applications **23**:904-923.

Bowman, D. M. J. S., J. K. Balch, P. Artaxo, W. J. Bond, J. M. Carlson, M. A. Cochrane, C. M. D'Antonio, R. S. DeFries, J. C. Doyle, S. P. Harrison, F. H. Johnston, J. E. Keeley, M. A. Krawchuk, C. A. Kull, J. B. Marston, M. A. Moritz, I. C. Prentice, C. I. Roos, A. C. Scott, T. W. Swetnam, G. R. van der Werf, and S. J. Pyne. 2009. Fire in the Earth System. Science **324**:481-484.

Carcaillet, C., Y. Bergeron, P. J. H. Richard, B. Frechette, S. Gauthier, and Y. T. Prairie. 2001. Change of fire frequency in the eastern Canadian boreal forests during the Holocene: does vegetation composition or climate trigger the fire regime? Journal of Ecology **89**:930-946.

Chapin, F. S., M. Sturm, M. C. Serreze, J. P. McFadden, J. R. Key, A. H. Lloyd, A. D. McGuire, T. S. Rupp, A. H. Lynch, J. P. Schimel, J. Beringer, W. L. Chapman, H. E. Epstein, E. S. Euskirchen, L. D. Hinzman, G. Jia, C. L. Ping, K. D. Tape, C. D. C. Thompson, D. A. Walker, and J. M. Welker. 2005. Role of land-surface changes in Arctic summer warming. Science **310**:657-660.

Chipman, M. L., V. Hudspith, P. E. Higuera, P. A. Duffy, R. Kelly, W. W. Oswald, and F. S. Hu. 2015. Spatiotemporal patterns of tundra fires: Late-Quaternary charcoal records from Alaska. Biogeosciences **12**:4017-4027.

Cochrane, M. A., A. Alencar, M. D. Schulze, C. M. Souza, D. C. Nepstad, P. Lefebvre, and E. A. Davidson. 1999. Positive feedbacks in the fire dynamic of closed canopy tropical forests. Science **284**:1832-1835.

Crausbay, S. D., P. E. Higuera, D. G. Sprugel, and L. B. Brubaker. 2017. Fire catalyzed rapid ecological change in lowland coniferous forests of the Pacific Northwest over the past 14,000 years. Ecology **98**:2356-2369.

Cumming, S. G. 2001. Forest type and wildfire in the alberta boreal mixedwood: What do fires burn? Ecological Applications **11**:97-110.

Dash, C. B., J. M. Fraterrigo, and F. S. Hu. 2016. Land cover influences boreal-forest fire responses to climate change: geospatial analysis of historical records from Alaska. Landscape Ecology **31**:1781-1793.

Duffy, P. A., J. E. Walsh, J. M. Graham, D. H. Mann, and T. S. Rupp. 2005. Impacts of large-scale atmospheric-ocean variability on Alaskan fire season severity. Ecological Applications **15**:1317-1330.

Erni, S., D. Arseneault, M. A. Parisien, and Y. Begin. 2017. Spatial and temporal dimensions of fire activity in the fire-prone eastern Canadian taiga. Global Change Biology **23**:1152-1166.

Flannigan, M., A. S. Cantin, W. J. de Groot, M. Wotton, A. Newbery, and L. M. Gowman. 2013. Global wildland fire season severity in the 21st century. Forest Ecology and Management **294**:54-61.

Flannigan, M. D., K. A. Logan, B. D. Amiro, W. R. Skinner, and B. J. Stocks. 2005. Future area burned in Canada. Climatic Change **72**:1-16.

Flannigan, M. D., B. M. Wotton, G. A. Marshall, W. J. de Groot, J. Johnston, N. Jurko, and A. S. Cantin. 2016. Fuel moisture sensitivity to temperature and precipitation: climate change implications. Climatic Change **134**:59-71.

Grimm, N. B., F. S. Chapin, B. Bierwagen, P. Gonzalez, P. M. Groffman, Y. Q. Luo, F. Melton, K. Nadelhoffer, A. Pairis, P. A. Raymond, J. Schimel, and C. E. Williamson. 2013. The impacts of climate change on ecosystem structure and function. Frontiers in Ecology and the Environment **11**:474-482.

Héon, J., D. Arseneault, and M. A. Parisien. 2014. Resistance of the boreal forest to high burn rates. Proceedings of the National Academy of Sciences of the United States of America **111**:13888-13893.

Hicke, J. A., G. P. Asner, E. S. Kasischke, N. H. F. French, J. T. Randerson, G. J. Collatz, B. J. Stocks, C. J. Tucker, S. O. Los, and C. B. Field. 2003. Postfire response of North American boreal forest net primary productivity analyzed with satellite observations. Global Change Biology **9**:1145-1157.

Higuera, P. E., L. B. Brubaker, P. M. Anderson, F. S. Hu, and T. A. Brown. 2009. Vegetation mediated the impacts of postglacial climate change on fire regimes in the south-central Brooks Range, Alaska. Ecological Monographs **79**:201-219.

Higuera, P. E., M. L. Chipman, J. L. Barnes, M. A. Urban, and F. S. Hu. 2011. Variability of tundra fire regimes in Arctic Alaska: millennial scale patterns and ecological implications. Ecological Applications **21**:3211-3226.

Hinzman, L. D., C. J. Deal, A. D. McGuire, S. H. Mernild, I. V. Polyakov, and J. E. Walsh. 2013. Trajectory of the Arctic as an integrated system. Ecological Applications **23**:1837-1868.

Hu, F. S., P. E. Higuera, P. Duffy, M. L. Chipman, A. V. Rocha, A. M. Young, R. Kelly, and M. C. Dietze. 2015. Arctic tundra fires: natural variability and responses to climate change. Frontiers in Ecology and the Environment **13**:369-377.

Hu, F. S., P. E. Higuera, J. E. Walsh, W. L. Chapman, P. A. Duffy, L. B. Brubaker, and M. L. Chipman. 2010. Tundra burning in Alaska: Linkages to climatic change and sea ice retreat. Journal of Geophysical Research-Biogeosciences **115**:G04002.

Johnson, E. A. 1992. Fire and vegetation dynamics: Studies from the North American boreal forest. Cambridge University Press, Cambridge.

Joly, K., P. A. Duffy, and T. S. Rupp. 2012. Simulating the effects of climate change on fire regimes in Arctic biomes: implications for caribou and moose habitat. Ecosphere **3**.

Kasischke, E. S., D. L. Verbyla, T. S. Rupp, A. D. McGuire, K. A. Murphy, R. Jandt, J. L. Barnes, E. E. Hoy, P. A. Duffy, M. Calef, and M. R. Turetsky. 2010. Alaska's changing fire regime - implications for the vulnerability of its boreal forests. Canadian Journal of Forest Research-Revue Canadienne De Recherche Forestiere **40**:1313-1324.

Kasischke, E. S., D. Williams, and D. Barry. 2002. Analysis of the patterns of large fires in the boreal forest region of Alaska. International Journal of Wildland Fire **11**:131-144.

Kelly, R., M. L. Chipman, P. E. Higuera, I. Stefanova, L. B. Brubaker, and F. S. Hu. 2013. Recent burning of boreal forests exceeds fire regime limits of the past 10,000 years. Proceedings of the National Academy of Sciences of the United States of America **110**:13055-13060.

Kelly, R., H. Genet, A. D. McGuire, and F. S. Hu. 2016. Palaeodata-informed modelling of large carbon losses from recent burning of boreal forests. Nature Climate Change **6**:79-82.

Krawchuk, M. A., S. G. Cumming, M. D. Flannigan, and R. W. Wein. 2006. Biotic and abiotic regulation of lightning fire initiation in the mixedwood boreal forest. Ecology **87**:458-468.

Krawchuk, M. A. and M. A. Moritz. 2011. Constraints on global fire activity vary across a resource gradient. Ecology **92**:121-132.

Krawchuk, M. A., M. A. Moritz, M. A. Parisien, J. Van Dorn, and K. Hayhoe. 2009. Global Pyrogeography: the Current and Future Distribution of Wildfire. PLoS ONE **4**.

Littell, J. S., D. McKenzie, D. L. Peterson, and A. L. Westerling. 2009. Climate and wildfire area burned in western U. S. ecoprovinces, 1916-2003. Ecological Applications **19**:1003-1021.

Macias Fauria, M. and E. A. Johnson. 2006. Large-scale climatic patterns control large lightning fire occurrence in Canada and Alaska forest regions. Journal of Geophysical Research-Biogeosciences **111**.

Macias Fauria, M. and E. A. Johnson. 2008. Climate and wildfires in the North American boreal forest. Philosophical Transactions of the Royal Society B-Biological Sciences **363**:2317-2329.

Macias Fauria, M., S. T. Michaletz, and E. A. Johnson. 2011. Predicting climate change effects on wildfires requires linking processes across scales. Wiley Interdisciplinary Reviews-Climate Change **2**:99-112.

Mack, M. C., M. S. Bret-Harte, T. N. Hollingsworth, R. R. Jandt, E. A. G. Schuur, G. R. Shaver, and D. L. Verbyla. 2011. Carbon loss from an unprecedented Arctic tundra wildfire. Nature **475**:489-492.

Marlon, J. R., P. J. Bartlein, A. L. Daniau, S. P. Harrison, S. Y. Maezumi, M. J. Power, W. Tinner, and B. Vanniere. 2013. Global biomass burning: a synthesis and review of Holocene paleofire records and their controls. Quaternary Science Reviews **65**:5-25.

McGuire, A. D., L. G. Anderson, T. R. Christensen, S. Dallimore, L. D. Guo, D. J. Hayes, M. Heimann, T. D. Lorenson, R. W. Macdonald, and N. Roulet. 2009. Sensitivity of the carbon cycle in the Arctic to climate change. Ecological Monographs **79**:523-555.

Moritz, M. A., M. A. Parisien, E. Batllori, M. A. Krawchuk, J. Van Dorn, D. J. Ganz, and K. Hayhoe. 2012. Climate change and disruptions to global fire activity. Ecosphere **3**.

Pan, Y. D., R. A. Birdsey, J. Y. Fang, R. Houghton, P. E. Kauppi, W. A. Kurz, O. L. Phillips, A. Shvidenko, S. L. Lewis, J. G. Canadell, P. Ciais, R. B. Jackson, S. W. Pacala, A. D. McGuire, S. L. Piao, A. Rautiainen, S. Sitch, and D. Hayes. 2011. A Large and Persistent Carbon Sink in the World's Forests. Science **333**:988-993.

Parisien, M. A., S. A. Parks, M. A. Krawchuk, J. M. Little, M. D. Flannigan, L. M. Gowman, and M. A. Moritz. 2014. An analysis of controls on fire activity in boreal Canada: comparing models built with different temporal resolutions. Ecological Applications **24**:1341-1356.

Pausas, J. G., R. A. Bradstock, D. A. Keith, J. E. Keeley, and G. F. Network. 2004. Plant functional traits in relation to fire in crown-fire ecosystems. Ecology **85**:1085-1100.

Pausas, J. G. and E. Ribeiro. 2013. The global fire productivity relationship. Global Ecology and Biogeography **22**:728-736.

Rocha, A. V., M. M. Loranty, P. E. Higuera, M. C. Mack, F. S. Hu, B. M. Jones, A. L. Breen, E. B. Rastetter, S. J. Goetz, and G. R. Shaver. 2012. The footprint of Alaskan tundra fires during the past half-century: implications for surface properties and radiative forcing. Environmental Research Letters **7**.

Rogers, B. M., J. T. Randerson, and G. B. Bonan. 2013. High-latitude cooling associated with landscape changes from North American boreal forest fires. Biogeosciences **10**:699-718.

Rogers, B. M., A. J. Soja, M. L. Goulden, and J. T. Randerson. 2015. Influence of tree species on continental differences in boreal fires and climate feedbacks. Nature Geoscience **8**:228-234.

Rothermel, R. C. 1972. A mathematical model for predicting fire spread in wildland fuels. U.S. Forest Service Research Paper. **INT-438**.

Serreze, M. C. and R. G. Barry. 2011. Processes and impacts of Arctic amplification: A research synthesis. Global and Planetary Change **77**:85-96.

Stocks, B. J., J. A. Mason, J. B. Todd, E. M. Bosch, B. M. Wotton, B. D. Amiro, M. D. Flannigan, K. G. Hirsch, K. A. Logan, D. L. Martell, and W. R. Skinner. 2002. Large forest fires in Canada, 1959-1997. Journal of Geophysical Research-Atmospheres **108**:8149.

Tarnocai, C., J. G. Canadell, E. A. G. Schuur, P. Kuhry, G. Mazhitova, and S. Zimov. 2009. Soil organic carbon pools in the northern circumpolar permafrost region. Global Biogeochemical Cycles **23**.

Tepley, A. J., E. Thomann, T. T. Veblen, G. L. W. Perry, A. Holz, J. Paritsis, T. Kitzberger, and K. Anderson-Teixeira. 2018. Influences of fire–vegetation feedbacks and post-fire recovery rates on forest landscape vulnerability to altered fire regimes. Journal of Ecology **00**:1-16.

van der Werf, G. R., J. T. Randerson, L. Giglio, T. T. van Leeuwen, Y. Chen, B. M. Rogers, M. Q. Mu, M. J. E. van Marle, D. C. Morton, G. J. Collatz, R. J. Yokelson, and P. S. Kasibhatla. 2017. Global fire emissions estimates during 1997-2016. Earth System Science Data **9**:697-720.

Veraverbeke, S., B. M. Rogers, M. L. Goulden, R. R. Jandt, C. E. Miller, E. B. Wiggins, and J. T. Randerson. 2017. Lightning as a major driver of recent large fire years in North American boreal forests. Nature Climate Change **7**:529-+.

Walker, D. A., M. K. Raynolds, F. J. A. Daniels, E. Einarsson, A. Evlvebakk, W. A. Could, A. E. Katenin, S. S. Kholod, C. J. Markon, E. S. Melnikov, N. G. Moskalenko, S. S. Talbot, and B. A. Yurtsev. 2005. The circumpolar Arctic vegetation map. Journal of Vegetation Science **16**:267-282.

Walther, G. R., E. Post, P. Convey, A. Menzel, C. Parmesan, T. J. C. Beebee, J. M. Fromentin, O. Hoegh-Guldberg, and F. Bairlein. 2002. Ecological responses to recent climate change. Nature **416**:389-395.

Westerling, A. L., H. G. Hidalgo, D. R. Cayan, and T. W. Swetnam. 2006. Warming and earlier spring increase western US forest wildfire activity. Science **313**:940-943.

Williams, J. W., S. T. Jackson, and J. E. Kutzbach. 2007. Projected distributions of novel and disappearing climates by 2100 AD. Proceedings of the National Academy of Sciences of the United States of America **104**:5738-5742.

Wooster, M. J. and Y. H. Zhang. 2004. Boreal forest fires burn less intensely in Russia than in North America. Geophysical Research Letters **31**.

Wotton, B. M., C. A. Nock, and M. D. Flannigan. 2010. Forest fire occurrence and climate change in Canada. International Journal of Wildland Fire **19**:253-271.

Chapter 1: Climatic thresholds shape northern high-latitude fire regimes and imply vulnerability to future climate change

Published in *Ecography* as:

Young, A.M., P. E. Higuera, P. A. Duffy, and F. S. Hu. 2017. Climatic thresholds shape northern high-latitude fire regimes and imply vulnerability to future climate change. Ecography **40**:606-617. doi: 10.1111/ecog.02205.

Abstract

Boreal forests and arctic tundra cover 33% of global land area and store an estimated 50% of total soil carbon. Because wildfire is a key driver of terrestrial carbon cycling, increasing fire activity in these ecosystems would likely have global implications. To anticipate potential spatiotemporal variability in fire-regime shifts, we modeled the spatially explicit 30-yr probability of fire occurrence as a function of climate and landscape features (i.e., vegetation and topography) across Alaska. Boosted regression tree (BRT) models captured the spatial distribution of fire across boreal forest and tundra ecoregions (AUC from 0.63-0.78 and Pearson correlations between predicted and observed data from 0.54-0.71), highlighting summer temperature and annual moisture availability as the most influential controls of historical fire regimes. Modeled fire-climate relationships revealed distinct thresholds to fire occurrence, with a nonlinear increase in the probability of fire above an average July temperature of 13.4 °C and below an annual moisture availability (i.e., P-PET) of approximately 150 mm. To anticipate potential fire-regime responses to 21st-century climate change, we informed our BRTs with Coupled Model Intercomparison Project Phase 5 climate projections under the RCP 6.0 scenario. Based on these projected climatic changes alone (i.e., not accounting for potential changes in vegetation), our results suggest an increasing probability of wildfire in Alaskan boreal forest and tundra ecosystems, but of

varying magnitude across space and throughout the 21st century. Regions with historically low flammability, including tundra and the forest-tundra boundary, are particularly vulnerable to climatically induced changes in fire activity, with up to a fourfold increase in the 30-yr probability of fire occurrence by 2100. Our results underscore the climatic potential for novel fire regimes to develop in these ecosystems, relative to the past 6,000-35,000 years, and spatial variability in the vulnerability of wildfire regimes and associated ecological processes to 21st-century climate change.

Introduction

Boreal forest and tundra ecosystems cover approximately 33% of Earth's terrestrial surface (McGuire et al. 1995) and are experiencing climatic warming at rates twice as fast as the global average (Serreze and Barry 2011). The ecosystem impacts of warming are well documented, including permafrost thawing (Schuur et al. 2008), shrub expansion (Myers-Smith et al. 2011), altered forest productivity (Beck et al. 2011), and increased fire activity (Kelly et al. 2013). Northern high-latitude ecosystems also play a key role in the global climate system, storing an estimated 50% of global soil carbon (McGuire et al. 2009). The fate of these massive carbon stocks is directly tied to wildfire (Bond-Lamberty et al. 2007, Kelly et al. 2016), and thus to potential shifts in 21st-century fire regimes (i.e., the expected pattern of burning over broad spatiotemporal scales; Baker, 2009). For example, the 2007 Anaktuvuk River Fire in the Brooks Foothills ecoregion of Alaska, an event locally unprecedented in the past 6,500 years (Chipman et al. 2015), resulted in an estimated 2.1 Tg C emitted to the atmosphere, comparable to the annual net carbon sink of the tundra biome (Mack et al. 2011). Thus, increased fire activity in this tundra region would likely result in

novel levels of burning, with important implications for ecosystem structure and function, including carbon storage.

Climate warming is expected to alter fire activity globally (Flannigan et al. 2009), but anticipating regional fire-regime shifts requires understanding how potential changes may manifest across space and time. The direction and impacts of shifting fire regimes will vary among ecosystems due to regional variation in climate change, vegetation composition, disturbance histories, ecosystem productivity, and carbon storage. For example, there is a wide range of fire-driven fuel consumption across boreal forests (0.6 to 12.9 kg C m^{-2}) due to regional differences in fuel composition and combustion efficiency (van Leeuwen et al. 2014). Therefore, regional differences in fire-regime changes could have important implications for wildfire emissions and carbon cycling. Spatial variability of northern high-latitude fire regimes (Rocha et al. 2012, Boulanger et al. 2013) is ultimately a product of climate and landscape controls on fuel productivity and fuel drying (Kasischke et al. 2010, Parisien et al. 2011). Anticipating potential fire-regime shifts and associated impacts of 21st-century climate change thus requires understanding the controls of spatial variability in historical fire regimes.

Statistical models of fire-climate relationships at annual timescales across broad regions of boreal forest or tundra suggest strong links between annual area burned and summer moisture deficits, highlighting mechanisms related to low fuel moisture (Duffy et al. 2005, Hu et al. 2015). Consequently, under future scenarios with higher summer moisture deficits, models project increased annual area burned, in some cases by up to 200% by the end of the 21st century (Balshi et al. 2009, Hu et al. 2015). Annual-scale models also have several

important limitations for projecting potential fire-regime shifts. First, annual-scale models generally trade off spatial for temporal resolution, with fire and climate information aggregated over broad spatial regions (e.g., Duffy et al. 2005, Hu et al. 2015). These models thereby average across regional or sub-regional variation in climate and landscape features that influence fire activity, masking regional variability in future fire activity. Second, these models are inherently sensitive to inter-annual climatic variability, a feature not well captured in global climate models (Rupp et al. 2013).

Multi-decadal scale statistical modeling offers a complementary approach to annual-scale models, trading off temporal for spatial resolution (Parisien et al. 2014). Using spatially resolved long-term (e.g., 30 yr) climatic averages and local landscape features, multi-decadal scale models explain fire occurrence at spatial resolutions from 1 to 100 km^2 (Krawchuk et al. 2009, Paritsis et al. 2013). These models help reveal mechanisms that drive spatial variation in modern fire activity (Parisien et al. 2014), and they may provide more robust scenarios of future fire activity because they are less sensitive to uncertainty in projections of inter-annual climatic variability (Moritz et al. 2012). While in many ecosystems annual-scale fire-climate relationships align with multi-decadal scale relationships (i.e., warm, dry conditions facilitate burning at both scales), alignment between these two scales is not ubiquitous. For example, fire activity is low in the warmest and driest biomes of Earth, due to consistently high fuel moisture or limited burnable biomass, respectively (Krawchuk and Moritz 2011). It remains unclear where tundra ecosystems fall along this "resource gradient" of burnable biomass. Global-scale analyses suggest that tundra fire regimes may be primarily fuel limited (Moritz et al. 2012), making them fundamentally different from fire regimes in North American boreal

forests. This contrasts with evidence from Alaskan tundra, which occupies some of the warmest, wettest regions of circumpolar tundra (Hu et al. 2015) and in some areas has burned as often as boreal forests (Higuera et al. 2011a).

Here we use multi-decadal scale statistical modeling to elucidate the historical drivers of regional fire-regime variability in boreal forest and tundra ecosystems, and then project potential fire-regime changes under 21st-century climate. To quantify historical and future fire regimes, we modeled the spatially explicit 30-yr probability of fire occurrence in Alaska at 2-km resolution using explanatory variables representing climate, vegetation, and topography. The 30-yr probability of fire occurrence can be related to the annual percent area burned, thus allowing a direct comparison to other fire-regime metrics from historical and paleo-fire records (e.g., fire frequency, mean fire return interval; Baker 2009, Chipman et al. 2015). Alaska is ideal for studying fire-climate relationships in boreal forest and tundra ecosystems, because estimated fire frequencies span several orders of magnitude, from one fire per 50 yr in areas of boreal forests (Kelly et al. 2013) to less than one fire per 10,000 yr in areas of tundra (Chipman et al. 2015). Alaska also offers one of the longest, most continuous fire records available for both boreal forest and tundra (http://fire.ak.blm.gov/), with high-resolution downscaled climate data available for the region (Scenarios Network for Alaska and Arctic Planning, 2015a, b). We expect multi-decadal climate to be an important control of Alaskan fire regimes, but we also expect the nature of fire-climate relationships to vary between boreal forest and tundra ecosystems across this vast region. Thus, two key questions we address in this work are: (1) what are the key climatic and landscape (e.g., vegetation, topography) factors controlling fire-regime variability in Alaskan boreal forest and tundra

ecosystems, and (2) how does vulnerability to climatically induced fire-regime shifts vary across Alaska throughout the 21st century?

Materials and methods

Response and explanatory variables

Fire presence-absence maps were constructed by converting fire-perimeter data from the Alaska Interagency Coordination Center (http://fire.ak.blm.gov/) to a 2-km gridded format, spanning the time period from 1950 through 2009 (Figure 1.1a). Fires prior to 1950 were excluded due to higher uncertainty in perimeter estimates (Kasischke et al. 2002). While similar studies (e.g., Moritz et al. 2012) used a presence-only approach, a presence/absence approach is justified here, as the fire perimeter data used accurately represents burned and unburned areas (Kasischke et al. 2002). Although small fires are almost certainly missing from this dataset, their omission likely has a negligible influence on our results, as most area burned is from large fires (Strauss et al. 1989, Randerson et al. 2012).

Our spatial domain and the distribution of boreal forest and tundra vegetation (Figure 1.1a) was defined using the 30-m resolution National Land Cover Database (NLCD) (Homer et al. 2007, Selkowitz and Stehman 2011) and the Circumpolar Arctic Vegetation Map (CAVM) (Walker et al. 2005). The spatial distribution of Alaskan boreal forest is influenced by climate, topography, and past disturbances. Coniferous taxa (*Picea mariana* and *Picea glauca*) dominate late-successional boreal forests, with deciduous taxa (*Betula*, *Populus*) dominant during early succession. A binary "forest" or "non-forest" classification was obtained by merging the NLCD classes, and then further classifying "non-forest" pixels above

650 meters in elevation as alpine tundra using a digital elevation model (USGS 1997). We classified all non-forested, but vegetated, pixels below 650 meters in elevation as "forest," as these pixels represent post-fire successional vegetation in boreal forest. This classification resulted in a single vegetation type for boreal forest. Tundra was further classified as graminoid, shrub, wetland, or barrens, by aggregating the 21 CAVM classifications. Graminoid tundra includes tussock tundra (80-100% vegetative cover) and non-tussock tundra (50-100% vegetative cover), which occur in warm and moderately dry regions of the tundra biome, and are dominated by *Carex* and *Eriophorum* (Walker et al. 2005). Shrub tundra includes erect dwarf-shrub (i.e., < 40 cm tall) and low-shrub (i.e., > 40 cm tall) tundra, which occur in warmer, wetter regions relative to graminoid tundra, and are characterized by *Betula*, *Alnus*, and *Salix*. Wetland tundra occurs on inundated soils, and vegetation can range from graminoid-dominated in cooler regions to shrub-dominated in warmer regions. Barren tundra occurs in cold, dry mountainous regions and is comprised of short-statured, discontinuous vegetation. In our analyses, we reclassified barren tundra as alpine tundra. For boreal forest and tundra, we removed perennial non-burnable areas from the analysis using NLCD classifications of snow/ice, rock, or water. NLCD data were resampled to 2-km resolution using the nearest neighbor procedure.

To account for potential topographic controls on fire occurrence, we constructed a topographic ruggedness (TR) metric (Figure 1.1b) (Riley et al. 1999). Topographic ruggedness influences fuel continuity and the density of potential fire breaks on the landscape, and thus regions with more topographic ruggedness likely have a lower probability of burning (Baker 2009). TR was calculated by averaging the absolute difference in elevation between

any pixel and its eight surrounding pixels using a 300-m digital elevation model (USGS 1997), which was then resampled using bilinear interpolation to 2-km resolution. TR values closer to zero represent a flatter landscape, while larger TR values represent areas of increased topographic ruggedness.

Climate variables representing energy and moisture availability were selected from 12 candidate variables (Supplementary material Appendix A.2, Table A.1) constructed from monthly mean temperature and total precipitation data from the climate research unit (CRU) (Harris et al. 2014). These CRU data were statistically downscaled via the "delta-change" method (Fowler et al. 2007) to 2-km resolution using data from the Parameter-elevation Relationships on Independent Slopes Model (PRISM Climate Group, Oregon State University, http://prism.oregonstate.edu) as the baseline map. Downscaling was conducted by and acquired from the Scenarios Network for Alaska and Arctic Planning (2015a). In addition, monthly potential evapotranspiration (PET) was calculated using monthly temperature and Thornthwaite's PET equation (Thornthwaite 1948; Supplementary material Appendix A.2, Table A.1). Specifically, we used calculations given in Willmott et al. (1985), which use monthly surface air temperature and day length to estimate total monthly PET for each 2-km pixel. Monthly moisture availability was subsequently calculated by subtracting total monthly PET estimates from the downscaled total monthly precipitation estimates. We performed an initial screening of candidate climate variables, using the Spearman rank correlation between 60-yr averages (1950-2009) of all climate variables (Supplementary material Appendix A.2, Table A.2). Each variable was then used individually to estimate fire presence and absence for the period spanning 1950-2009. We chose climate variables that had

low correlation with each other ($|r_s| \leq 0.5$) and performed best when predicting fire presence and absence, as measured by the area under the receiver operating characteristic curve (see *Assessing model performance*). This process resulted in the selection of mean temperature of the warmest month (T_{WARM}; Figure 1.1c) and total annual moisture availability ($P\text{-}PET_{ANN}$; Figure 1.1d) as our two climatic explanatory variables.

Modeling the probability of fire occurrence

We modeled the presence or absence of fire using boosted regression trees (BRTs) (Elith et al. 2008), implemented with the "gbm" package (Ridgeway 2015) in the R computing environment (v3.2.2, R Core Team). We constructed three sets of models, each comprised of 100 BRTs, which included the entire study domain ("AK"; i.e., both boreal forest and tundra vegetation), only boreal forest ("BOREAL"), and only tundra ("TUNDRA"). Stratifying by these domains allowed us to directly compare fire-climate relationships between boreal forest and tundra, and evaluate the relative influence of boreal forest and tundra vegetation when included in the AK model. We used a modified version of the Alaskan ecoregions map (Levels I and III; Figure 1.1e) by Nowacki et al. (2001) to define the spatial domains for each set of models. The primary modification was the addition of the Noatak River Watershed at the Level III stratification, defined using the Noatak National Preserve perimeter. Details on the meta-parameters used to fit BRTs and model diagnostics are provided as supplementary information (Supplementary materials Appendix A.1 and Appendix A.2, Figure A.1).

To guard against overfitting of historical fire-climate relationships and account for spatial autocorrelation among 2-km pixels, we developed models using only a randomly

sampled subset of 2-km pixels from each spatial domain. Specifically, we conducted a sensitivity analysis that evaluated the tradeoff between varying sampling rates and model performance, with sampling rates determined as a function of the fire-size distribution within each sampling domain (Supplementary materials Appendix A.1 and Appendix A.2, Table A.3). Based on this analysis, we used sampling rates that correspond to randomly selecting a single 2-km pixel every 114 km^2, 122 km^2, and 74 km^2, for the AK, BOREAL, and TUNDRA domains, respectively, areas equivalent to the 85^{th} percentile of the fire-size distribution in each domain.

Training datasets were constructed for BRTs using a randomly selected set of 30 (non-continuous) years of paired fire and climate data, and the remaining set of 30 years was designated as a testing dataset. This partitioning ensured distinct training and testing datasets, to help assess each model's predictive power. Thirty year time periods are also common for expressing climatological normals, making our results consistent with the context of other global change studies. This 30-yr randomization was done for each of the 100 BRTs.

Assessing model performance

To assess model performance, we used the area under the receiver operating characteristic curve (AUC), commission error rates, and observed vs. predicted fire rotation period estimates. AUC values indicate how well BRTs discriminate between observed fire presence and absence in the testing dataset, with 0.5 suggesting no predictive power and 1.0 indicating perfect accuracy. To evaluate how well BRTs captured the potential distribution of fire occurrence, we used a threshold, derived by maximizing the summation of the true positive and true negative rates, to calculate commission error rates (Jimenez-Valverde 2012).

To assess how well predicted probabilities characterized fire regimes, we compared predicted and observed fire rotation periods (FRPs). The FRP (Eqn. 1.1) is defined as the amount of time it takes to burn an area equal in size to an area of interest

$$FRP = \frac{t}{\left(\sum_{i=1}^{n} a_i \Big/ A \right)} \tag{1.1}$$

where t is the number of years of observed fire data, a_i is the area burned of each i^{th} of n fires during this time period, and A is the size of the area of interest (Baker 2009). Within each Alaskan ecoregion (i.e. our areas of interest, Figure 1.1e) we calculated predicted FRPs by equating probability values with area burned per pixel in 30 years (Baker 2009). Observed FRPs were calculated from area burned data using the thirty years in the testing dataset, which included re-burning of pixels. To assess goodness of fit, we calculated Pearson correlation coefficients for each of the 100 BRTs for all three models to evaluate the linear relationship between predicted and observed FRPs.

By sampling 30 years non-continuously, we assume that 30 years is enough time to accurately characterize Alaskan fire regimes at the spatial scales considered here, and that fire regimes have been stationary from 1950-2009 at 30-yr timescales. We evaluated these assumptions by comparing the distribution of 100 non-continuous, randomly sampled 30-yr FRPs to the 60-yr FRP from1950-2009 for each ecoregion (Supplementary material Appendix A.2, Figure A.2), and by calculating and comparing FRPs for continuous 30-yr periods at a one-year time step from 1950-2009 (Supplementary material Appendix A.2, Figure A.3). Our data meet these assumptions, with one important exception. FRPs in the least flammable ecoregions (e.g., Brooks Foothills) were sensitive to the inclusion or exclusion of individual

fire events (Supplementary material Appendix A.2, Figure A.2). Thus, characterizing fire regimes in these regions at 30 - 60 year time periods is more uncertain than in more flammable regions.

Historical fire-regime controls

We characterized the controls of boreal forest and tundra fire regimes using relative influence values and partial dependence plots. The relative influence of explanatory variables was calculated by summing the number of times a variable was chosen in a BRT, weighted by the BRT improvement of each partition (Elith et al. 2008). The sample mean and standard deviation of the relative influence values from the 100 BRTs were plotted for comparison and visually assessed. Partial dependence plots capture the marginal relationship(s) among response and explanatory variable(s) (i.e., integrating out the influence of other explanatory variables) (Friedman 2001). Partial dependence plots from preliminary analyses revealed nonlinear fire-climate relationships, suggesting climatic thresholds to fire occurrence. To quantify potential thresholds we used a piecewise linear regression (Supplementary material Appendix A.1).

Projecting 21st-century fire regimes

We compared historical and future projections of the probability of fire occurrence to understand potential fire regimes under projected climate changes. We used downscaled (2 km) 21st-century projections from five global climate models (GCMs) from the Coupled Model Intercomparison Project Phase 5, provided by the Scenarios Network for Alaska and Arctic Planning (2015b), under the Representative Concentration Pathway 6.0 scenario

(CCSM4, GFDL-CM3, GISS-E2-R, IPSL-CM5A-LR, and MRI-CGCM3). These specific models were selected because they were evaluated as most skillful for Alaska, based on methods from Walsh et al. (2008). We informed our models with 30-yr averages of T_{WARM} and $P\text{-}PET_{ANN}$ for 2010-2039, 2040-2069, 2070-2099 for each 2-km pixel under each GCM. Our BRTs were then driven with 30-yr climatological normals, while keeping our topographic and vegetation variables unchanged.

To quantify fire-regime responses to future climate change projections, we calculated the fire rotation period for each 2-km pixel using the AK model. To quantify the direction and magnitude of potential fire-regime changes, we present a ratio between projected future fire rotation periods (FRP_{Future}) and historical fire rotation periods ($FRP_{Historical}$), for each pixel (i.e., FRP_{Future} / $FRP_{Historical}$) (e.g., Boulanger et al. 2013). This ratio is < 1.0 if fire activity increases and projected fire rotation periods shorten, and > 1.0 if fire activity decreases and projected fire rotation periods lengthen. For both projected FRPs and the relative change in FRPs, we displayed the median predicted value from all 5 GCMs, as well as projections from the warmest GCM (GFDL-CM3) and the coldest GCM (MRI-CGCM3), defined as T_{WARM} averaged over Alaska from 2010-2099.

Data available from the Dryad Digital Repository: http://dx.doi.org/10.5061/dryad.r217r (Young et al. 2016).

Results

Model evaluation

All models adequately discriminated between burned and unburned areas using climate and landscape data, with mean (SD) AUC values of 0.78 (0.02), 0.63 (0.03), and 0.73 (0.06) in the AK, BOREAL, and TUNDRA models, respectively. AK and BOREAL models had low commission error rates, 14% for AK and 20% for BOREAL models, indicating an ability to identify the spatial distribution of fire in Alaska. TUNDRA models were the least accurate in identifying the spatial distribution of fire, with the highest commission errors rates (34%) and the highest variability in commission error rates (SD of 18%, compared to 4% for AK and 8% for BOREAL models). Predicted probabilities of fire occurrence captured the spatial distribution of area burned across Alaska (Figure 1.2b, c, and d). Median Pearson correlation coefficients ranged from 0.54 in BOREAL models to 0.71 in AK (Figure 1.2e, f, and g), indicating overall robust linear relationships between predicted and observed fire rotation periods. Despite the general goodness of fit, models over-predicted the probability of fire occurrence in less flammable ecoregions (Figure 1.2e).

Historical fire-regime controls

Temperature of the warmest month (T_{WARM}) and annual moisture availability ($P\text{-}PET_{ANN}$) had the highest relative influence in all three models, although the magnitude varied among models (Figure 1.3). For example, $P\text{-}PET_{ANN}$ was more important in the BOREAL model than in the TUNDRA model. Topographic ruggedness (TR) had low to moderate

influence in all three models, and vegetation type had the lowest relative influence in both the AK and TUNDRA models (and was 0 by definition in the BOREAL model).

All three models featured a nonlinear, positive relationship between T_{WARM} and the 30-yr probability of fire occurrence (Figure 1.4a, c, e). In addition, the 30-yr probability of fire occurrence was negatively related to $P\text{-}PET_{ANN}$ in the AK and BOREAL models (Figure 1.4b, d). In the TUNDRA model, the relationship between $P\text{-}PET_{ANN}$ and fire occurrence was non-monotonic, with the wettest and driest regions exhibiting the lowest predicted probabilities compared to regions of moderate moisture availability (Figure 1.4f). Interactions between T_{WARM} and $P\text{-}PET_{ANN}$ were apparent in all three models (Figure 1.5a, b, and c), highlighting fire-conducive conditions in warm and dry climates. The relationship between TR and the probability of fire occurrence was non-monotonic for the AK and BOREAL models, with the flattest and most rugged areas exhibiting low probabilities of fire relative to regions with moderate topographic relief (Supplementary material Appendix A.2, Figure A.4). In the TUNDRA model, the probability of fire occurrence decreased as TR increased (Supplementary material Appendix A.2, Figure A.4).

Segmented regressions analysis revealed temperature (T_{WARM}) and annual moisture availability ($P\text{-}PET_{ANN}$) thresholds to fire occurrence that were generally similar among all three models. From the bootstrapped samples the average (95% CI) threshold for T_{WARM} was 13.36 °C (13.29-13.45), 13.5 °C (13.4-13.6), and 13.65 °C (13.50-13.83), for the AK, BOREAL, and TUNDRA models, respectively (Figure 1.4a, c, and e). For $P\text{-}PET_{ANN}$ threshold estimates averaged 215 mm (40-255) and 151 mm (79-223) for the AK and

BOREAL models, respectively, and -207 mm (-225 - -187) and 153 mm (124-182) for the TUNDRA model.

Projected 21st-century changes in climate and fire regimes

The average projected climate change among all five GCMs under RCP 6.0 suggests increases in summer temperature (T_{WARM}) across all ecoregions, ranging from 0.73 – 1.19 °C during 2010-2039, to 2.33-3.08 °C by 2070-2099 (Supplementary material Appendix A.2, Figure A.5). Projected annual moisture availability ($P\text{-}PET_{ANN}$) exhibits much more spatial variability compared to T_{WARM} for the 21st-century (Supplementary material Appendix A.2, Figure A.6). For example, in the Cook Inlet Basin the average projected $P\text{-}PET_{ANN}$ for the 2010-2039 period increases by 80 mm relative to the historical period (1950-2009). Comparatively, the Yukon River Lowlands is projected to experience approximately a 60 mm decrease in $P\text{-}PET_{ANN}$ during this same time period.

Using the median probability of fire value from among the five GCMs, the AK model predicts shorter fire rotation periods (i.e., more frequent burning) (Figure 1.6) in 87%, 93%, and 97% of our study region for 2010-2039, 2040-2069, and 2070-2099, respectively (Figure 1.7). In 43% of our study area, the probability of burning is projected to more than double by mid-century, resulting in fire rotation periods less than half of that predicted for the historical period. In contrast, 13% of our study region is projected to have no change or reduced fire activity for 2010-2039, primarily in boreal forest regions (Figure 1.7).

In regions projected to experience an increase in the probability of fire occurrence, the magnitude of change was variable across space and time (Figure 1.7). The largest relative

increases occur in tundra regions and the cooler boreal forest regions. In regions such as the Brooks Foothills, Yukon-Kuskokwim Delta, or Nulato Hills, fire rotation periods are projected to decrease from greater than 800 to less than 200 years by the end of the 21st century. In boreal forest the relative magnitude of change is smaller than in tundra and forest-tundra regions, but across most of the boreal forest fire rotation periods are projected to decrease to less than 100 years by end of the 21st century (Figure 1.6).

Discussion

Historical drivers of northern high-latitude fire regimes at multi-decadal timescales

Our study elucidates varying regional vulnerability to climatically induced fire-regime shifts under future climate change. This variability reflects fire-climate relationships shaped by thresholds to fire occurrence, and important interactions between temperature and moisture. Our results indicate that regions characterized by warmer and drier climates support both burnable biomass and frequent fire-conducive weather conditions necessary for fuel drying, ignition, and fire spread. The importance of summer warmth and moisture availability is consistent with annual-scale models from both boreal forest (Duffy et al. 2005, Balshi et al. 2009) and tundra ecosystems (Hu et al. 2010, Hu et al. 2015), which highlight warmer and drier summer conditions as key determinants of annual flammability. This congruence in the importance of summer climate at annual and multi-decadal timescales suggests that both Alaskan tundra and boreal forest are characterized by climate- rather than fuel-limited fire regimes. The primary difference between boreal and tundra fire-regime controls identified in this study is the lower importance of moisture availability in tundra (Figure 1.3). This lower importance may reflect the impacts of permafrost underlying tundra soils, which impedes

drainage and results in higher fuel moisture than in boreal forest under similar moisture levels (Eugster et al. 2000).

Interactions between summer warmth and moisture availability at 30-yr timescales also determine fuel loading, thereby explaining low fire activity in drier, yet cooler, regions of tundra (e.g., Brooks Range) (Figure 1.4f, 5c). In these cool and dry tundra regions, the low predicted probability of fire occurrence provides the only limited evidence of fuel-limited fire regimes in Alaska; however we note also that fire occurrence is quite sparse in these tundra regions. Reduced moisture availability, in combination with cooler temperatures, likely results in lower productivity (Walker et al. 2005) and thus reduced fuel availability (Moritz et al. 2012). Finally, lower fire activity in cool and dry tundra regions could also reflect reduced lightning ignitions, due to limited convection and thunderstorm formation (Pfeiffer et al. 2013). Together, this body of work highlights the nature of climatic controls of northern high-latitude fire regimes, from timescales of years to decades, providing key information to anticipate potential fire-regime shifts in the 21st century.

Climatic thresholds drive spatial variability in fire regimes

Fire-climate relationships in boreal forest and tundra ecosystems are characterized by climate thresholds (Figure 1.4) that drive regional variation in historical fire regimes. Temperature and moisture thresholds to burning were distinct and consistent across boreal forest and tundra ecosystems, implying that even small shifts in climate could result in large increases or decreases in potential fire activity. Thresholds to burning are also apparent in the Canadian boreal forest at annual (Ali et al. 2012) and multi-decadal timescales (Parisien et al. 2011), and in Alaskan tundra at annual timescales (Hu et al. 2010, Hu et al. 2015). This

consistency across timescales suggests links to fundamental mechanisms of wildfire ignition and spread. Specifically, high summer temperatures enhance landscape connectivity of dry fuels, regardless of landcover type, facilitating large fires and thus a high probability of fire occurrence across landscapes (Turner and Romme 1994).

Identification of climatic thresholds to burning also improves our understanding of the climatic drivers of fire-regime changes in historical and paleo-fire records. Increases in fire activity over the past 10-30 years in Alaska suggest that climatic thresholds to burning are being surpassed, particularly in regions where climate conditions are near temperature thresholds identified by our models. For example, in boreal forests, ecoregions such as the Davidson Mountains and North Ogilvie Mountains are characterized by July temperatures of 14.2 and 14.4 °C, respectively (Supplementary material Appendix A.2, Figure A.5), with both regions experiencing large increases in area burned between 2000 and 2010 (Kasischke et al. 2010). Identifying these thresholds also provides context for paleoecological records. For example, Chipman et al. (2015) highlight spatial variability in burning across Alaskan tundra based on paleoecological records spanning the past 6000-35,000 years. While tundra ecosystems in the south-central Brooks Range experienced frequent burning between c. 14,000 and 10,000 years ago (Higuera et al. 2008), tundra of the Yukon-Kuskokwim Delta experienced little burning during this same period (Chipman et al. 2015). This contrast likely reflects persistent climatic differences between these regions, with summer temperatures generally above (in the south-central Brooks Range) and below (in the Yukon-Kuskokwim Delta) the approximate 13.4 °C threshold.

Vulnerability of northern high-latitude fire regimes to 21st-century climate change

Our modeling results suggest increased fire activity will be widespread across most ecoregions during the 21st century under the RCP 6.0 scenario, equaling or exceeding the maximum levels of burning inferred from historical and paleoecological records. Across broad regions of Alaskan boreal forests, projected fire rotation periods of 50-100 years are similar to the highest levels of burning observed during the historical period in the Yukon Flats ecoregion (i.e., since 1950), the most flammable region in Alaska. In some tundra regions (e.g., Brooks Foothills and Yukon-Kuskokwim Delta), projected fire rotation periods of less than 200 yr would be unprecedented in the context of the past 6,000-35,000 years (Higuera et al. 2011b, Chipman et al. 2015). Compared to FRP estimates of 4,700 years for the late Quaternary (Chipman et al. 2015), our models suggest an approximately 20-fold decrease in the FRP in the Brooks Foothills. Although our models overpredict fire activity in low flammability tundra regions during the historical period (Figure 1.2e), even a more conservative 5- to 10-fold decrease in the FRP would represent a substantial increase in fire activity.

Projected fire regimes further highlight tundra and cooler boreal forest regions (i.e., the forest-tundra boarder) as the most vulnerable to climatically induced fire-regime shifts, as indicated by the largest changes relative to the historical period (Figure 1.7). The vulnerability of these regions is a consequence of exceeding temperature thresholds to burning (Figure 1.4), rather than greater rates of climatic warming compared to boreal forests (Figure A.5). Forest-tundra regions are also sensitive to other climatically induced ecological changes, including vegetation shifts (Pearson et al. 2013) and permafrost thaw (Schuur et al. 2008). These

ecological changes could interact with wildfire to enhance future landscape flammability in tundra and forest-tundra, forming a positive feedback that would accelerate ecosystem shifts, with important implications for northern high-latitude carbon storage. Temperature-induced shrub expansion (Myers-Smith et al. 2011) and drier soils due to permafrost thaw could also serve to increase the probability of fire occurrence (Higuera et al. 2008). In turn, more frequent and potentially repeat burning would likely accelerate permafrost thaw (Rocha and Shaver, 2011) and alter vegetation successional trajectories (Jones et al. 2013), further altering soil hydrology and biogeochemical cycling (Mack et al. 2011). The impacts of these potential interactions and feedbacks in tundra and forest-tundra may also be manifested at broader spatial scales, as increased burning (Turetsky et al. 2011), productivity (Euskirchen et al. 2009), and permafrost thaw (Schuur et al. 2015) all alter soil and ecosystem carbon storage, and thus influence atmospheric greenhouse gas concentrations.

Limitations to anticipating future fire regimes

Our future projections have several important limitations. First, projected climate changes have high uncertainty, due to the dynamics represented in GCMs as well as the scenarios represented by the alternative RCPs (Overland et al. 2014). Second, no-analog climate conditions, relative to 1950-2009, will likely exist in the 21st century. Boosted regression tree models control for extrapolation into these no-analog conditions by "clamping down" on predicted values at the upper and lower limits of each explanatory variable (Elith and Graham 2009), leaving our models constrained and unable to project values of fire activity higher or lower than existed from 1950-2009. Finally, our models do not account for future changes in vegetation, permafrost, or lightning ignitions. Given these constraints, our

future projections are best interpreted as indicating the potential location and degree of fire-conducive climatic conditions throughout the 21st century. The inability to represent vegetation changes is particularly limiting, given the known importance of fire-climate-vegetation feedbacks (Higuera et al. 2009, Johnstone et al. 2010, Kelly et al. 2013). The lack of vegetation influence in our models was surprising, but is at least partially an artifact of the categorical nature of our vegetation variables, which are not used as effectively as continuous variables (e.g., TWARM) with our methods. In North American boreal forests, burning can reduce subsequent landscape flammability for years to decades, by causing a shift from more flammable coniferous forests to less flammable deciduous forests (Kelly et al. 2013), or due a reduction in burnable biomass through a shift from landscapes dominated by older to younger forest stands (Héon et al. 2014). Thus, initial climate-induced increases in fire activity during the early 21st century (e.g., Figure 1.6) may result in decreased fire activity by mid-century, even if climate becomes more conducive for burning. Conversely, decreased fire activity in the early 21st century may have the opposite effect, as regions with little or decreased burning could serve as "fire refugia," thus helping maintain landscape heterogeneity and flammable coniferous taxa on the landscape (Johnstone et al. 2010).

Despite these limitations, our results highlight the climatic potential for novel fire regimes to develop in tundra and forest-tundra regions by the end of the 21st century, a consequence of climatic thresholds to fire occurrence being surpassed. By quantifying the vulnerability of fire regimes to future climate change, our work helps global change scientists and land managers anticipate the environmental and socioeconomic consequences of climatically mediated fire-regime shifts. Better understanding the potential implications of

climatically induced fire-regime shifts will require additional work identifying the mechanisms underlying these 30-yr climatological thresholds to burning at finer spatial scales. How these thresholds interact with non-climatic controls of burning, including ignition variability and human activity, is also a key unknown that will ultimately dictate future fire regimes in northern high-latitude ecosystems.

Acknowledgements

This research and manuscript benefited from discussions with J. Abatzoglou, L. Boschetti, M. Chipman, M. Dietze, R. Kelly, and J. Morris. Funding was provided by NSF grants ARC-1023669 to PEH and PAD, ARC-1023477 to FSH, and a NSF GK12 Fellowship, NASA Earth and Space Science Fellowship NNX14AK86H, and Joint Fire Science Program GRIN Award 14-3-01-7 to AMY. All data and scripts used in this manuscript are publicly available via the Dryad repository (http://dx.doi.org/10.5061/dryad.r217r), and the NSF Arctic Data Center (http://dx.doi.org/10.18739/A2MP8P/).

References

Ali, A. A., O. Blarquez, M. P. Girardin, C. Hely, F. Tinquaut, A. El Guellab, V. Valsecchi, A. Terrier, L. Bremond, A. Genries, S. Gauthier, and Y. Bergeron. 2012. Control of the multimillennial wildfire size in boreal North America by spring climatic conditions. Proceedings of the National Academy of Sciences of the United States of America **109**:20966-20970.

Baker, W. L. 2009. Fire Ecology in Rocky Mountain Landscapes. Island Press.

Balshi, M. S., A. D. McGuire, P. Duffy, M. Flannigan, J. Walsh, and J. Melillo. 2009. Assessing the response of area burned to changing climate in western boreal North America using a Multivariate Adaptive Regression Splines (MARS) approach. Global Change Biology **15**:578-600.

Beck, P. S. A., G. P. Juday, C. Alix, V. A. Barber, S. E. Winslow, E. E. Sousa, P. Heiser, J. D. Herriges, and S. J. Goetz. 2011. Changes in forest productivity across Alaska consistent with biome shift. Ecology Letters **14**:373-379.

Bond-Lamberty, B., S. D. Peckham, D. E. Ahl, and S. T. Gower. 2007. Fire as the dominant driver of central Canadian boreal forest carbon balance. Nature **450**:89-92.

Boulanger, Y., S. Gauthier, D. R. Gray, H. Le Goff, P. Lefort, and J. Morissette. 2013. Fire regime zonation under current and future climate over eastern Canada. Ecological Applications **23**:904-923.

Chipman, M. L., V. Hudspith, P. E. Higuera, P. A. Duffy, R. Kelly, W. W. Oswald, and F. S. Hu. 2015. Spatiotemporal patterns of tundra fires: Late-Quaternary charcoal records from Alaska. Biogeosciences **12**:4017-4027.

Duffy, P. A., J. E. Walsh, J. M. Graham, D. H. Mann, and T. S. Rupp. 2005. Impacts of large-scale atmospheric-ocean variability on Alaskan fire season severity. Ecological Applications **15**:1317-1330.

Elith, J. and C. H. Graham. 2009. Do they? How do they? WHY do they differ? On finding reasons for differing performances of species distribution models. Ecography **32**:66-77.

Elith, J., J. R. Leathwick, and T. Hastie. 2008. A working guide to boosted regression trees. Journal of Animal Ecology **77**:802-813.

Eugster, W., W. R. Rouse, R. A. Pielke, J. P. McFadden, D. D. Baldocchi, T. G. F. Kittel, F. S. Chapin, G. E. Liston, P. L. Vidale, E. Vaganov, and S. Chambers. 2000. Land-atmosphere energy exchange in Arctic tundra and boreal forest: available data and feedbacks to climate. Global Change Biology **6**:84-115.

Euskirchen, E. S., A. D. McGuire, F. S. Chapin, S. Yi, and C. C. Thompson. 2009. Changes in vegetation in northern Alaska under scenarios of climate change, 2003-2100: implications for climate feedbacks. Ecological Applications **19**:1022-1043.

Flannigan, M. D., M. A. Krawchuk, W. J. de Groot, B. M. Wotton, and L. M. Gowman. 2009. Implications of changing climate for global wildland fire. International Journal of Wildland Fire **18**:483-507.

Fowler, H. J., S. Blenkinsop, and C. Tebaldi. 2007. Linking climate change modelling to impacts studies: recent advances in downscaling techniques for hydrological modelling. International Journal of Climatology **27**:1547-1578.

Friedman, J. H. 2001. Greedy function approximation: A gradient boosting machine. Annals of Statistics **29**:1189-1232.

Harris, I., P. D. Jones, T. J. Osborn, and D. H. Lister. 2014. Updated high-resolution grids of monthly climatic observations - the CRU TS3.10 Dataset. International Journal of Climatology **34**:623-642.

Héon, J., D. Arseneault, and M. A. Parisien. 2014. Resistance of the boreal forest to high burn rates. Proceedings of the National Academy of Sciences of the United States of America **111**:13888-13893.

Higuera, P. E., L. B. Brubaker, P. M. Anderson, T. A. Brown, A. T. Kennedy, and F. S. Hu. 2008. Frequent Fires in Ancient Shrub Tundra: Implications of Paleorecords for Arctic Environmental Change. PLoS ONE **3**:e0001744.

Higuera, P. E., L. B. Brubaker, P. M. Anderson, F. S. Hu, and T. A. Brown. 2009. Vegetation mediated the impacts of postglacial climate change on fire regimes in the south-central Brooks Range, Alaska. Ecological Monographs **79**:201-219.

Higuera, P. E., M. L. Chipman, J. L. Barnes, M. A. Urban, and F. S. Hu. 2011a. Variability of tundra fire regimes in Arctic Alaska: millennial scale patterns and ecological implications. Ecological Applications **21**:3211-3226.

Higuera, P. E., J. L. Barnes, M. L. Chipman, M. Urban, and F. S. Hu. 2011b. Tundra fire history over the past 6000 years in the Noatak National Preserve, northwestern Alaska. Alaska Park Science **10**:37-41.

Homer, C., J. Dewitz, J. Fry, M. Coan, N. Hossain, C. Larson, N. Herold, A. McKerrow, J. N. VanDriel, and J. Wickham. 2007. Completion of the 2001 National Land Cover Database for the conterminous United States. Photogrammetric Engineering and Remote Sensing **73**:337-341.

Hu, F. S., P. E. Higuera, P. Duffy, M. L. Chipman, A. V. Rocha, A. M. Young, R. Kelly, and M. C. Dietze. 2015. Arctic tundra fires: natural variability and responses to climate change. Frontiers in Ecology and the Environment **13**:369-377.

Hu, F. S., P. E. Higuera, J. E. Walsh, W. L. Chapman, P. A. Duffy, L. B. Brubaker, and M. L. Chipman. 2010. Tundra burning in Alaska: Linkages to climatic change and sea ice retreat. Journal of Geophysical Research-Biogeosciences **115**:G04002.

Jimenez-Valverde, A. 2012. Insights into the area under the receiver operating characteristic curve (AUC) as a discrimination measure in species distribution modelling. Global Ecology and Biogeography **21**:498-507.

Johnstone, J. F., F. S. Chapin, T. N. Hollingsworth, M. C. Mack, V. Romanovsky, and M. Turetsky. 2010. Fire, climate change, and forest resilience in interior Alaska. Canadian Journal of Forest Research-Revue Canadienne De Recherche Forestiere **40**:1302-1312.

Jones, B. M., A. L. Breen, B. V. Gaglioti, D. H. Mann, A. V. Rocha, G. Grosse, C. D. Arp, M. L. Kunz, and D. A. Walker. 2013. Identification of unrecognized tundra fire events on the north slope of Alaska. Journal of Geophysical Research-Biogeosciences **118**:1334-1344.

Kasischke, E. S., D. L. Verbyla, T. S. Rupp, A. D. McGuire, K. A. Murphy, R. Jandt, J. L. Barnes, E. E. Hoy, P. A. Duffy, M. Calef, and M. R. Turetsky. 2010. Alaska's changing fire regime - implications for the vulnerability of its boreal forests. Canadian Journal of Forest Research-Revue Canadienne De Recherche Forestiere **40**:1313-1324.

Kasischke, E. S., D. Williams, and D. Barry. 2002. Analysis of the patterns of large fires in the boreal forest region of Alaska. International Journal of Wildland Fire **11**:131-144.

Kelly, R., M. L. Chipman, P. E. Higuera, I. Stefanova, L. B. Brubaker, and F. S. Hu. 2013. Recent burning of boreal forests exceeds fire regime limits of the past 10,000 years. Proceedings of the National Academy of Sciences of the United States of America **110**:13055-13060.

Kelly, R., H. Genet, A. D. McGuire, and F. S. Hu. 2016. Palaeodata-informed modelling of large carbon losses from recent burning of boreal forests. Nature Climate Change **6**:79-82.

Krawchuk, M. A. and M. A. Moritz. 2011. Constraints on global fire activity vary across a resource gradient. Ecology **92**:121-132.

Krawchuk, M. A., M. A. Moritz, M. A. Parisien, J. Van Dorn, and K. Hayhoe. 2009. Global Pyrogeography: the Current and Future Distribution of Wildfire. PLoS ONE **4**.

Mack, M. C., M. S. Bret-Harte, T. N. Hollingsworth, R. R. Jandt, E. A. G. Schuur, G. R. Shaver, and D. L. Verbyla. 2011. Carbon loss from an unprecedented Arctic tundra wildfire. Nature **475**:489-492.

McGuire, A. D., L. G. Anderson, T. R. Christensen, S. Dallimore, L. D. Guo, D. J. Hayes, M. Heimann, T. D. Lorenson, R. W. Macdonald, and N. Roulet. 2009. Sensitivity of the carbon cycle in the Arctic to climate change. Ecological Monographs **79**:523-555.

McGuire, A. D., J. M. Melillo, D. W. Kicklighter, and L. A. Joyce. 1995. Equilibrium responses of soil carbon to climate change: Empirical and process-based estimates. Journal of Biogeography **22**:785-796.

Moritz, M. A., M. A. Parisien, E. Batllori, M. A. Krawchuk, J. Van Dorn, D. J. Ganz, and K. Hayhoe. 2012. Climate change and disruptions to global fire activity. Ecosphere **3**.

Myers-Smith, I. H., B. C. Forbes, M. Wilmking, M. Hallinger, T. Lantz, D. Blok, K. D. Tape, M. Macias-Fauria, U. Sass-Klaassen, E. Levesque, S. Boudreau, P. Ropars, L. Hermanutz, A. Trant, L. S. Collier, S. Weijers, J. Rozema, S. A. Rayback, N. M. Schmidt, G. Schaepman-Strub, S. Wipf, C. Rixen, C. B. Menard, S. Venn, S. Goetz, L. Andreu-Hayles, S. Elmendorf, V. Ravolainen, J. Welker, P. Grogan, H. E. Epstein, and D. S. Hik. 2011. Shrub expansion in tundra ecosystems: dynamics, impacts and research priorities. Environmental Research Letters **6**.

Nowacki, G., P. Spencer, T. Brock, M. Fleming, and T. Jorgenson. 2001. Ecoregions of Alaska and neighboring territories - US Geological Survey Open-File Report 02-297 (map). Online at http://agdc.usgs.gov/data/projects/fhm/#H, USGS, Reston, VA.

Overland, J. E., M. Wang, J. E. Walsh, and J. C. Stroeve. 2014. Future Arctic Climate Changes: Adaptation and mitigation time scales. Earth's Future **2**:68-74.

Parisien, M. A., S. A. Parks, M. A. Krawchuk, M. D. Flannigan, L. M. Bowman, and M. A. Moritz. 2011. Scale-dependent controls on the area burned in the boreal forest of Canada, 1980-2005. Ecological Applications **21**:789-805.

Parisien, M. A., S. A. Parks, M. A. Krawchuk, J. M. Little, M. D. Flannigan, L. M. Gowman, and M. A. Moritz. 2014. An analysis of controls on fire activity in boreal Canada: Comparing models built with different temporal resolutions. Ecological Applications **24**:1341-1356.

Paritsis, J., A. Holz, T. T. Veblen, and T. Kitzberger. 2013. Habitat distribution modeling reveals vegetation flammability and land use as drivers of wildfire in SW Patagonia. Ecosphere **4**.

Pearson, R. G., S. J. Phillips, M. M. Loranty, P. S. A. Beck, T. Damoulas, S. J. Knight, and S. J. Goetz. 2013. Shifts in Arctic vegetation and associated feedbacks under climate change. Nature Climate Change **3**:673-677.

Pfeiffer, M., A. Spessa, and J. O. Kaplan. 2013. A model for global biomass burning in preindustrial time: LPJ-LMfire (v1.0). Geoscientific Model Development **6**:643-685.

Randerson, J. T., Y. Chen, G. R. van der Werf, B. M. Rogers, and D. C. Morton. 2012. Global burned area and biomass burning emissions from small fires. Journal of Geophysical Research **117**:G04012.

Ridgeway, G. with contributions from others. 2015. gbm: Generalized Boosted Regression Models. R package version 2.1.1. http://CRAN.R-project.org/package = gbm.

Riley, S. J., S. D. DeGloria, and R. Elliot. 1999. A terrain ruggedness index that quantifies topographic heterogeneity. Intermountain Journal of Sciences **5**:23-27.

Rocha, A. V. and G. R. Shaver. 2011. Postfire energy exchange in arctic tundra: the importance and climatic implications of burn severity. Global Change Biology **17**:2831-2841.

Rocha, A. V., M. M. Loranty, P. E. Higuera, M. C. Mack, F. S. Hu, B. M. Jones, A. L. Breen, E. B. Rastetter, S. J. Goetz, and G. R. Shaver. 2012. The footprint of Alaskan tundra fires during the past half-century: implications for surface properties and radiative forcing. Environmental Research Letters **7**.

Rupp, D. E., J. T. Abatzoglou, K. C. Hegewisch, and P. W. Mote. 2013. Evaluation of CMIP5 20th century climate simulations for the Pacific Northwest USA. Journal of Geophysical Research-Atmospheres **118**:10884-10906.

Scenarios Network for Alaska and Arctic Planning, University of Alaska. 2015a. Historical monthly and derived precipitation products – 2 km CRU TS. http://ckan.snap.uaf.edu/dataset/historical-monthly-and-derived-precipitation-products-2-km-cru-ts, accessed January 2015.

Scenarios Network for Alaska and Arctic Planning, University of Alaska. 2015b. Projected monthly and derived precipitation products – 2 km CMIP5/AR5. http://ckan.snap.uaf.edu/dataset/projected-monthly-and-derived-precipitation-products-2km-cmip5-ar5, accessed January 2015.

Schuur, E. A. G., J. Bockheim, J. G. Canadell, E. Euskirchen, C. B. Field, S. V. Goryachkin, S. Hagemann, P. Kuhry, P. M. Lafleur, H. Lee, G. Mazhitova, F. E. Nelson, A. Rinke, V. E. Romanovsky, N. Shiklomanov, C. Tarnocai, S. Venevsky, J. G. Vogel, and S. A. Zimov. 2008. Vulnerability of permafrost carbon to climate change: Implications for the global carbon cycle. Bioscience **58**:701-714.

Schuur, E. A. G., A. D. McGuire, C. Schadel, G. Grosse, J. W. Harden, D. J. Hayes, G. Hugelius, C. D. Koven, P. Kuhry, D. M. Lawrence, S. M. Natali, D. Olefeldt, V. E. Romanovsky, K. Schaefer, M. R. Turetsky, C. C. Treat, and J. E. Vonk. 2015. Climate change and the permafrost carbon feedback. Nature **520**:171-179.

Selkowitz, D. J. and S. V. Stehman. 2011. Thematic accuracy of the National Land Cover Database (NLCD) 2001 land cover for Alaska. Remote Sensing of Environment **115**:1401-1407.

Serreze, M. C. and R. G. Barry. 2011. Processes and impacts of Arctic amplification: A research synthesis. Global and Planetary Change **77**:85-96.

Strauss, D., L. Bednar, and R. Mees. 1989. Do One Percent of Forest Fires Cause 99-Percent of the Damage. Forest Science **35**:319-328.

Thornthwaite, C. W. 1948. An Approach toward a Rational Classification of Climate. Geographical Review **38**:55-94.

Turetsky, M. R., E. S. Kane, J. W. Harden, R. D. Ottmar, K. L. Manies, E. Hoy, and E. S. Kasischke. 2011. Recent acceleration of biomass burning and carbon losses in Alaskan forests and peatlands. Nature Geoscience **4**:27-31.

Turner, M. G. and W. H. Romme. 1994. Landscape dynamics in crown fire ecosystems. Landscape Ecology **9**:59-77.

USGS. 1997. Alaska 300m digital elevation model. U.S. Geological Survey EROS Alaska Field Office, Anchorage, AK.

van Leeuwen, T. T., G. R. van der Werf, A. A. Hoffmann, R. G. Detmers, G. Rucker, N. H. F. French, S. Archibald, J. A. Carvalho, G. D. Cook, W. J. de Groot, C. Hely, E. S. Kasischke, S. Kloster, J. L. McCarty, M. L. Pettinari, P. Savadogo, E. C. Alvarado, L. Boschetti, S. Manuri, C. P. Meyer, F. Siegert, L. A. Trollope, and W. S. W. Trollope. 2014. Biomass burning fuel consumption rates: a field measurement database. Biogeosciences **11**:7305-7329.

Walker, D. A., M. K. Raynolds, F. J. A. Daniels, E. Einarsson, A. Evlvebakk, W. A. Could, A. E. Katenin, S. S. Kholod, C. J. Markon, E. S. Melnikov, N. G. Moskalenko, S. S. Talbot, and B. A. Yurtsev. 2005. The circumpolar Arctic vegetation map. Journal of Vegetation Science **16**:267-282.

Walsh, J. E., W. L. Chapman, V. Romanovsky, J. H. Christensen, and M. Stendel. 2008. Global Climate Model Performance over Alaska and Greenland. Journal of Climate **21**:6156-6174.

Willmott, C. J., C. M. Rowe, and Y. Mintz. 1985. Climatology of the terrestrial seasonal water cycle. Journal of Climatology **5**:589-606.

Young, A. M., P.E. Higuera, P. A. Duffy, and F. S. Hu. 2016. Data from: Climatic thresholds shape northern high-latitude fire regimes and imply vulnerability to future climate change. Dryad Digital Repository, http://dx.doi.org/10.5061/dryad.r217r.

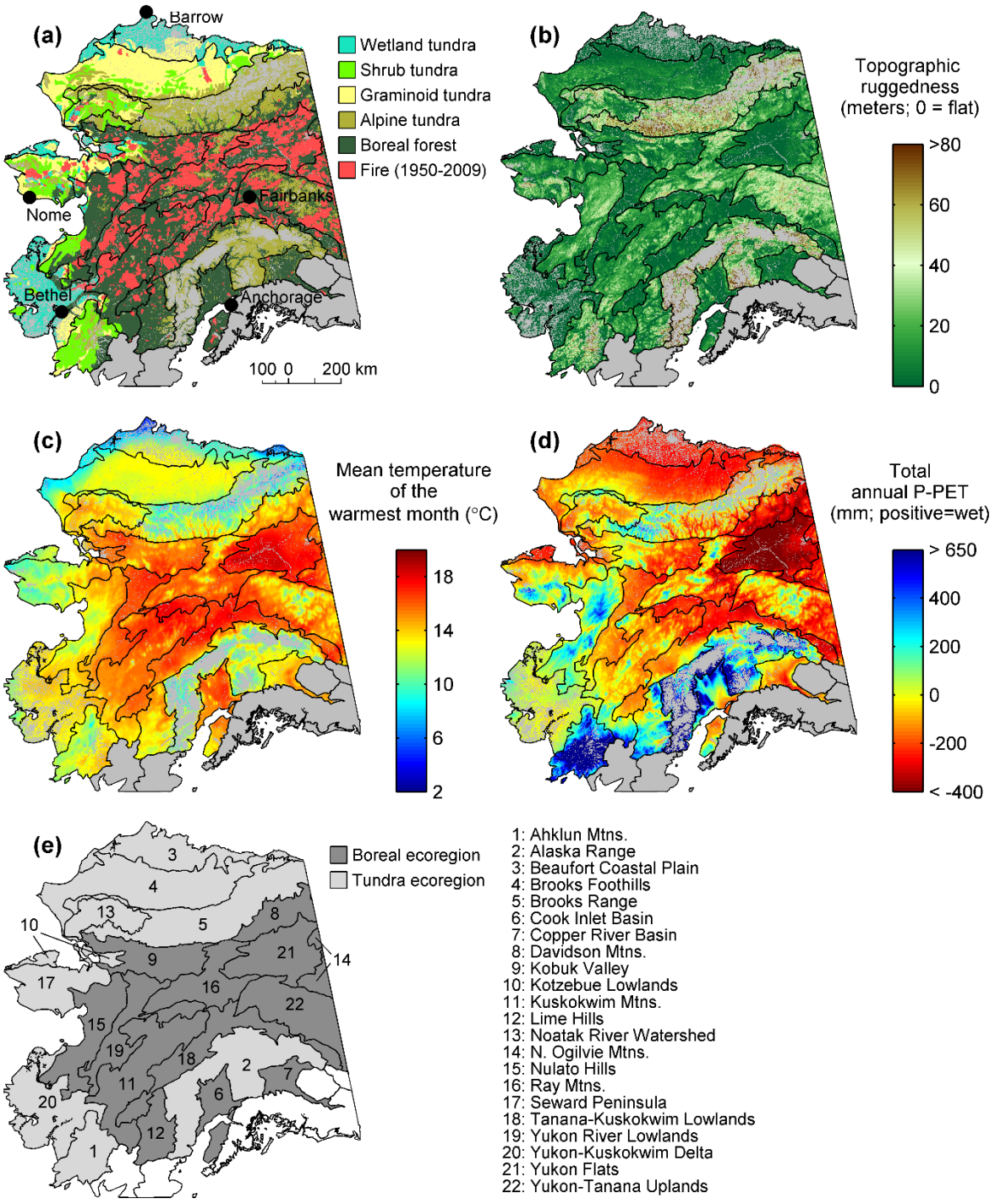

Figure 1.1. Spatial domain of the study area, including (a) the spatial distribution of vegetation and fire occurrence (1950-2009), (b) topographic ruggedness, (c) 1950-2009 mean temperature of the warmest month (T_{WARM}), (d) 1950-2009 mean total annual moisture availability ($P\text{-}PET_{ANN}$), and (e) ecoregion classification. Boreal and Tundra classifications of each ecoregion are at the Level I stratification, while individual ecoregions are classified at Level III. These classifications are slightly modified from those in Nowacki et al. (2001).

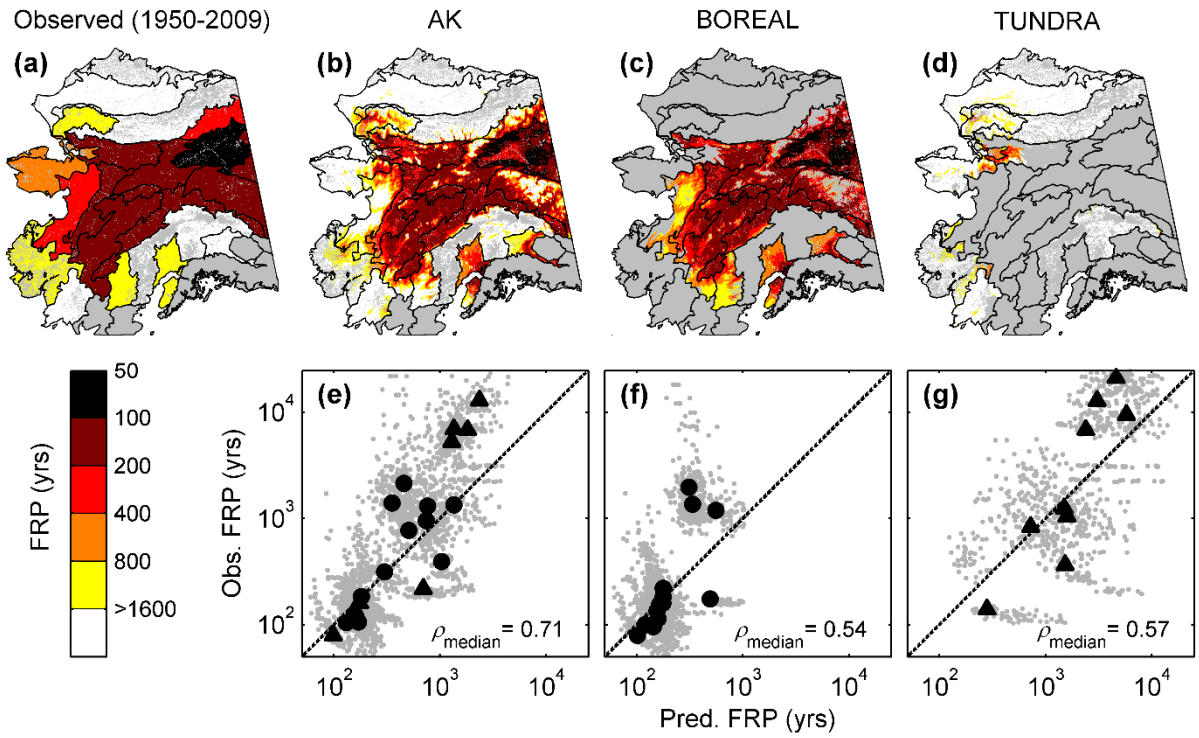

Figure 1.2. Depictions of model performance, including (a) observed fire rotation periods (FRPs) from 1950-2009 for Alaskan ecoregions as a reference, (b-d) model predicted fire rotation periods for each 2 × 2 km pixel in Alaska, and (e-g) plots comparing observed fire rotation periods against model predictions per ecoregion. Grey colored points in panels e-g are individual predictions and observations from the 100 boosted regression tree models (BRTs), while the filled darker colored circles and triangles are the median predicted and observed FRPs from the 100 BRTs for boreal and tundra ecoregions, respectively. Pearson correlation coefficients (ρ_{median}) are the median recorded Pearson correlation coefficient from a distribution of 100 Pearson correlations comparing the linear relationship between predicted and observed FRPs for each BRT. The x- and y-axes in panels e-g are on the $\log_e$ scale. Correlations were calculated on untransformed data.

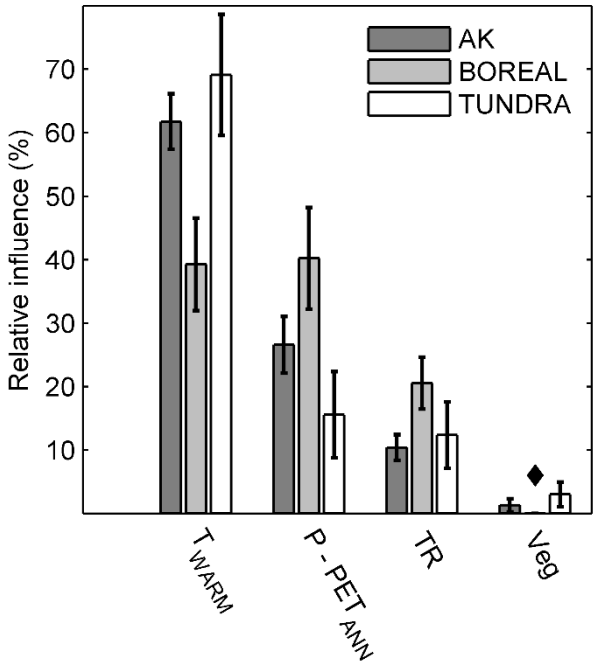

Figure 1.3. Relative influence of explanatory variables for the Alaska (AK), boreal forest (BOREAL), and tundra (TUNDRA) models. Bar heights represent the sample means and error bars represent ± 1 standard deviation from 100 boosted regression tree models. For the BOREAL model, the relative influence of vegetation (Veg) is 0 by default, as the BOREAL vegetation model has only one class (indicated by the black diamond).

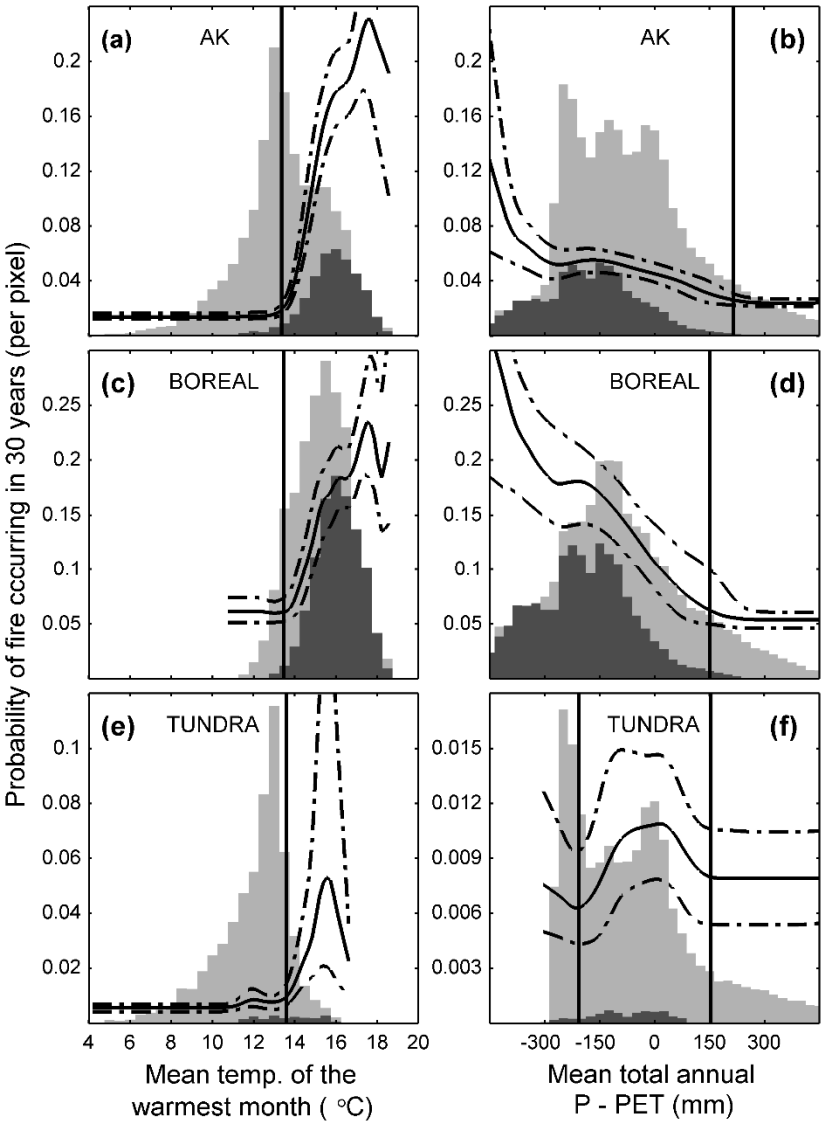

Figure 1.4. Partial dependence plots illustrating the relationships between the most important explanatory variables and the 30-yr predicted probability of fire occurrence. Rows separate different models, with the Alaska (AK), boreal forest (BOREAL), and tundra (TUNDRA) models displayed from top to bottom. The solid black lines represent the median predicted probability of fire occurrence, and the dashed lines represent the interquartile range from 100 boosted regression tree models. Probability values (y axis) are presented only for the range of climate conditions (x axis) observed from 1950-2009. A lowess function (span = 0.1) was used to smooth the plotted predicted median and interquartile lines. Vertical lines highlight thresholds, identified as the mean breakpoint from the segmented regression analysis. As a reference, lighter (darker) colored histograms represent the historical distribution of each climate variable among unburned (burned) pixels from 1950 to 2009. Histograms heights were scaled individually and are not associated with y-axis values.

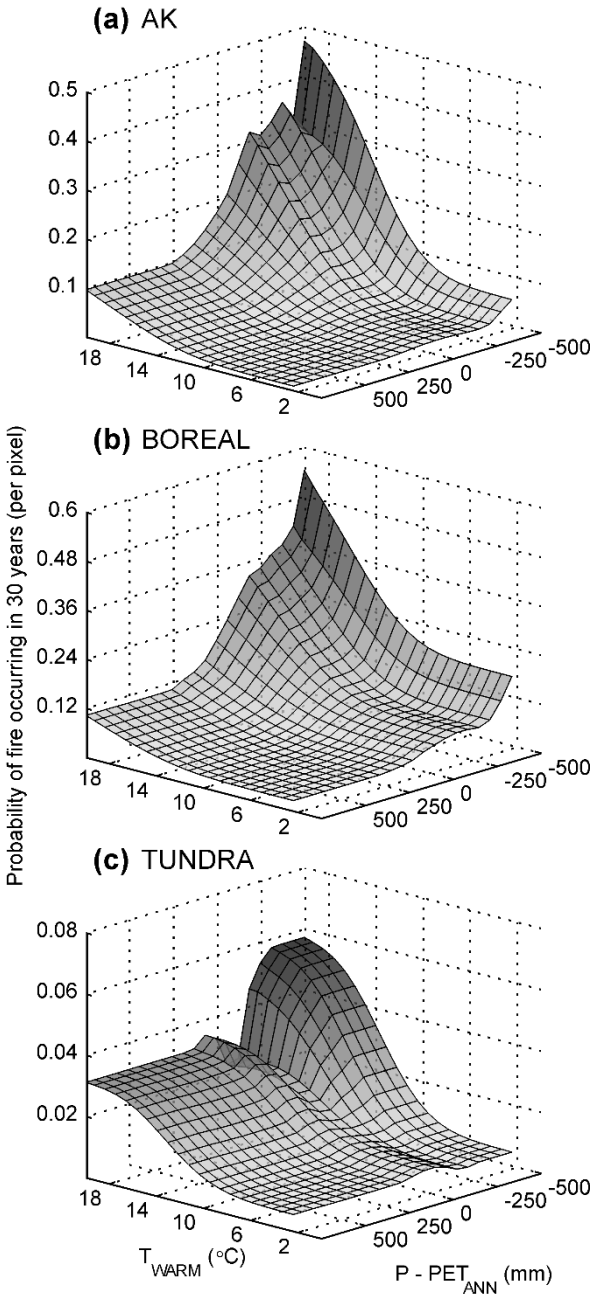

Figure 1.5. Interactions between the mean temperature of the warmest month (T_{WARM}) and annual moisture availability ($P\text{-}PET_{ANN}$), and the 30-yr probability of fire occurrence per pixel for the (a) AK, (b) BOREAL, and (c) TUNDRA models. The response surface represents the median predicted probability of fire occurrence from 100 boosted regression tree models for each model type. Darker (lighter) colors in the response surface represent higher (lower) probabilities of fire occurrence. A lowess function (span=0.1) was used to smooth the response surface.

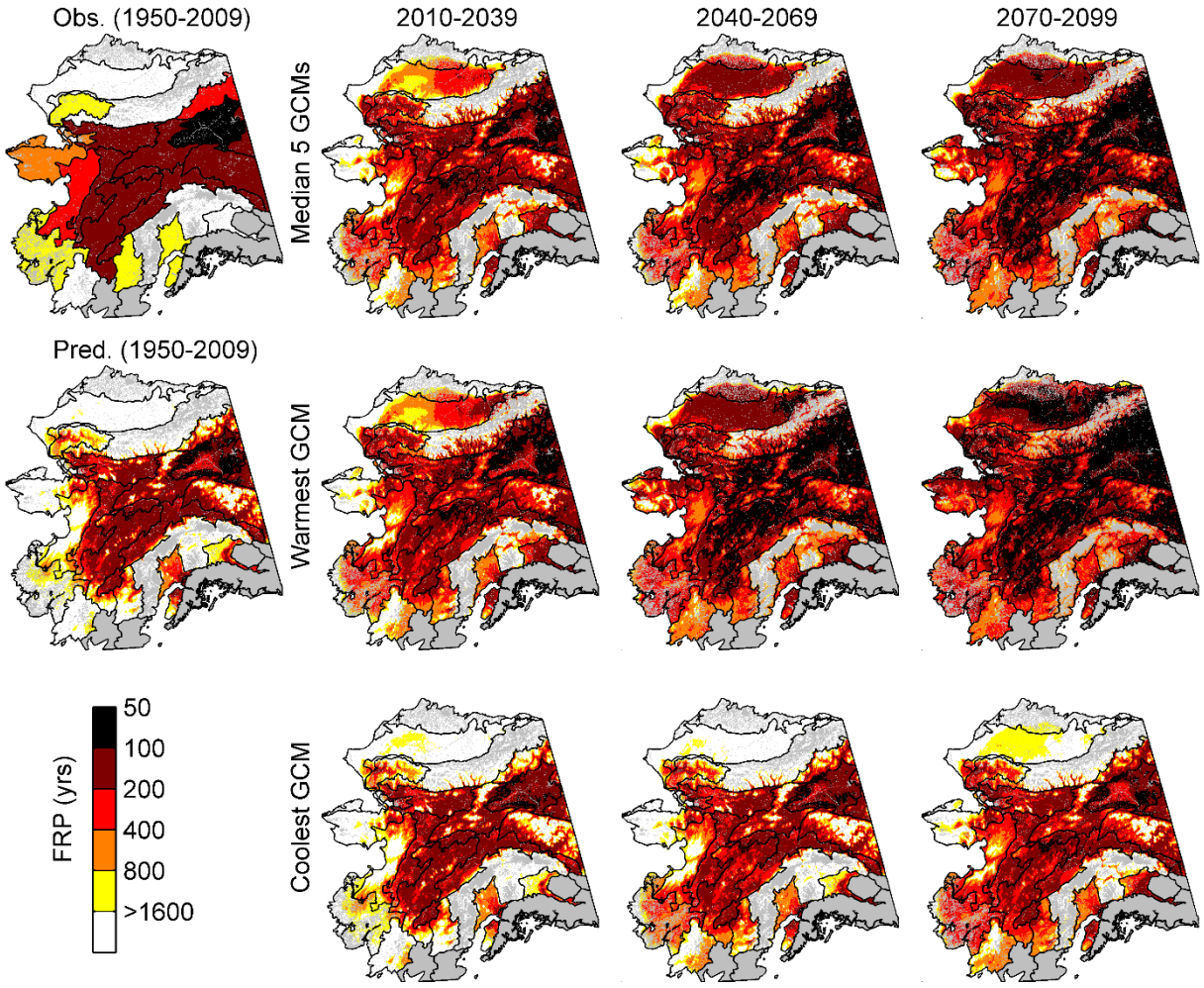

Figure 1.6. Projected fire rotation periods for three different time periods in the 21st century from the AK model. The left-most column represents historical observed (first row) and predicted (second row) fire rotation periods in Alaska, as a reference.

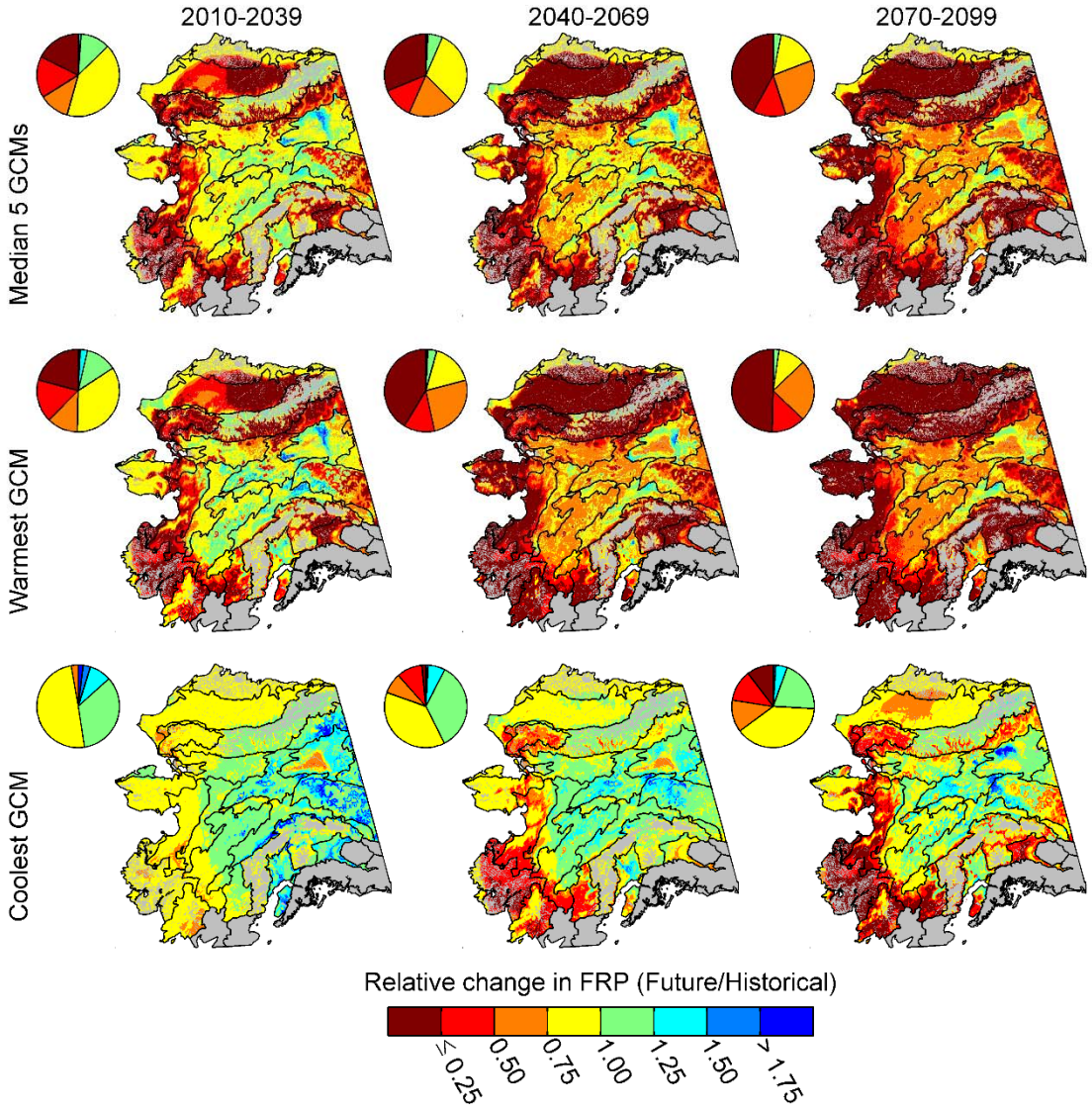

Figure 1.7. Relative change in the fire rotation period (FRP_{FUTURE} / $FRP_{HISTORICAL}$) per pixel for three different time periods in the 21st century. Change is depicted on a nonlinear scale, where a ratio of 0.5 is equal to a 100% increase in area burned, and a ratio 2.0 is equal to a 50% decrease in area burned. Warmer colors indicate an increase in the future probability of fire and thus decreasing fire rotation periods (i.e., relative difference < 1.0); cooler colors indicate a decrease in the future probability of fire and thus increasing fire rotation periods (i.e., relative difference > 1.0). Pie charts depict the proportions of all pixels in the study domain projected to experience a given level of relative change.

Chapter 2: Evidence and impacts of negative fire-vegetation feedbacks in the North American boreal forest biome

Abstract

Annual area burned in North American boreal forests is projected to increase 50-300% by 2100, in direct response to climatic change. These projections, however, generally do not account for post-fire vegetation changes, which alter landscape flammability and can change the probability of future burning, setting up fire-vegetation feedbacks. Here we use fire-history records spanning the North American boreal forest biome, MODIS data characterizing tree cover (MOD44B), and various sources of annual-scale climate data, to characterize the strength of and impact of fire-vegetation feedbacks in boreal forest ecosystems. We explicitly quantified the relative importance of vegetation as a control of annual fire activity, the magnitude and duration of post-fire vegetation change, and the presence and magnitude of fire-vegetation feedbacks. Our study domain was the entirety of the North American boreal forest biome (4.24×10^6 km^2), from 1950-2016.

We found strong evidence for negative fire-vegetation feedbacks across North American boreal forests. When comparing areas that burned only once in the past 36 years to areas that burned multiple times, we found that the distributions of single- and re-burned areas were significantly different (p-value < 0.05). Furthermore, we estimate the magnitude of this negative feedback accounts for a decrease in area burned of ≈ 27,000-36,000 km^2 (2.7-3.6 $\times 10^6$ ha, 4-5% of total area burned). Annual fire activity also lead to tree-cover loss of up to 40%, with reductions from pre-fire levels lasting for decades (35-55 yr). Finally, we found that burned-area reductions caused by negative fire-vegetation feedbacks are analogous in effect to a one-unit decrease in the 90th percentile of the Canadian fire weather index (FWI_{90})

across our entire study domain (e.g., from 10 to 9). This change in climate is comparable in magnitude to climate projections through the early-to-mid 21st century (i.e., 2030-2040) under RCP 8.5 for the IPSL-CM5A-LR global climate model. Overall, our results indicate that negative fire-vegetation feedbacks have a significant, detectable influence on biome-wide area burned. Such fire-driven decreases in landscape flammability will likely be influential in mediating the impacts of 21st-century climate change, at least until fire-conducive climate conditions exceed ranges experienced over the past several decades.

Introduction

Fire is a prominent disturbance and biophysical process in North American boreal forest ecosystems, tightly linked and responsive to climatic variability across multiple spatial and temporal scales (Duffy et al. 2005, Parisien et al. 2011, Parisien et al. 2014, Young et al. 2017). The strong relationship between climate and fire suggests fire regimes will be sensitive to ongoing and future climate over the 21st century (Moritz et al. 2012, Boulanger et al. 2013, Young et al. 2017). Indeed, recent evidence highlights increases in fire activity over the past half century (Kasischke et al. 2010, Kelly et al. 2013), and current projections of future area burned suggest a 50-300% increases by 2100 (Flannigan et al. 2005, Balshi et al. 2009, Boulanger et al. 2013, Young et al. 2017). Such increases in boreal-forest burning would have significant impacts on ecosystem structure and function, with impacts lasting years to decades (Chambers et al. 2005, Randerson et al. 2006, Johnstone et al. 2010, Beck et al. 2011, Rogers et al. 2013). For example, because fire is a dominant driver of boreal carbon dynamics, increasing fire activity could shift boreal forest regions from a carbon sink to a carbon source

(Balshi et al. 2007, Bond-Lamberty et al. 2007, Turetsky et al. 2011, Kelly et al. 2016), with potential regional and global implications (McGuire et al. 2009, Tarnocai et al. 2009).

The role of vegetation in mediating the response of fire regimes to climate change is poorly understood. Fire-vegetation interactions, documented across multiple ecosystems and scales, highlight how fire-induced changes in vegetation can increase or decrease the likelihood of subsequent burning (Héon et al. 2014, Paritsis et al. 2015, Parks et al. 2015a, Parks et al. 2016, Erni et al. 2017, Tepley et al. 2018). For example, in temperate beech (*Nothofagus*) forests of the Southern Hemisphere, fire can induce shifts to more flammable landscapes through post-fire increases in shrub abundance, creating a positive feedback whereby subsequent fire is more likely (Paritsis et al. 2015). Conversely, in coniferous forests of the western United States, fire activity decreases the likelihood of subsequent fire ignitions and spread, for years to decades, likely through the removal of biomass and overall lowering of landscape flammability (Parks et al. 2015a, Parks et al. 2016). Similar mechanisms have been proposed for North American boreal forests, where post-fire vegetation mosaics intrinsically have low flammability, due to a higher proportion of deciduous trees, relative to more homogenous, late successional conifer-dominated landscapes (Johnstone et al. 2010, Héon et al. 2014, Dash et al. 2016, Marchal et al. 2017). These studies provide strong evidence for a negative fire-vegetation feedback in North American conifer-dominated ecosystems.

Understanding the prevalence and magnitude of negative fire-vegetation feedbacks is critical for anticipating future fire regimes in boreal forest ecosystems, as these mechanisms could potentially offset and mediate projected increases in fire-conducive weather and climate

(e.g., Mann et al. 2012, Kelly et al. 2013, Pastick et al. 2017). In this study, our primary objective was to elucidate and quantify if and how negative feedbacks between fire and vegetation mediate the direct impact of climate on area burned in North American boreal forests. We use multiple analyses calling on spatial datasets of fire, vegetation, and climate to explore and quantify the controls and impacts of fire, specifically addressing three questions: (1) what is the importance of tree cover, relative to climate, in controlling annual area burned; (2) what is the magnitude and duration of tree-cover loss due to fire activity; (3) is there evidence for negative feedbacks between fire activity and tree-cover loss, and if so, what is the magnitude of this feedback? Overall, this work addresses a key source of uncertainty accompanying climatically driven projections of fire for the 21st century: the role that fire-induced changes in vegetation plays in mediating fire-regime responses to climate change.

Methods and materials

Our study area encompasses the entirety of the North American boreal forest (4.2×10^6 km^2), as defined by the World Wildlife Fund ecoregions map (Olson et al. 2001) (Figure 2.1), stretching ≈ 6200 km from the Atlantic Ocean to the Bering Strait and from 47 °N to 69 °N latitude. We aggregated and summarized multiple 1 km^2 datasets to a 500 km^2 resolution, using non-overlapping hexagons as our spatial sampling unit (hereafter referred to as “hexels," e.g., Parks et al. 2014, Parks et al. 2015b). In total, this study area was divided into 8482 individual hexels.

Fire Data

Fire data were obtained from the Canadian Forest Service National Fire Database (http://cwfis.cfs.nrcan.gc.ca/ha/nfdb) and the Alaska Large Fire Database (https://fire.ak.blm.gov/). Each dataset contains estimates for individual fire perimeters from the present (i.e., 2016) to 1917 (Canada) and 1939 (Alaska). We primarily used fire perimeters from 1981-present (Figure 2.1a), to avoid the potentially confounding influence of missing fires (i.e., false negatives). Fire-perimeter data were converted to 1-km raster grids for each year, and the total burned area for each hexel in each year was calculated and used in further analyses.

Vegetation and topography data

To characterize boreal forest vegetation, we used the MODIS Vegetation Continuous Fields product (MOD44B, collection 6), which provides estimates for the percentage of tree cover, non-tree cover, and non-vegetation cover at a ≈ 250-m resolution (DiMiceli et al. 2015). For each year from 2001-2016, we re-projected and resampled vegetation data to 1-km Albers Equal Area projection using the MODIS Reprojection Tool (https://lpdaac.usgs.gov/tools/modis_reprojection_tool_swath). These 1-km data were averaged for each vegetation coverage type (i.e., tree, non-tree, and non-vegetated) across each hexel. Additionally, we calculated the percentage of water in each hexel. We considered water and non-vegetated areas as unburnable, and hexels with > 50% unburnable cover were excluded from our analyses (e.g., Parks et al. 2015b). We used the quality science dataset from the MOD44B product to identify low-quality pixels. For analyses using the MOD44B product, we removed any hexels where the total number of low-quality pixels over the

summer months (i.e., day of year 161-289) exceeded 10% of the entire hexel area (i.e., 50 km^2).

We calculated topographic ruggedness (Riley et al. 1999) at a 1-km resolution for our entire study area by combining an Alaska Digital Elevation Model (DEM, USGS 1997) and a Canadian DEM (Natural Resources Canada 2001). The topographic ruggedness for each hexel was calculated as the median value from among all 1-km pixels contributing to each hexel.

Climate data

We used multiple climate variables to quantify the contribution of temperature and moisture to fire danger from 1981-2016. First, we used precipitation and potential evapotranspiration estimates from the Climate Research Unit (CRU) Time Series dataset (version 4.01) to calculate monthly precipitation minus potential-evapotranspiration (P-PET) (Harris et al. 2014). Second, we used variables from the Canadian Forest Fire Danger Rating System (CFFDRS, Van Wagner 1987), derived from two different climate-data sources: the MERRA2 reanalysis product (Rienecker et al. 2011), specifically using CFFDRS estimates published by Field et al. (2015), and the ERA-Interim Reanalysis (ERAI) data product (Dee et al. 2011). For the MERRA2-based CFFDRS estimates, we used the "raw" precipitation output, as opposed to "corrected" output or output based on rain-gauge datasets (Field et al. 2015). The CRU, MERRA2, and ERAI datasets have native spatial resolutions of 0.5 × 0.5°, 0.5 × 2/3°, and 0.75 × 0.75° latitude by longitude, respectively. For each climate dataset, we used bilinear interpolation to obtain climate variable estimates at the centroid of each hexel.

Measuring fire-related vegetation change

To evaluate how fire alters vegetation in North American boreal forests, we quantified changes in tree cover (%) as function of the total burned area per hexel (in any given year), and time-since-fire. Specifically, tree-cover change over time was calculated as the ratio of post-fire tree cover to tree cover in the year immediately prior of burning (i.e., post/pre, e.g., Figure 2.1d, e); this metric was calculated for each hexel that burned in each of the first 10 post-fire years. Post-fire tree-cover change was only analyzed for hexels that had (pre-fire) tree cover >20%, to avoid unreasonably large change values due to initial low values in tree cover (i.e., a small denominator in the change metric). We evaluated tree-cover changes as a function of burned area by averaging tree-cover change per hexel over the first 10 years post-fire, and then plotting these values as a function of burned area in the relevant hexel. We also evaluated tree-cover change for each year following fire, for the first 10 years, and compared these changes to those from a random subset of unburned hexels over the same time period. For unburned hexels, we identified all hexels in our study area that did not burn from 2002-2016, and then sampled these unburned hexels at random, equal in size to the number of sampled burned hexels (n = 250), and calculated tree-cover change over time. These time series represent multiple series among individual hexels, with the starting years (i.e., year of burn) ranging from 2002-2015. We did not evaluate time series longer than 10 years, which would only reflect tree-cover changes after fire in four years (2002-2005).

In addition to measuring changes in tree cover for the first 10 years after fire, we also estimated longer-term patterns of post-fire tree-cover change in our study area using a chronosequence approach (e.g., Beck et al. 2011, Rogers et al. 2013). This allowed us to

estimate the timing and patterns of post-fire recovery across the study area. Specifically, we identified all hexels that experienced fire activity from 1950-2015 and calculated the difference between the year-of-fire and the years spanned by the MOD44B data product (2001-2016). For example, if a hexel burned in 1950, we estimated tree-cover for the 51-66 years post-fire (i.e., [2001 thru 2016] minus 1950). For this analysis, we only evaluated post-fire tree-cover change after the year that experienced the highest burned area for each hexel. This approach is conservative, as it avoids quantifying change after years with little area burned, where post-fire change may still mainly reflect impacts of larger fires from the past. As a final part of the analysis, to understand how long it takes for boreal landscapes to reach pre-fire levels of tree cover, we estimated pre-fire tree-cover for the entire study area by identifying hexels that did not record fires over the entire study period (i.e., 1950-2015). From these unburned hexels, we calculated the median tree-cover value as an estimate of tree cover in hexels with > 65 years since fire.

Quantifying the annual controls of burning in boreal forests

To understand the strength and nature of climate, vegetation, and topography each as a control of annual burning, we developed statistical models using boosted regression trees (BRTs) (Friedman 2001, 2002). BRTs are a machine learning algorithm well suited for characterizing the strength of explanatory variables (i.e. "relative importance"), and the nature of ecological relationships (via partial dependence plots; [De'ath 2007]). Here, we modeled annual fire activity at the hexel level as a binary variable, instead of area burned, considering any hexel with area burned above 25 km^2 as "burned" (i.e., 1), and all hexels below this value as unburned (i.e., 0).

We develop three sets of BRTs, with each set based on a unique climate explanatory variable; each set included 50 individual BRTs to account for stochasticity in the BRT algorithm. Climate predictor variables included annual value of (1) total June-August P-PET (P-PET$_{JJA}$), (2) average June-August drought code (DC$_{JJA}$), and the (3) 90th-percentile of the daily Fire Weather Index from June-August (FWI$_{90}$). For each of the three sets of models, additional explanatory variables included % tree cover per hexel, % unburnable area per hexel, and topographic ruggedness. For BRTs that used DC$_{JJA}$ and FWI$_{90}$, we trained models using both the MERRA2 and ERAI climate-data sources separately, specifically to account for potential differences in the reanalysis products. Thus, we had five sets of models total: P-PET$_{JJA}$, DC$_{JJA}$ (MERRA2 and ERAI), and FWI$_{90}$ (MERRA2 and ERAI). For each climate variable, we imposed the functional fit to be either strictly monotonically decreasing (P-PET$_{JJA}$) or increasing (DC$_{JJA}$ and FWI$_{90}$) using the 'var.monotone' meta-parameter in the 'gbm' function. This *a priori* assumption for the nature of these fire-climate relationships is well justified, given the annual scale of this analysis and known climatic controls of burning in boreal ecosystems (Johnson 1992, Bessie and Johnson 1995, Macias Fauria and Johnson 2006). Goodness of fit for each model was assessed using AUC (Fawcett 2006). BRTs were implemented in R (R Core Team 2017) using the 'gbm' package (Ridgeway 2017). The optimal number of regression trees was estimated using the "test" method by randomly partitioning all available data into training (10%) and testing (10%) subsets. The remaining 80% of available data was used to assess model goodness-of-fit. For the meta-parameters in this BRT analysis, the shrinkage parameter was 0.01, the total number of regression trees was 5000, there was a minimum of one observation per regression tree node, and the interaction depth was set at three. To simplify our results, we present findings using only ERAI-based

FWI_{90}, the climate variable that provided the highest goodness-of-fit (Table B.1). Full results from all five sets of BRTs are provided as an Appendix (Table B.1 and Figure B.1).

Quantifying feedbacks between fire and vegetation

To understand if and how negative fire-vegetation feedbacks alter the direct influence of climate on annual fire activity, we tested if the distribution of annual area burned per hexel differed between hexels that burned only once vs. those that burned more than once over the analysis period (1981-2016). Specifically, we tested the hypotheses:

H_0: Area burned is independent of past fire activity

H_A: Area burned is dependent on and influenced by past fire activity

Therefore, under the null hypothesis (H_0), and the assumption that hexels that burned only once represent late-successional landscapes, we would expect these distributions to be statistically indistinct. To test this null hypothesis, we split our fire dataset into two populations: (1) hexels that burned once over the analysis period (i.e., "single-burned" hexels), and (2) hexels that burned two or more times over the analysis period (i.e., "multi-burned hexels"). We compared the empirical distributions of area burned for the single-burned and multi-burned hexels using the non-parametric Kolmogorov-Smirnov test (Massey 1951) and the non-parametric Anderson-Darling test (Pettitt 1976). Each test was implemented using R (R Core Team 2017) with the 'ks.test' function in the base R 'stats' package and 'ad.test' function in 'kSamples' package (Scholz and Zhu 2017). Additionally, to visually compare the distributions, we used empirical survival functions. These functions

depict the probability of observing burned area greater than a pre-specified value (e.g., 400 km^2).

In addition to comparing the annual fire size distribution between single- and multi-burned hexels, we also compared total area burned from 1981-2016 that would be expected under the null hypothesis vs. observed total area burned. To estimate expected area burned under the null hypothesis, we conducted repeated random sampling of observed single-burned hexels, with each random sample equal in size to the number of multi-burned hexels from 1981-2016 (i.e., n_{mult}). Under the null hypothesis, the total area burned in only multi-burned hexels should be approximated through repeated random sampling of single-burned hexels. We generated 1000 random samples from the population of single-burned hexels, each of size n_{mult}, calculating total burned area for each random sample. From this sampling distribution of expected total area burned, we calculated the mean and 95% confidence intervals. The differences between expected and observed area burned provides an estimate of the total difference in area burned from 1981-2016 attributable to any fire-vegetation feedbacks.

The above analyses required two selection decisions. First, we removed all hexels that recorded fires prior to 1981, to help avoid misclassifying hexels as single-burned. Second, we considered three different minimum cutoff values for classifying hexels as "burned" or "unburned." These cutoff values were based on the 99^{th}, 95^{th}, and 90^{th} percentiles of cumulative total area burned in our study area across all years: 29 km^2, 16 km^2, and 5 km^2, respectively. These minimum cutoff values were used specifically to remove the influence of the numerous hexels in our study area that experience small area burned per year. For

example, hexels with burned area values < 5 km^2 account for only 1% of total area burned, but comprise more than 20% of all hexels that experienced fire.

Comparing negative fire-vegetation feedbacks and climate change impacts on area burned

To assess the impacts of fire-vegetation feedbacks relative to the impacts of climate on area burned, we conducted a sensitivity analysis. We fit a model to predict the expected area burned under the null hypothesis (of no fire-vegetation feedbacks), specifically modelling how the distribution of single-burned hexels varied in response to climate. This model therefore provides a means to predict the expected area burned for a given change in climate, where "climate" refers to FWI_{90}. To model the distribution of single-burned hexels, we used a tapered Pareto distribution (Kagan and Schoenberg 2001), chosen due to its success in modelling fire-size distributions (Schoenberg et al. 2003, Marchal et al. 2017). If X is a tapered Pareto random variable, then its distribution function is

$$F_X(x) = 1 - \left(\frac{a}{z}\right)^{\sigma} \exp\{(a-x)/\theta\}, \quad a \le z,\ 0 < \sigma \tag{2.1}$$

(Kagan and Schoenberg 2001). In (Eqn. 2.1), a is a lower truncation value, considered known. We tested three different values for a, identical to the three lower-cutoff values described previously (i.e., 99th, 95th, and 90th percentiles of cumulative area burned). The shape and scale parameters are σ and θ, respectively. There is no upper limit on the support for x, so we derived a right-truncated tapered Pareto distribution, using 500 km^2 as this upper truncation point (i.e., the size of a hexel). To relate hexel burned area to climatic variability through a truncated-tapered Pareto distribution, we used regression functions to model σ and θ

$$\sigma = \exp\left(\beta_0 + \beta_1 \mathrm{FWI}_{90}\right) \tag{2.2}$$

$$\theta = \gamma_0 + \gamma_1 \mathrm{FWI}_{90} \ . \tag{2.3}$$

Since $\sigma > 0$, we used an exponential function in (Eqn. 2.2) to ensure only nonnegative values were estimated. This method of using regression functions to estimate parameters was based off of past work studying fire-size distribution in Canadian boreal forest ecosystems (Cumming 2001, Marchal et al. 2017).

To estimate parameters in (Eqn. 2.2) and (Eqn. 2.3), we first conducted repeated random subsampling of the entire population of single-burned hexels, and then used maximum likelihood estimation (MLE) in each subsample. We generated 1000 subsamples, each 20% of the total number of single burned hexels. This subsampling approach was necessary to meet independence assumptions required to derive maximum likelihood estimates using the MATLAB 'mle' function (MATLAB 2017), specifically to account for spatial auto-correlation among hexels in a given year. The sampling rate of 20% was chosen based on visual inspection of empirical semi-variograms (Figure B.2). Semi-variograms were calculated using the 'geoR' package (Ribeiro Jr. and Diggle 2016) in R (R Core Team 2017). Histograms for the parameter sampling distributions are available in in Figure B.3. We evaluated goodness of fit for the truncated-tapered Pareto distribution using QQ-plots (Figure B.4) and by quantifying differences between predictions and observations of total area burned.

To conduct our sensitivity analysis, we systematically decreased FWI_{90} for every observation that experienced burning from 1981-2016, in 0.5 increments, from -0.5 to -2.0.

For each of these incremental decreases in in FWI_{90}, we generated a random sample from a truncated-tapered Pareto distribution using (Eqn. 2.2) and (Eqn. 2.3). To generate random variables from the truncated-tapered Pareto distribution, we used the Accept-Reject algorithm (Devroye 1986, Robert and Casella 2004). From this random sample, equal in size to the number of burned hexels in our study area, we calculated expected total area burned. We then plotted our results to identify at what change in FWI_{90} does total expected area burned matched observed area burned. Finally, to contextualize the magnitude of any fire-vegetation feedbacks in terms of FWI_{90} units, we compared this value to projected changes in FWI_{90} throughout the 21st century, using the IPSL-CM5A-LR global climate model under the Representative Concentration Pathway (RCP) 8.5 emissions scenario.

Results

Annual controls of boreal forest burning

Our boosted regression tree models were able to distinguish between hexels that experience extensive burning (i.e., > 25 km^2) and those that did not, with mean (SD) AUC values ranging from 0.75 (0.01) to 0.80 (0.01) (Table B.1). Climate variables had average relative influences ranging from 36% (SD = 3.6%) for P-PET and 40% (SD=4.1%) for ERAI-based FWI_{90}. Tree cover consistently had the second highest relative influence, regardless of the climate variable or data source used (e.g., MERRA2 or ERAI) (Figure B.1). Among the five different climate variables considered (Figure B.1), the average relative importance for tree cover ranged from 19-28%. Our other landscape variables, unburnable area and topographic ruggedness, had relatively low influence, approximately 14-22% and 5-17%, respectively (Figures 2.2, B.1).

The probability that a hexel experienced area burned > 25 km^2 increased nonlinearly with FWI_{90} (Figure 2.2a). While we specifically constrained this functional relationship to only increase with FWI_{90}, the nonlinear nature of this relationship indicates that that the probability of extensive burning rises dramatically as FWI_{90} increases, particularly above FWI_{90} values of 25-30. The nature of the relationship between tree cover and the probability of burned area > 25 km^2 was non-monotonic, with noticeable decreases in the probability of burning below ≈20% and above ≈50% in tree cover (Figure 2.2).

Fire-caused changes on boreal tree cover

Fire notably decreased tree cover across North American boreal forest ecosystems. When considering hexels that experienced ≥ 100 km^2 in burned area, tree cover decreased by approximately 14% on average (SD = 12%) in the first 10 years after fire (Figure 2.3b-c). Comparatively, hexels that did not experience any fire from 2002-2016 exhibited an average tree-cover change of 2% (SD = 11%) (Figure 2.3a, c). The magnitude of post-fire tree-cover change was strongly related to burned area, with more tree-cover loss in hexels that experienced higher levels of burning (Figure 2.3d). Using a simple least-squares model, burned area explained approximately 41% of the variability in observed tree-cover change over the first 10 years after fire (Figure 2.3d).

In addition to short-term changes in tree cover, we also found evidence that the legacy of past fire can last from 35-55 years in boreal forests (Figure 2.3e). The high variability in this "recovery" was strongly related to the extent of burning; for example, it took approximately 25-35 years for tree cover to return to estimated pre-fire levels after fires that

burned less than 10 km^2 (in a single hexel), vs. up to 55 years if burned area was greater than 475 km^2 (Figure 2.3e).

Impacts of fire-vegetation feedback on annual area burned

We found little support for our null hypothesis (H_0) that area burned per hexel is independent of past activity. Instead, non-parametric hypothesis testing provided evidence that the distribution of annual area burned from single-and multi-burned hexels came from different populations (p-value < 0.05; Figure 2.4c). The only non-parametric hypothesis test to suggest that single- and multi-burned hexels are from the same population was the Kolmogorov-Smirnov test, specifically for the distributions using a 99^{th} percentile lower cutoff value (p-value = 0.055). From the survival plots (Figure 2.4a-c), single-burned hexels have a significantly higher probability of burning, compared to multi-burned hexels. For example, the probability that burned area is ≥ 400 km^2 is 5% in single-burned hexels, vs. only 2% in multi-burned hexels (Figure 2.4c). Additionally, the expected total burned area under the null hypothesis was significantly higher than observed total area burned. Overall, we estimate that negative fire-vegetation feedbacks have reduced total area burned in our study region from 27,000-33,000 km^2 (Table 2.1) over the past 36 yr. This reduction in burned area is approximately equal to a 12-30 year increase in the fire rotation period, using our entire study area as the area of interest (Table 2.1).

Comparing negative fire-vegetation feedback and climate change impacts on area burned

The truncated-tapered Pareto distribution fits the distribution of single-burned hexels well, as suggested by QQ-plots (Figure B.4). Our fitted truncated-tapered Pareto distribution

model successfully predicted the total area burned observed in single-burned hexels, which were used to fit these models. For example, the mean difference between predicted and observed area burned, when using the 99th-percentile cutoff value, was -3600 km^2 (95% CI = -14000 to 6500 km^2), corresponding to an approximate 1% under-prediction relative to total area burned among only single-burned hexels. These same models significantly over-predicted total area burned in only multi-burned hexels. For example, for hexels that used the 99th-percentile of total area burned as a lower cutoff value, there was a mean difference of 34,000 km^2 (95% CI = 21000 to 45000 km^2), or approximately 13% of total area burned, between predictions and observations of multi-burned hexels. Our sensitivity analysis indicated that burned-area reductions attributable to negative fire-vegetation feedbacks are analogous to an approximate "global" decrease in FWI_{90} by one unit across our entire study area (i.e., observed FWI_{90} – 1) (Figure 2.5). This magnitude of climate change is comparable to the increase in FWI_{90} anomalies (relative to the 1981-2010 average) projected through the early-mid 21st century (i.e., 2030-2040) under the RCP 8.5 emissions scenario for the IPSL-CM5A-LR global climate model.

Discussion

Our results add support to an extensive body of work highlighting climate as the leading driver of fire in the North American boreal forest biome, from regional to continental spatial scales (Duffy et al. 2005, Parisien et al. 2011, Moritz et al. 2012, Parisien et al. 2014, Bedia et al. 2015, Young et al. 2017). By quantifying post-fire tree-cover change and the likelihood of fire in once- vs. multi-burned regions, our results also reveal tree cover is a key secondary control of fire activity. These findings broadly highlight the overall importance of

vegetation, and vegetation change, for anticipating fire activity in boreal forest ecosystems. Strong links between tree cover and fire activity imply the potential for negative feedbacks between increased burning and landscape flammability (Figure 2.2), an important mechanism dictating fire-regime responses to future climate change.

Evidence and impacts of negative fire-vegetation feedbacks

The likelihood of fire occurrence in North American boreal forests was strongly dependent on past fire activity, suggesting the presence of a significant negative fire-vegetation feedback (Table 2.1 and Figure 2.4). Negative fire-vegetation feedbacks were likely driven by fire-induced changes in vegetation, which result in an overall reduction in landscape flammability. While the satellite-derived metrics of tree cover used in this study do not discriminate among species, we suggest this reduction in flammability is due to either shifts from coniferous to deciduous taxa, which tends to increase fuel moisture relative to conifer-dominated stands (Krawchuk et al. 2006, Barrett et al. 2011, Beck et al. 2011), and/or shifts to younger stands, which would lower fuel loading (Héon et al. 2014). At the continental scale of this study, we found clear evidence of decreases in post-fire tree cover, by up to a 40% (Figure 2.3), supporting the hypothesis of decreased fuel loading and lower crown bulk density as mechanisms leading to reduced fire activity. This loss in tree cover, particularly after extensive burning (Figure 2.3c), is the result of high-intensity surface and crown fires removing significant proportions of the forest canopy through combustion, and killing living trees through bole and root mortality (Johnson 1992)

We estimate that the negative fire-vegetation feedback documented here has reduced total area burned by approximately 27,000-36,000 km^2 (2.7-3.6 $\times 10^6$ ha) over the past 36

years (Table 2.1). This is equivalent to a 12-30 year increase in the fire rotation period (FRP; Johnson and Gutsell 1994), when considering our entire study area as the "area of interest." Recent evidence from eastern Canada also reveals a significant negative feedback between fire activity and the subsequent probability of burning (Erni et al. 2017). Specifically, Erni et al. (2017) suggest burn rates (i.e., % area burned per year) in eastern Canadian boreal forests would have more than doubled, from approximately 2% to 5% (i.e. >100% increase in burn rate), in the absence of negative fire-vegetation feedbacks. While we also documented evidence of a negative fire-vegetation feedback across the entire North American boreal forest biome, the magnitude of this impact is lower at the biome scale. By converting our FRP values to burn rates (Table 2.1), we estimate that burn rates across our study area would increase from approximately 0.42 to 0.44 % in the absence of negative fire-vegetation feedbacks (i.e., a 5.3% increase in burn rate). The lower magnitude of our estimate is likely due to the inclusion of a much broader spatial area, including ecoregions that experienced significantly less burning than the region studied by Erni et al. (2017), as well as other highly flammable ecoregions in western North America (Figure 2.1). Nonetheless, our results highlight a distinct and significant impact of past fire activity influencing the probability of subsequent burning.

The significance of negative fire-vegetation feedbacks for influencing future fire activity in the boreal forest biome will also depend upon the duration of reduced landscape flammability, as vegetation will eventually return to pre-fire levels (at least under successional trajectories within the historic range of variability) (e.g., Erni et al. 2017). Here, we found that fire-related vegetation changes were immediate, and lasted for decades, with forest recovery

estimated to take 35-55 yr, based on patterns of post-fire vegetation change over the past six decades (Figure 2.3). This duration is consistent with other observational studies at finer spatial scales, where factors such canopy cover and basal area have decadal-scale recovery rates (Bartels et al. 2016). Variability in the duration of forest recovery was also strongly dependent on the total annual area burned that initiated succession: boreal forest vegetation, as measured by tree cover, took longer to recover when more area burned in a given year (Figure 2.3e). This relationship between burned area and forest recovery highlights the potential for increased fire activity to reduce landscape flammability through longer recovery times. Under future projections of increasing aridity (Flannigan et al. 2016) and higher fire activity (Young et al. 2017), larger areas could experience this decreasing landscape flammability due to burning (Mann et al. 2012, Kelly et al. 2013, Pastick et al. 2017). Additionally, shorter fire-return intervals that accompany increased area burned (Johnson and Gutsell 1994, Kelly et al. 2013) may further enhance this negative fire-vegetation feedback, by favoring deciduous-tree dominance (and thus lower fuel moisture) at landscape scales (Johnstone and Chapin 2006, Brown and Johnstone 2012).

Integrating past evidence to anticipate future climate-change impacts on fire regimes

By reducing area burned, the impact of negative fire-vegetation feedbacks on total area burned in North American boreal forests is analogous to a decrease in fire-conducive climate conditions (e.g., FWI_{90}). We estimate the magnitude of negative fire-vegetation feedbacks to be equivalent to a "global" one-unit decrease in FWI_{90} across our entire study domain. We suggest that a one-unit change in FWI_{90} is significant in the context of climate change, as it is comparable to the increase in FWI_{90} projected through the first half of the 21st

century (2020-2040; Figure 2.5b). While this comparison provides a general understanding of the importance of fire-vegetation feedbacks relative to the direct impacts of climate change, it should be interpreted with caution. Specifically, this comparison implicitly assumes that for a given increase in FWI_{90} there is an equitable change in vegetation capable of offsetting the climatically driven increase in the probability of burning. Because fire-climate relationships are nonlinear (e.g., Figure 2a; Young et al. 2017), a one-unit change in FWI_{90} in the past or across space will not necessarily have the same impact as a one-unit change in the future under different climate conditions. Additionally, boreal forest landscapes will continue to change over the course of the century, integrating the legacies of past fire events and future area burned. Therefore, extrapolating this impact of past vegetation feedbacks to future landscapes is untenable, as these past and future ecosystems will fundamentally differ in their structure and function

Limitations and directions for future work

There are several additional key assumptions and limitations to consider when interpreting our results. First, we currently only take into account one GCM and one RCP scenario. Our interpretations regarding the importance of past negative fire-vegetation feedbacks, in the context of future climate change (e.g., Figure 2.5), may alter if we were to consider a wider range of GCMs and RCPs. Second, we only consider a 36-yr period (1981-2016) for evaluating the influence of negative fire-vegetation feedbacks, a relatively short time period compared to the length of secondary succession. By only representing the first three decades of succession, our results may overestimate the impacts of fire-vegetation feedbacks, as we are likely only considering the stages of succession where landscape

flammability is at a minimum. Finally, the fire-history records used here each have a diminishing record, with the likelihood of missed fires in the dataset higher prior to 1981. Such undetected fires could lead to misclassifying hexels as "single burned," when in reality they may have burned in the recent past relative to the year of burning. Not accounting for this unrecorded burning would underestimate the impact of the negative fire-vegetation feedbacks, as hexels classified as "single-burned" may more closely resemble "multi-burned" hexels in reality, and thus have an intrinsically lower probability of burning.

Despite these limitations, our findings provide strong evidence that negative fire-vegetation feedbacks have a significant impact on subsequent area burned in North American and boreal forest ecosystems. Future work should focus on linking these different interactions and relationships among fire, vegetation, and climate through statistical or process-based models that can explicitly capture post-fire vegetation changes, as well as the climatic controls of burning (Williams and Abatzoglou 2016). While regional-scale models can accomplish this task (e.g., ALFRESCO; Rupp et al. 2000, Mann et al. 2012), expanding such models to include broader spatial scales is needed to contextualize the impacts of climate change on area burned, and associated impacts on surface-energy partitioning (i.e., radiative forcing) and fire-related carbon emissions.

Acknowledgements

This research was supported by a NASA Earth and Space Science Fellowship (NNX14AK86H) and a Joint Fire Science Program GRIN Award (14-3-01-7) to AMY, NSF grants ARC-1023669 to PEH and PAD, and ARC-1023477 to FSH.

References

Balshi, M. S., A. D. McGuire, P. Duffy, M. Flannigan, J. Walsh, and J. Melillo. 2009. Assessing the response of area burned to changing climate in western boreal North America using a Multivariate Adaptive Regression Splines (MARS) approach. Global Change Biology **15**:578-600.

Balshi, M. S., A. D. McGuire, Q. Zhuang, J. Melillo, D. W. Kicklighter, E. Kasischke, C. Wirth, M. Flannigan, J. Harden, J. S. Clein, T. J. Burnside, J. McAllister, W. A. Kurz, M. Apps, and A. Shvidenko. 2007. The role of historical fire disturbance in the carbon dynamics of the pan-boreal region: A process-based analysis. Journal of Geophysical Research-Biogeosciences **112**.

Barrett, K., A. D. McGuire, E. E. Hoy, and E. S. Kasischke. 2011. Potential shifts in dominant forest cover in interior Alaska driven by variations in fire severity. Ecological Applications **21**:2380-2396.

Bartels, S. F., H. Y. H. Chen, M. A. Wulder, and J. C. White. 2016. Trends in post-disturbance recovery rates of Canada's forests following wildfire and harvest. Forest Ecology and Management **361**:194-207.

Beck, P. S. A., S. J. Goetz, M. C. Mack, H. D. Alexander, Y. F. Jin, J. T. Randerson, and M. M. Loranty. 2011. The impacts and implications of an intensifying fire regime on Alaskan boreal forest composition and albedo. Global Change Biology **17**:2853-2866.

Bedia, J., S. Herrera, J. M. Gutierrez, A. Benali, S. Brands, B. Mota, and J. M. Moreno. 2015. Global patterns in the sensitivity of burned area to fire-weather: Implications for climate change. Agricultural and Forest Meteorology **214**:369-379.

Bessie, W. C. and E. A. Johnson. 1995. The Relative importance of fuels and weather on fire behavior in sub-alpine forests. Ecology **76**:747-762.

Bond-Lamberty, B., S. D. Peckham, D. E. Ahl, and S. T. Gower. 2007. Fire as the dominant driver of central Canadian boreal forest carbon balance. Nature **450**:89-92.

Boulanger, Y., S. Gauthier, D. R. Gray, H. Le Goff, P. Lefort, and J. Morissette. 2013. Fire regime zonation under current and future climate over eastern Canada. Ecological Applications **23**:904-923.

Brown, C. D. and J. F. Johnstone. 2012. Once burned, twice shy: Repeat fires reduce seed availability and alter substrate constraints on Picea mariana regeneration. Forest Ecology and Management **266**:34-41.

Chambers, S. D., J. Beringer, J. T. Randerson, and F. S. Chapin. 2005. Fire effects on net radiation and energy partitioning: Contrasting responses of tundra and boreal forest ecosystems. Journal of Geophysical Research-Atmospheres **110**.

Cumming, S. G. 2001. A parametric model of the fire-size distribution. Canadian Journal of Forest Research-Revue Canadienne De Recherche Forestiere **31**:1297-1303.

Dash, C. B., J. M. Fraterrigo, and F. S. Hu. 2016. Land cover influences boreal-forest fire responses to climate change: geospatial analysis of historical records from Alaska. Landscape Ecology **31**:1781-1793.

De'ath, G. 2007. Boosted trees for ecological modeling and prediction. Ecology **88**:243-251.

Dee, D. P., S. M. Uppala, A. J. Simmons, P. Berrisford, P. Poli, S. Kobayashi, U. Andrae, M. A. Balmaseda, G. Balsamo, P. Bauer, P. Bechtold, A. C. M. Beljaars, L. van de Berg, J. Bidlot, N. Bormann, C. Delsol, R. Dragani, M. Fuentes, A. J. Geer, L. Haimberger, S. B. Healy, H. Hersbach, E. V. Holm, L. Isaksen, P. Kallberg, M. Kohler, M. Matricardi, A. P. McNally, B. M. Monge-Sanz, J. J. Morcrette, B. K. Park, C. Peubey, P. de Rosnay, C. Tavolato, J. N. Thepaut, and F. Vitart. 2011. The ERA-Interim reanalysis: configuration and performance of the data assimilation system. Quarterly Journal of the Royal Meteorological Society **137**:553-597.

Devroye, L. 1986. Non-uniform random variate generation. Springer-Verlag, New York.

DiMiceli, C., M. Carroll, R. Sohlberg, D. H. Kim, M. Kelley, and J. R. G. Townshend. 2015. MOD44B MODIS/Terra Vegetation Continuous Fields Yearly L3 Global 250m SIN Grid Version 006. NASA EOSDIS Land Processes DAAC, USGS Earth Resources Observation and Science (EROS) Center, Sioux Falls, South Dakota, accessed July 7, 2017, at doi: 10.5067/MODIS/MOD44B.006.

Duffy, P. A., J. E. Walsh, J. M. Graham, D. H. Mann, and T. S. Rupp. 2005. Impacts of large-scale atmospheric-ocean variability on Alaskan fire season severity. Ecological Applications **15**:1317-1330.

Erni, S., D. Arseneault, M. A. Parisien, and Y. Begin. 2017. Spatial and temporal dimensions of fire activity in the fire-prone eastern Canadian taiga. Global Change Biology **23**:1152-1166.

Fawcett, T. 2006. An introduction to ROC analysis. Pattern Recognition Letters **27**:861-874.

Field, R. D., A. C. Spessa, N. A. Aziz, A. Camia, A. Cantin, R. Carr, W. J. de Groot, A. J. Dowdy, M. D. Flannigan, K. Manomaiphiboon, F. Pappenberger, V. Tanpipat, and X. Wang. 2015. Development of a Global Fire Weather Database. Natural Hazards and Earth System Sciences **15**:1407-1423.

Flannigan, M. D., K. A. Logan, B. D. Amiro, W. R. Skinner, and B. J. Stocks. 2005. Future area burned in Canada. Climatic Change **72**:1-16.

Flannigan, M. D., B. M. Wotton, G. A. Marshall, W. J. de Groot, J. Johnston, N. Jurko, and A. S. Cantin. 2016. Fuel moisture sensitivity to temperature and precipitation: climate change implications. Climatic Change **134**:59-71.

Friedman, J. H. 2001. Greedy function approximation: A gradient boosting machine. Annals of Statistics **29**:1189-1232.

Friedman, J. H. 2002. Stochastic gradient boosting. Computational Statistics & Data Analysis **38**:367-378.

Harris, I., P. D. Jones, T. J. Osborn, and D. H. Lister. 2014. Updated high-resolution grids of monthly climatic observations - the CRU TS3.10 Dataset. International Journal of Climatology **34**:623-642.

Héon, J., D. Arseneault, and M. A. Parisien. 2014. Resistance of the boreal forest to high burn rates. Proceedings of the National Academy of Sciences of the United States of America **111**:13888-13893.

Johnson, E. A. 1992. Fire and vegetation dynamics: Studies from the North American boreal forest. Cambridge University Press, Cambridge.

Johnson, E. A. and S. L. Gutsell. 1994. Fire frequency models, methods and interpretations. Advances in Ecological Research, Vol 25 **25**:239-287.

Johnstone, J. F. and F. S. Chapin. 2006. Fire interval effects on successional trajectory in boreal forests of northwest Canada. Ecosystems **9**:268-277.

Johnstone, J. F., F. S. Chapin, T. N. Hollingsworth, M. C. Mack, V. Romanovsky, and M. Turetsky. 2010. Fire, climate change, and forest resilience in interior Alaska. Canadian Journal of Forest Research-Revue Canadienne De Recherche Forestiere **40**:1302-1312.

Kagan, Y. Y. and F. Schoenberg. 2001. Estimation of the upper cutoff parameter for the tapered Pareto distribution. Journal of Applied Probability **38A**:158-175.

Kasischke, E. S., D. L. Verbyla, T. S. Rupp, A. D. McGuire, K. A. Murphy, R. Jandt, J. L. Barnes, E. E. Hoy, P. A. Duffy, M. Calef, and M. R. Turetsky. 2010. Alaska's changing fire regime - implications for the vulnerability of its boreal forests. Canadian Journal of Forest Research-Revue Canadienne De Recherche Forestiere **40**:1313-1324.

Kelly, R., M. L. Chipman, P. E. Higuera, I. Stefanova, L. B. Brubaker, and F. S. Hu. 2013. Recent burning of boreal forests exceeds fire regime limits of the past 10,000 years. Proceedings of the National Academy of Sciences of the United States of America **110**:13055-13060.

Kelly, R., H. Genet, A. D. McGuire, and F. S. Hu. 2016. Palaeodata-informed modelling of large carbon losses from recent burning of boreal forests. Nature Climate Change **6**:79-82.

Krawchuk, M. A., S. G. Cumming, M. D. Flannigan, and R. W. Wein. 2006. Biotic and abiotic regulation of lightning fire initiation in the mixedwood boreal forest. Ecology **87**:458-468.

Macias Fauria, M. and E. A. Johnson. 2006. Large-scale climatic patterns control large lightning fire occurrence in Canada and Alaska forest regions. Journal of Geophysical Research-Biogeosciences **111**.

Mann, D. H., T. S. Rupp, M. A. Olson, and P. A. Duffy. 2012. Is Alaska's boreal forest now crossing a major ecological threshold? Arctic Antarctic and Alpine Research **44**:319-331.

Marchal, J., S. G. Cumming, and E. J. B. McIntire. 2017. Land cover, more than monthly fire weather, drives fire-size distribution in Southern Quebec forests: Implications for fire risk management. PLoS ONE **12**:e0179294.

Massey, F. J. 1951. The Kolmogorov-Smirnov test for goodness of fit. Journal of the American Statistical Association **46**:68-78.

MATLAB and Statistics Toolbox Release 2017a. 2017. The MathWorks, Inc., Natick, Massachusetts, United States.

McGuire, A. D., L. G. Anderson, T. R. Christensen, S. Dallimore, L. D. Guo, D. J. Hayes, M. Heimann, T. D. Lorenson, R. W. Macdonald, and N. Roulet. 2009. Sensitivity of the carbon cycle in the Arctic to climate change. Ecological Monographs **79**:523-555.

Moritz, M. A., M. A. Parisien, E. Batllori, M. A. Krawchuk, J. Van Dorn, D. J. Ganz, and K. Hayhoe. 2012. Climate change and disruptions to global fire activity. Ecosphere **3**.

Natural Resources Canada. 2001. Canada3D: Digital Elevation Model of the Canadian landmass. Centre for Topographic Information, Sherbrooke, QC, Canada. http://ftp.geogratis.gc.ca/pub/nrcan_rncan/elevation/canada3d/

Olson, D. M., E. Dinerstein, E. D. Wikramanayake, N. D. Burgess, G. V. N. Powell, E. C. Underwood, J. A. D'Amico, I. Itoua, H. E. Strand, J. C. Morrison, C. J. Loucks, T. F. Allnutt, T. H. Ricketts, Y. Kura, J. F. Lamoreux, W. W. Wettengel, P. Hedao, and K. R. Kassem. 2001. Terrestrial ecoregions of the worlds: A new map of life on Earth. Bioscience **51**:933-938.

Parisien, M. A., S. A. Parks, M. A. Krawchuk, M. D. Flannigan, L. M. Bowman, and M. A. Moritz. 2011. Scale-dependent controls on the area burned in the boreal forest of Canada, 1980-2005. Ecological Applications **21**:789-805.

Parisien, M. A., S. A. Parks, M. A. Krawchuk, J. M. Little, M. D. Flannigan, L. M. Gowman, and M. A. Moritz. 2014. An analysis of controls on fire activity in boreal Canada: Comparing models built with different temporal resolutions. Ecological Applications **24**:1341-1356.

Paritsis, J., T. T. Veblen, and A. Holz. 2015. Positive fire feedbacks contribute to shifts from Nothofagus pumilio forests to fire-prone shrublands in Patagonia. Journal of Vegetation Science **26**:89-101.

Parks, S. A., L. M. Holsinger, C. Miller, and C. R. Nelson. 2015a. Wildland fire as a self-regulating mechanism: the role of previous burns and weather in limiting fire progression. Ecological Applications **25**:1478-1492.

Parks, S. A., C. Miller, L. M. Holsinger, L. S. Baggett, and B. J. Bird. 2016. Wildland fire limits subsequent fire occurrence. International Journal of Wildland Fire **25**:182-190.

Parks, S. A., M. A. Parisien, C. Miller, and S. Z. Dobrowski. 2014. Fire Activity and Severity in the Western US Vary along Proxy Gradients Representing Fuel Amount and Fuel Moisture. PLoS ONE **9**:e99699.

Parks, S. A., C. Miller, M. A. Parisien, L. M. Holsinger, S. Z. Dobrowski, and J. Abatzoglou. 2015b. Wildland fire deficit and surplus in the western United States, 1984-2012. Ecosphere **6**.

Pastick, N. J., P. Duffy, H. Genet, T. S. Rupp, B. K. Wylie, K. D. Johnson, M. T. Jorgenson, N. Bliss, A. D. McGuire, E. E. Jafarov, and J. F. Knight. 2017. Historical and projected trends in landscape drivers affecting carbon dynamics in Alaska. Ecological Applications **27**:1383-1402.

Pettitt, A. N. 1976. A two-sample Anderson-Darling rank statistic. Biometrika **63**:161-168.

R Core Team. 2017. R: A language and environment for statistical computing. R Foundation for Statistical Computing, Vienna, Austria. URL https://www.R-project.org/.

Randerson, J. T., H. Liu, M. G. Flanner, S. D. Chambers, Y. Jin, P. G. Hess, G. Pfister, M. C. Mack, K. K. Treseder, L. R. Welp, F. S. Chapin, J. W. Harden, M. L. Goulden, E. Lyons, J. C. Neff, E. A. G. Schuur, and C. S. Zender. 2006. The impact of boreal forest fire on climate warming. Science **314**:1130-1132.

Ribeiro Jr., P. J. and P. J. Diggle. 2016. geoR: Analysis of Geostatistical Data. R package version 1.7-5.2. https://CRAN.R-project.org/package=geoR.

Ridgeway, G. with contributions from others. 2017. gbm: Generalized Boosted Regression models. R package version 2.1.3. https://CRAN.R-project.org/package=gbm.

Rienecker, M. M., M. J. Suarez, R. Gelaro, R. Todling, J. Bacmeister, E. Liu, M. G. Bosilovich, S. D. Schubert, L. Takacs, G. K. Kim, S. Bloom, J. Y. Chen, D. Collins, A. Conaty, A. Da Silva, W. Gu, J. Joiner, R. D. Koster, R. Lucchesi, A. Molod, T. Owens, S. Pawson, P. Pegion, C. R. Redder, R. Reichle, F. R. Robertson, A. G. Ruddick, M. Sienkiewicz, and J. Woollen. 2011. MERRA: NASA's Modern-Era Retrospective Analysis for Research and Applications. Journal of Climate **24**:3624-3648.

Riley, S. J., S. D. DeGloria, and R. Elliot. 1999. A terrain ruggedness index that quantifies topographic heterogeneity. Intermountain Journal of Sciences **5**:23-27.

Robert, C. P. and G. Casella. 2004. Monte Carlo statistical methods. Springer Science+Business Media Inc., New York.

Rogers, B. M., J. T. Randerson, and G. B. Bonan. 2013. High-latitude cooling associated with landscape changes from North American boreal forest fires. Biogeosciences **10**:699-718.

Rupp, T. S., A. M. Starfield, and F. S. Chapin. 2000. A frame-based spatially explicit model of subarctic vegetation response to climatic change: comparison with a point model. Landscape Ecology **15**:383-400.

Schoenberg, F. P., R. Peng, and J. Woods. 2003. On the distribution of wildfire sizes. Environmetrics **14**:583-592.

Scholz, F. and A. Zhu. 2017. kSamples: K-Sample Rank Tests and their Combinations. R package version 1.2-7. https://CRAN.R-project.org/package=kSamples.

Tarnocai, C., J. G. Canadell, E. A. G. Schuur, P. Kuhry, G. Mazhitova, and S. Zimov. 2009. Soil organic carbon pools in the northern circumpolar permafrost region. Global Biogeochemical Cycles **23**.

Tepley, A. J., E. Thomann, T. T. Veblen, G. L. W. Perry, A. Holz, J. Paritsis, T. Kitzberger, and K. Anderson-Teixeira. 2018. Influences of fire–vegetation feedbacks and post-fire recovery rates on forest landscape vulnerability to altered fire regimes. Journal of Ecology **00**:1-16.

Turetsky, M. R., E. S. Kane, J. W. Harden, R. D. Ottmar, K. L. Manies, E. Hoy, and E. S. Kasischke. 2011. Recent acceleration of biomass burning and carbon losses in Alaskan forests and peatlands. Nature Geoscience **4**:27-31.

USGS. 1997. Alaska 300m digital elevation model. U.S. Geological Survey EROS Alaska Field Office, Anchorage, AK.

Van Wagner, C. E. 1987. Development and structure of the Canadian Forest Fire Weather Index System. Technical Report 35. Canadian Forest Service, Ottawa, Ontario, Canada.

Williams, A. P. and J. Abatzoglou. 2016. Recent advances and remaining uncertainties in resolving past and future climate effects on global fire activity. Current Climate Change Reports **2**:1-14.

Young, A. M., P. E. Higuera, P. A. Duffy, and F. S. Hu. 2017. Climatic thresholds shape northern high-latitude fire regimes and imply vulnerability to future change. Ecography **40**:606-617.

Table 2.1. Summaries comparing expected and observed total area burned in North American boreal forests (1981-2016). Expected area burned is calculated under the null hypothesis (H_0) that burning is independent of past fire activity. Values in square brackets represent the percent increase in total area burned. The FRP is the fire rotation period, the amount of time it takes to burn an area equal in size to the study area (Johnson and Gutsell 1994), here the North American boreal forest (total area $\approx 4.24\times10^6$ km^2) over the period 1981-2016 (36 yr).

	Total Area Burned (km^2 $\times10^5$)			Fire Rotation Period (yr)		
Lower threshold (percentile)	**Observed**	**Mean expected under H_0 (90% CI)**	**Exp. – Obs. (90% CI)**	**Observed**	**Mean expected under H_0 (90% CI)**	**Exp. – Obs. (90% CI)**
29 km^2 (90th)	6.36	6.69 [5.2%] (6.61, 6.76)	0.33 (0.25, 0.40)	240	228 (226, 231)	-12 (-14, -9)
16 km^2 (95th)	6.70	7.06 [5.4%] (6.97, 7.16)	0.36 (0.27, 0.46)	228	216 (213, 219)	-12 (-15, -9)
5 km^2 (99th)	6.99	7.26 [3.9%] (7.15, 7.38)	0.27 (0.16, 0.39)	219	210 (207, 214)	-30 (-33, -26)

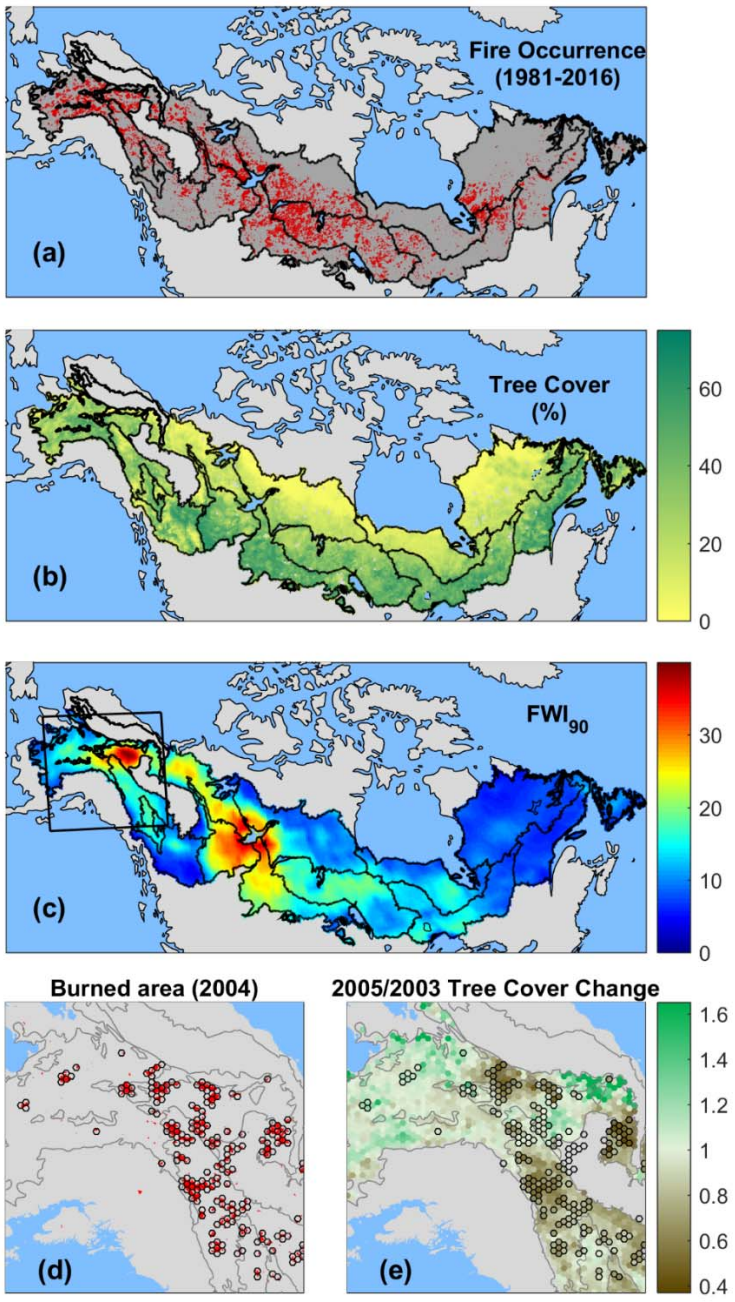

Figure 2.1. Study area, including the spatial distribution of key explanatory and response variables, and an example of post-fire tree-cover change. From top panel to bottom: the spatial distribution of historical fire perimeters from 1981-2016; percent tree cover for 2004; the 90th percentile of the FWI estimate (FWI_{90}) for the year 2004 (a large fire year in western North America). The bottom two panels display an example of tree-cover change following the fires in 2004, displayed as the ratio of tree cover in 2005, relative to tree cover in 2003. The 500 km^2 hexels in the bottom two panels highlight localities that experienced >50 km^2 in area burned in 2004. In all panels, polygon delineations represent Level-III Ecoregion classifications (Olson et al. 2001).

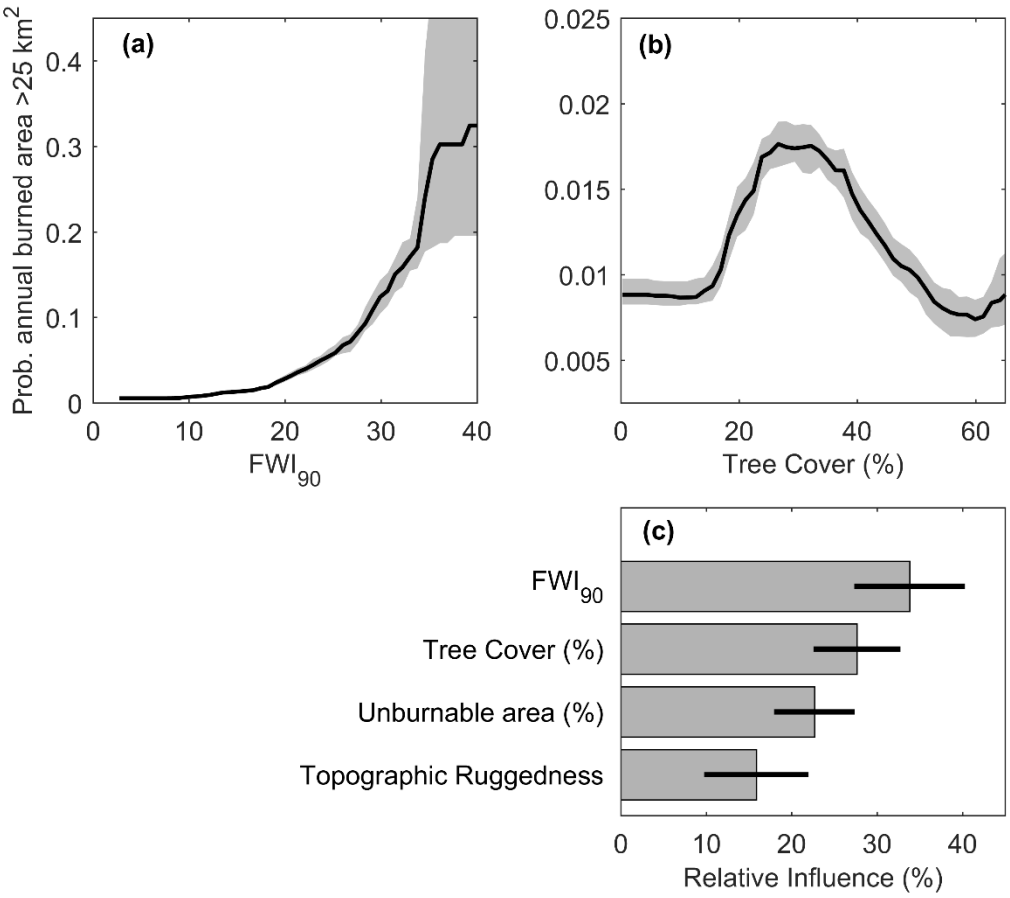

Figure 2.2. Partial dependence and relative influence plots depicting the controls of extensive burning (i.e., >25 km^2 per hexel) in North American boreal forests. (a-b) Partial dependence plots displaying the marginal relationship between fire weather (a) and tree cover (b). The solid black line represents the median, while shaded regions represents the 25^{th}-75^{th} percentiles for 50 individual boosted regression tree models (BRTs). (c) Relative influence of the explanatory variables. Bar widths represent the average relative influence for 50 BRTs (±2 SD).

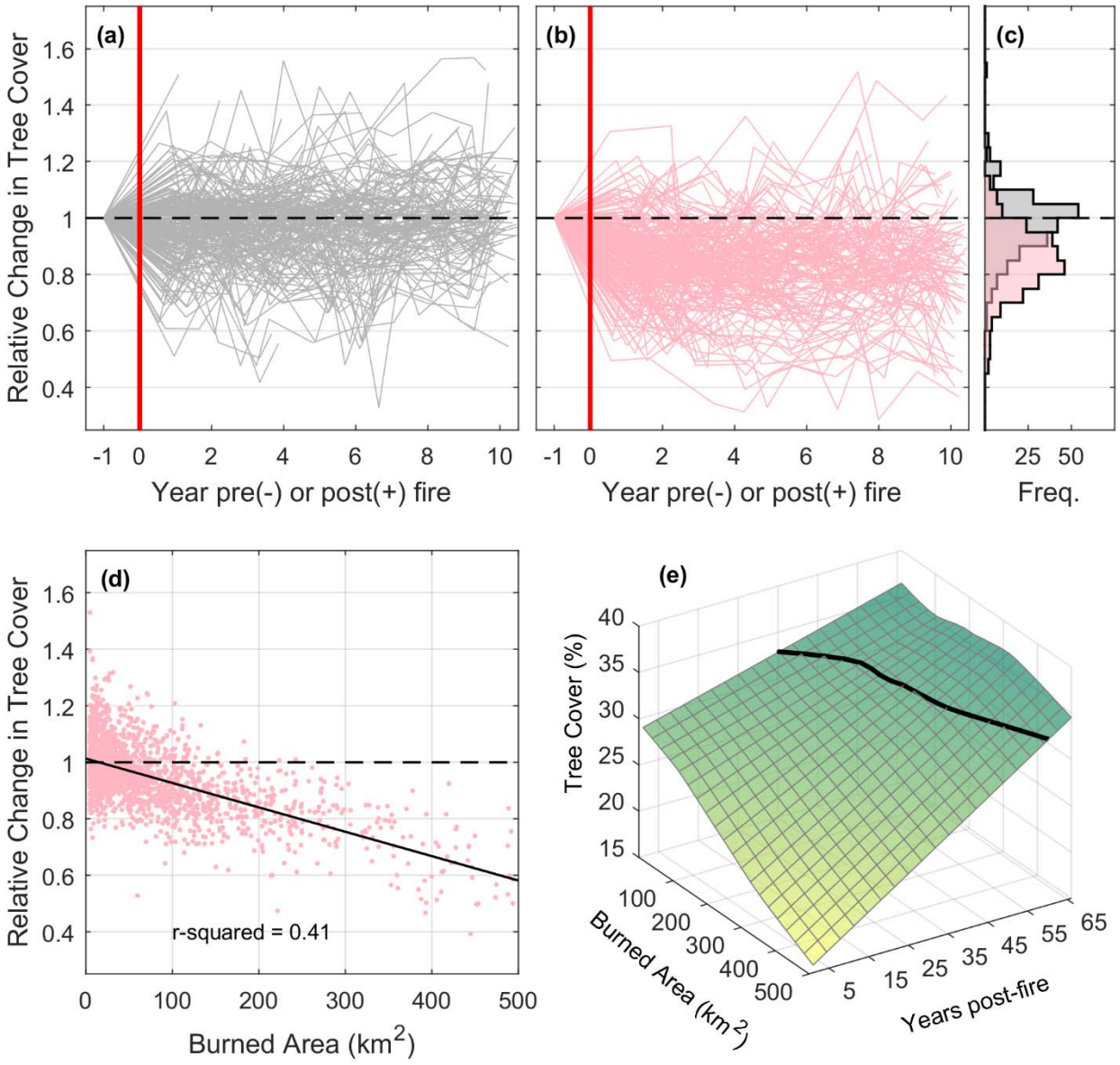

Figure 2.3. Short-term changes (a-d) and long-term trends (e) in tree cover after fire in North American boreal forests. (a-b) Time series of tree-cover change for hexels that experienced ≥ 0 km^2 and < 100 km^2 in burned area (a), and ≥ 100 km^2 (b). A value of 1 (horizontal dashed line) indicates no change in tree cover, and the vertical red line represents year of burning. (c) A summary of the distribution of tree-cover change from years 1-10 following fire, for hexels that burned (pink) or did not burn (gray). (d) The relationship between burned area per hexel and tree-cover change in the 10 yr following fire. The solid line is the least squares fit. (e) Tree cover, calculated using a chronosequence approach from 1950-2016, as a function of time-since-fire and burned area per hexel. The surface plot was calculated using a bivariate locally weighted regression (span = 0.7). The solid black line is an estimate of where the surface plot intersects with our estimate of tree cover for areas that have not experienced any fire for a length of 51-66 yr.

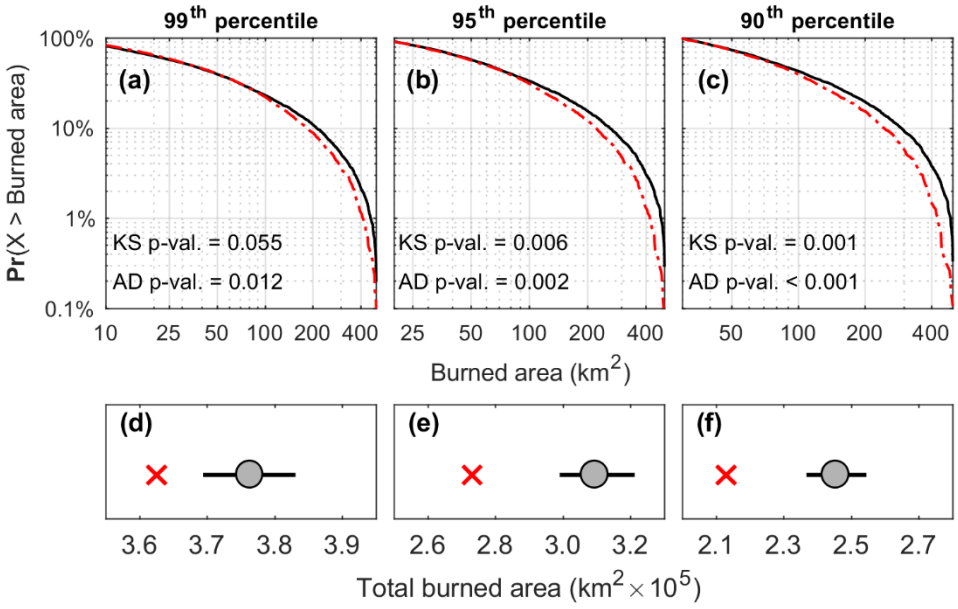

Figure 2.4. A comparison of the burned-area distributions between single- and multi-burned hexels from 1981-2016. (a-c) Empirical survival functions for burned area per hexel for single-burned (solid black line) and multi-burned hexels (dashed red line), with each panel depicting empirical functions for different lower threshold values (i.e., 99th, 95th, and 90th percentiles). "KS" and "AD" refer to two-sample non-parametric hypothesis tests using the Kolmogorov-Smirnov and Anderson Darling tests, respectively, testing the null hypothesis that the two empirical distributions are from the same population. (d-f) Observed total area burned for multi-burned hexels (red "x"), compare to the expected total area burned under H_0. Gray points represent the mean expected total area burned from this resampling, while the black lines represent the empirical 95% empirical confidence interval.

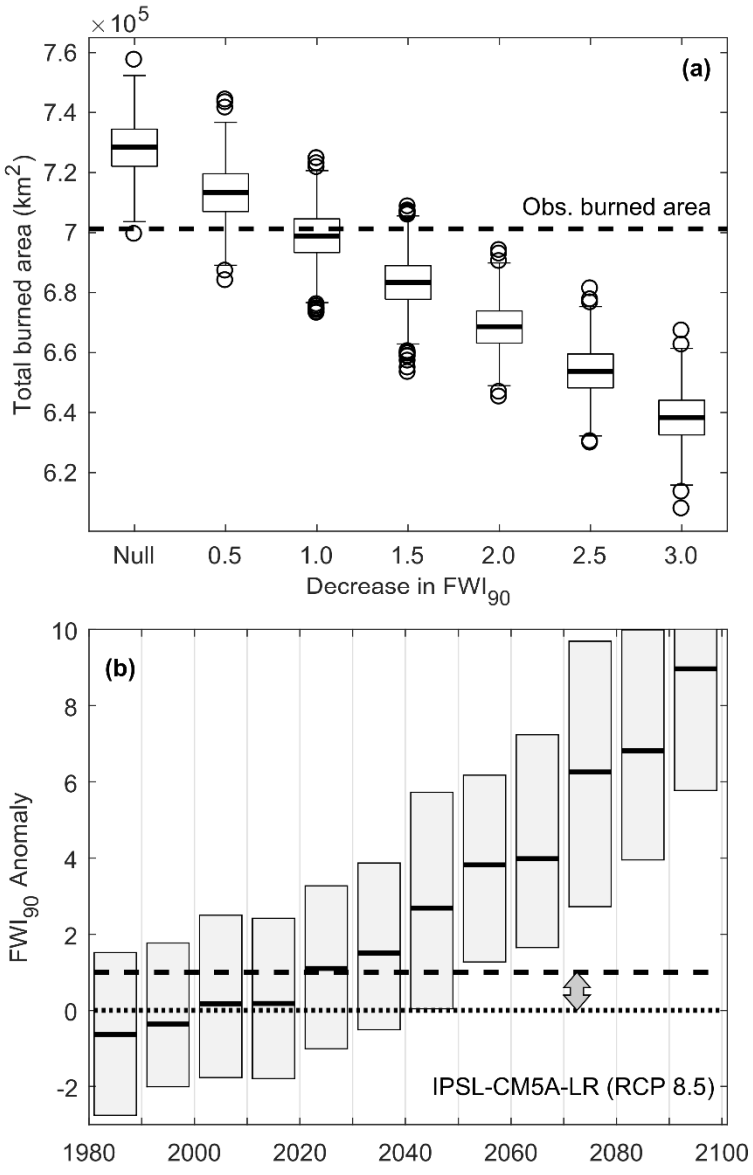

Figure 2.5. (a) Sensitivity analysis evaluating changes of total burned area in response to pre-specified decreases in the fire weather (i.e., FWI_{90}). Each boxplot represents the distribution of 1000 predictions of total area burned across the entire study area for a given "global" decrease in FWI_{90}, with predictions based on the truncated-tapered Pareto distribution. The horizontal dashed line represents total observed area burned in the study area from 1981-2016. (b) Projected change in FWI_{90} from the IPSL-CM5A-LR GCM (RCP 8.5) across the entire study area, for each decade of the 21st century. The horizontal black lines and shaded grey boxes represent the median and 25th-75th percentiles, respectively, of annual anomalies. The difference between the dotted line at y = 0 and the dashed line at y = 1 (highlighted by the grey arrow) represents the magnitude of the potential mediating influence of vegetation on fire activity, estimated from the sensitivity analysis in panel (a).

Chapter 3: Consequences of climatic thresholds to burning for projecting fire activity and ecological change

In revision for publication in *Global Ecology and Biogeography* as:

Young, A.M., P.E. Higuera, J. Abatzoglou, P. A. Duffy, and F. S. Hu. In Revision. Consequences of climatic thresholds to burning for projecting fire activity and ecological change. Global Ecology and Biogeography.

Abstract

Aim: Ecological properties governed by threshold relationships can exhibit heightened sensitivity to small changes in climate, creating an inherent source of uncertainty when anticipating future change. We investigated the impact of threshold relationships on our ability to project ecological change outside the observational record, using the challenge of projecting fire-regime responses to climate change in Alaskan boreal forest and tundra ecosystems during the late Holocene.

Location: Alaskan boreal forest and tundra ecosystems.

Time period: 850-2100 CE.

Methods: We informed a set of published statistical models, designed to predict the 30-yr probability of fire occurrence based on climatological normals, with downscaled Global Climate Model data for 850-1850 CE. To evaluate model performance outside the observational record, we compared projections to mean fire return intervals estimated from 29 published paleofire reconstructions from lake-sediment records.

Results: Model-paleodata comparisons highlight spatially varying projection accuracy across boreal forest and tundra regions, with variability strongly related to climatic proximity to the

summer temperature threshold to burning: sites closer to this threshold exhibited larger prediction errors than sites further away from this threshold. Modifying the modern (i.e., 1950-2009) fire-climate relationship also resulted in significant changes in projection accuracy. Under 21st-century climate projections, increasing proportions of Alaskan tundra and boreal forest will approach and surpass the temperature threshold to burning, with > 50% lying within 2 °C of the threshold by 2010-2039, and > 50% exceeding this threshold by more than 2 °C by 2070-2099.

Main conclusions: Our results highlight a high sensitivity of statistical projections to changing threshold relationships and/or data uncertainty, implying projections of future ecosystem change in threshold-governed ecosystems will be accompanied by notable uncertainty. This work further suggests that ecological responses to climate change will exhibit significant spatiotemporal variability, as different regions approach and surpass climatic thresholds over the 21st century.

Introduction

Understanding the impacts of 21st-century climatic and environmental change is a key challenge for ecologists, with implications for biogeochemical cycling, natural resources management, and human livelihoods (Walther et al. 2002, Grimm et al. 2013). This challenge is particularly acute for ecosystem properties governed by non-linear or threshold relationships. Under threshold relationships, ecosystem properties are relatively insensitive to changing drivers until a threshold is crossed; beyond the threshold, properties shift suddenly, and in some cases irreversibly (Scheffer et al. 2001). Clear examples are found throughout hydrological systems, which undergoes large changes in structure and function as

temperatures cross 0 °C (Vaughan et al. 2013). Threshold relationships characterize ecological responses in ecosystems worldwide (Hunsicker et al. 2016), and they are critical for understanding foundational concepts in ecology, including resilience and alternative stable states (Gunderson 2000, Suding and Hobbs 2009). Understanding how ecosystem properties behave in threshold-governed systems is thus fundamental to ecology, with direct implications for anticipating future ecosystem change.

Climatically driven fire activity is a globally relevant example of an ecological relationship characterized by nonlinearities and thresholds relationships. Across multiple temporal and spatial scales, fire activity can be explained by nonlinear relationships with temperature and moisture variables, ultimately reflecting fuel moisture and landscape flammability (Moritz et al. 2012, Pausas and Paula 2012, Bedia et al. 2015, Young et al. 2017). The nature of these fire-climate relationships dictates, in part, how climate change will impact future fire regimes. For example, consider a system where the relationship between fire and climate is characterized by a distinct threshold, where a small change in climate can result in a fire-regime shift (e.g., Figure 3.1a); in contrast, in a system with a more linear fire-climate relationship, changes are more gradual and fire regimes exhibit a more constant rate of change for a similar change in climate (Figure 3.1b, c). In the context of anticipating future ecosystem change, predictions in threshold-governed systems will inherently be more sensitive to variability or uncertainty in ecosystem drivers. Specifically, even slight deviations or uncertainties in an ecosystem driver around a threshold will result in a wide range of predictions of the ecosystem response (Peters et al. 2004a).

The inherent difficulty in predicting future conditions in threshold-governed systems is particularly relevant when using statistical models, for example to anticipate species range shifts (i.e., species distribution models; Elith and Leathwick 2009), fire activity (Moritz et al. 2012, Young et al. 2017), and biotic disturbance agents (e.g., Buotte et al. 2016). Projections from statistical models are also subject to significant uncertainty when applied geographically outside of their calibration domain (Veloz et al. 2012), in the past or future (Diniz-Filho et al. 2009, Moreno-Amat et al. 2015). This uncertainty may partly reflect the influence of threshold relationships, as threshold responses can interact with and amplify other methodological sources of uncertainty when projecting beyond the observational record, such as model specification (e.g., non-stationary ecological relationships) and/or uncertainty in the data used to inform the model (Barry and Elith 2006).

Here we highlight the implications that threshold relationships may have for anticipating future ecosystem change, and how heightened variability near thresholds can lead to significant inaccuracy and/or uncertainty in future projections. To develop and illustrate this understanding, we use the challenge of projecting climatically driven changes in fire activity in boreal forest and tundra ecosystems of Alaska, which span broad gradients in climate and fire activity, with well-developed fire-history records spanning both historical and pre-historical periods. We specifically address the following three questions: (1) how do threshold relationships impact predictions of fire activity outside the observational record; (2) how sensitive are predictions to varying fire-climate relationships (e.g., Figure 3.1); and (3) what are the implications for anticipating future ecological change in threshold-governed systems? We test the ability of existing statistical models, calibrated to 1950-2009 CE

(Common Era) and designed to model fire presence/absence, to predict fire activity from 850-1850 CE in Alaskan boreal forest and tundra ecosystems through model-paleodata comparisons. We use paleoecologial records because they are a key independent source of information for evaluating projections outside the observational record (Martínez-Meyer et al. 2004, Pearman et al. 2008). Furthermore, by evaluating the ability to project fire activity in the past, we provide an explicit example of the challenges and implications that accompany projecting ecosystem properties in threshold-governed ecosystems under future climate change.

Methods and materials

Our study area includes the boreal forest and tundra biomes of mainland Alaska (Figure 3.2). Boreal forests generally experience moderate- to high-severity fires, with fire rotation periods generally ranging from 120-360 yr (Kasischke et al. 2002). In the Noatak River Watershed (Figure 3.2), the most flammable tundra region in Alaska, mean fire return intervals are comparable to those in interior boreal forest (Higuera et al. 2011). In cooler tundra ecoregions, such as the Brooks Foothills and Yukon-Kuskokwim Delta, mean fire return intervals exceed 3500 yr (Hu et al. 2010, Chipman et al. 2015). A detailed description of the vegetation communities in these Alaskan ecosystems is described in Young et al. (2017).

Statistical models of fire presence/absence

To understand the impacts of predicting fire activity outside the observational record, we used a published set of statistical models from Alaska (Young et al. 2017), testing their

predictive ability during the past millennium (850-1850 CE). These models are designed to predict the spatially explicit probability of fire occurrence at 2-km resolution in Alaskan boreal forest and tundra ecosystems, comparable to species distribution models (Elith and Leathwick 2009). Models were constructed by relating the spatial distribution of fire presence/absence to 30-yr climatological normals of average temperature of the warmest month (hereafter "summer temperature," [°C]) and total annual moisture availability (i.e., precipitation minus potential evapotranspiration, P-PET [mm]), as well as topographic ruggedness and vegetation type. The relationships among fire, climate, topography, and vegetation were quantified using Boosted Regression Tree models (BRTs), a machine learning tool (De'ath 2007). Young et al., (2017) provide a set of 100 individual BRTs, with each BRT unique due to internal model-building stochasticity and a random selection of observations from the study area. As part of this model-building process in Young et al. (2017), three separate sets of 100 BRTs were constructed for different spatial domains in Alaska: (1) all of mainland Alaska (i.e., both boreal forest and tundra), (2) only boreal forest, and (3) only tundra. In this study, we used the models constructed using data from all of mainland Alaska. Finally, a key finding from Young et al. (2017) was the importance of summer temperature as an explanatory variable for fire occurrence, and a distinct threshold response between summer temperature and the 30-yr probability of fire occurrence. The estimated mean (bootstrapped 95% CI) threshold value for summer temperature was 13.40 °C (13.29, 13.45) (Figure 3.2c), calculated using a segmented regression analysis (Muggeo 2003).

We used the published models from Young et al. (2017) for this study, with one notable modification. Here, we use mean total annual precipitation instead of annual moisture availability (i.e., P-PET, as used in Young et al., [2017]). Temperature-based estimates of PET can be sensitive to temperature biases, specifically due to the nonlinear nature of the calculations (McAfee 2013). Thus, we chose to use moisture variables provided directly from the GCMs (i.e., precipitation, see *Past-millennium climate data*), rather than risk exacerbating potential biases through subsequent PET calculations. Results from these updated BRT models were similar to those from Young et al. (2017), as quantified by AUC values (a measure of goodness-of-fit for presence/absence models): AUC averaged 0.78 (SD = 0.02) when using summer temperature and precipitation vs. 0.78 (SD = 0.02) when using summer temperature and P-PET (Young et al. 2017).

Past-millennium climate data

To predict fire activity over the past millennium, we informed the statistical models with bias-corrected and spatially downscaled paleo-climate data spanning 850-1850 CE, a time period outside the 1950-2009 CE observational record. Specifically, we used GCM simulations from the Paleoclimate Intercomparison Project Phase 3 (PMIP3, Braconnot et al. 2012), a component of the Coupled Model Intercomparison Project (CMIP5, Taylor et al. 2012). Given the spatially explicit nature of our statistical models, we used GCMs instead of paleoclimate reconstructions because most paleoclimate reconstructions in Alaska do not spatially coincide with the paleoecological fire-history records used in our model-paleodata comparisons. We selected GCMs available from the PMIP3 experiments that provided monthly output from 850-1850 CE for surface air temperature and precipitation. Of the five

GCMs from the Earth System Grid Federation repository (https://www.earthsystemcog.org/projects/cog/) that met these requirements (as of March 1, 2017), we evaluated their performance over the observational record using a ranking analysis (Appendix C.1). We used the top three GCMs from this analysis (i.e., GISS-E2-R, MPI-ESM-P, and MRI-CGCM3), individually, to drive our statistical models and calculate prediction error. To account for differences in the spatial resolution between our statistical models (2 km) and GCMs (i.e., > 1.0° latitude × longitude), we conducted a bias correction and downscaling analysis using the delta-change method (Giorgi and Mearns 1991). Full details on this downscaling analysis are described in Appendix C.2. To drive our statistical models with these downscaled climate data, we calculated 30-yr climatological averages, at one-year time steps, from 850-1850 CE (e.g., 850-879, 851-880).

Model-paleofire comparisons

We used existing paleofire records as an independent data source to evaluate our statistical models when applied outside the observational record. Specifically, we compared model projections to published fire-history reconstructions from 29 lake-sediment charcoal records that span seven ecoregions in Alaska (Figure 3.2). Here, ecoregion perimeters were defined using the Level-III classifications from Nowacki et al. (2001). In each record, local fire events were estimated using a statistical technique that identifies significant peaks in charcoal accumulation rates (CHAR) relative to background CHAR (Higuera et al. 2009), with "local" defined as a radius of approximately 500-1000 meters around each lake. Thus, the approximate spatial scale represented by each lake-sediment record (0.8-3.1 km^2) is reasonably well matched to the 2-km pixel resolution (i.e., 4 km^2) used in the statistical

models. Details and metadata for each of these records is presented in Appendix C.3. Using these charcoal peaks, fire frequency metrics and mean fire return intervals were calculated for each lake location over a given time period. Since the statistical models used here are based on fire presence/absence at multidecadal timescales, instead of fire frequency, predictions approximate, rather than equate to, the 30-yr probability of fire occurrence for a specific 4 km^2 pixel on the landscape, and thus approximate the annual probability of fire occurrence for a given pixel. Through the cumulative summation of the predicted annual probability of fire occurrence, we can calculate fire frequency (Johnson and Gutsell 1994). In this analysis, we specifically used the inverse of fire frequency (*FF*) to compare predictions and observations, $FF^{-1} = t/N_{FIRES}$. Here, t is the number of years during the time period of prediction or reconstruction (in this analysis 1000 yr [850-1850 CE]), and N_{FIRES} is equal to the number of fire events predicted or reconstructed during this 1000-yr period. We used the inverse *FF* to compare predictions and observations, as under large-samples the inverse *FF* can approximate the mean fire return interval (*MFI* [yr]), a more commonly used metric to interpret fire frequency across different landscapes (i.e., $FF^{-1} = t/N_{FIRES} \approx MFI$).

We measured prediction error to evaluate differences between model projections and reconstructed *MFI* and to understand the relative accuracy of our model predictions. Specifically, we used a standardized prediction-error metric (Eqn. 3.1)

$$E_{i,j,k} = \frac{P_{i,j,k} - O_{i,j}}{\overline{O}_{\bullet,j}} \times 100\% \qquad (3.1)$$

Here, $E_{i,j,k}$ is the standardized error metric for the k^{th} BRT (k = 1, 2, …, 100), j^{th} ecoregion (j = 1, 2, …, 7), and i^{th} lake-sediment record (i = 1, 2, …, n_j), where n_j is the number of lakes in

the j^{th} ecoregion. P is the model prediction, O is the observed *MFI* for the time period of 850-1850 CE, and $\overline{O}$ in the denominator (Eqn. 3.1) is the average *MFI* from all lakes within each ecoregion (i.e., $n_j^{-1}\sum_{i=1}^{n_j} MFI_i$). Standardizing this error metric by the average *MFI* accounts for differing levels of fire frequency among ecoregions. Additionally, by standardizing our prediction error metric we also reduce the potential influence that a false positive or false negative in the charcoal record could significantly alter our results. A tradeoff with this standardization is the possibility for ecoregions to have no fires from 850-1850 CE, resulting in a denominator value equal to zero and an undefined *MFI* (i.e., 1000 yr / 0 fires). To account for this outcome, if a lake had no fires within the past millennium, we calculated $\overline{O}$ based on an extended time period that captured the most recent fire event in the paleo-fire record. Among all lakes, only four required an extended time period, which averaged 3271 BCE (i.e., Before Common Era; Appendix C.3). Finally, the discrete nature (i.e., fire presence/absence) and relatively short record (i.e., 1000 yr) made it impractical to evaluate our model projections throughout the course of the past millennium, and thus we chose to evaluate prediction error using a single metric summarized for this 1000-yr period.

Sensitivity analysis

To evaluate the sensitivity of model projections to changing fire-climate relationships and/or uncertainty in the data, we modified observational fire-climate relationships in Alaska, comparing predictions between modified and unmodified relationships. Modified fire-climate relationships altered the marginal relationship between summer temperature and the probability of fire occurrence, based on results from Young et al. (2017), which indicate that

summer temperature is the most important explanatory variable. We modified two specific aspects of observational relationships, to reflect two different ways in which fire-climate relationships could vary: (1) the shape of the relationship, and (2) the location of the summer-temperature threshold. We modified the shape of the relationship between summer temperature and the probability of fire by altering the training dataset; the result is three modified shapes (Shape 1 – Shape 3), each increasingly more linear compared to the original (Appendix C.4). We modified the location of the summer temperature threshold by adding 0.5 °C, 1.0 °C, and 1.5 °C to the downscaled GCM-based temperature estimates. Here, we only increased temperature values for our sensitivity analysis, rather than also explore decreases, because initial results suggested that GCMs were underestimating past-millennium temperatures.

Impacts of threshold responses for 21st-century projections

Initial results from using our statistical models to project fire activity over the past millennium revealed increased prediction error in regions near the summer temperature threshold, implying spatially varying uncertainty in future projections. To understand the spatial distribution of Alaskan landscapes that are relatively close to the summer temperature threshold, and thus where projections may be most sensitive to threshold-driven uncertainty, we conducted an additional analysis. Specifically, we classified each pixel in Alaska by its proximity to the temperature threshold (i.e., 13.4 °C) identified in Young et al. (2017), as either below (≤ 11.4 °C), near (>11.4 °C and ≤ 15.4 °C), or above (>15.4 °C) the threshold. This classification was done for four separate 30-yr time periods (1971-2000, 2010-2039, 2040-2069, and 2070-2099), utilizing the three GCMs selected from our ranking analysis. We

used GCM projections under the Representative Concentration Pathway (RCP) 8.5 emissions scenarios.

Results

For the past millennium (850-1850 CE), two of the top-three-ranked GCMs in Alaska (GISS-E2-R and MRI-CGCM3) generally simulate cooler summer temperatures relative to a historical baseline period of 1971-2000, with some spatial variability among Alaskan ecoregions and GCMs (Figure C.8). For example, both the GISS-E2-R and MRI-CGCM3 GCMs project temperatures on average 0.87 °C (SD = 0.32 °C) and 0.64 °C (SD = 0.26 °C) cooler over the 1000-yr period, respectively, among all 29 lake locations and across all 1000 yr (850-1850 CE). Temporal variability in these anomalies ranged from 0.75-1.61 °C across GCMs and ecoregions (Figure C.8). The warmest projections were from the MPI-ESM-P GCM, which on average projected summer temperatures 0.08 °C (SD = 0.30 °C) higher relative to the 1971-2000 normal. Past projections of total annual precipitation were similar or slightly drier relative to the 1971-2000 baseline period. Specifically, total annual precipitation was 99% (SD = 0.03%), 90% (SD = 0.2%), and 99% (SD = 0.02%) relative to 1971-2000 period, for GISS-E2-R, MPI-ESM-P, and MRI-CGCM3, respectively. Time series depicting these GCM-based climate anomalies are available in Appendix C.5.

Prediction errors in *MFI* over the past millennium differed significantly among ecoregions, highlighting the varying accuracy of the statistical models when applied outside of the observational record. Errors were highest in regions closer (in climate space) to the summer temperature threshold of 13.4 °C and relatively low in regions further away from this temperature threshold (Table 3.1 and Figure 3.3). For example, in the Yukon Flats, which is

on average 4.6 °C (SD = 0.4 °C) above the summer temperature threshold, the median prediction error among all lakes, GCMs, and BRTs (i.e., 14 lakes × 3 GCMs × 100 BRTs) was -28%, with an interquartile range of 33% (IQR; i.e., third minus first quartile). Therefore, in the Yukon Flats our models slightly over predicted the rate of burning relative to paleo-fire records. In contrast, regions sitting closer to the identified threshold, such as the Copper River Basin (0.7 °C above the threshold [SD = 1.2 °C]) and the Noatak River Watershed (1.4 °C above threshold [SD = 0.3 °C]), had median prediction errors of 453% (IQR = 203%) and 148% (IQR = 413%), respectively (Table 3.1 and Figure 3.3). The exception to this pattern occurred in tundra regions that experienced little fire activity over the past millennium. For example, the prediction error in the Yukon-Kuskokwim Delta, which today sits relatively close to the 13.4 °C threshold (0.13 °C above), had a median prediction error of -75% on average (IQR = 9%; Figure 3.3).

Modifying the temperature threshold to burning significantly altered prediction errors in ecoregions closer to the observed threshold, while causing relatively no change in other ecoregions (Table 3.1 and Figure 3.4). For example, in the Noatak River Watershed and the Kobuk Valley, decreasing threshold values by only 0.5 °C relative to the original relationship decreased the median prediction error by approximately 99% and 95%, respectively. Conversely, in the Yukon Flats and less-flammable tundra regions (e.g., Brooks Foothills), increasing the temperature threshold, even as much as 1.5 °C, did not significantly alter the prediction errors (Table 3.1 and Figure 3.4).

Prediction errors in most ecoregions were also sensitive to changes in the shape of the observed fire-climate relationships (Figure 3.4). When using any of the three modified

relationships, the distribution of prediction errors changed considerably in ecoregions near the summer temperature threshold. Specifically, when fire-climate relationships are only moderately modified (i.e., Shape 1 and Shape 2; Appendix C.4), median prediction errors only showed significant decreases in the Copper River Basin (158% under Shape 1 and 236% under Shape 2). However, dispersion in prediction errors (measured with the IQR) narrowed considerably in Noatak River Watershed, Kobuk Valley, and Copper River Basin, thus indicating a change in the distribution of prediction errors. Specifically, there was greater change in IQR under Shapes 1 and 2 in these ecoregions closer to the summer temperature threshold (Table 3.1 and Figure 3.4). Conversely, in the Yukon Flats, the ecoregion furthest away from the observed threshold, the median (IQR) prediction error was stable when using either the original relationship (median = -28%, IQR = 38%), or the three modified relationships (i.e., Shapes 1-3): -27% (34%), -29% (31%), and -28% (33%) (Table 3.1 and Figure 3.4).

Historical estimates and future projections obtained from global climate models (GCMs) highlight how the total area and spatial distribution of pixels close to the observed temperature threshold to burning are projected to shift during the 21st century, indicating spatially varying levels of projection uncertainty. During the historical (i.e., 1971-2000) and early 21st century (i.e., 2010-2039), the majority of Alaskan land area is estimated to lie within 2 °C of the temperature threshold (i.e., 13.4 °C +/- 2 °C), while under projections for the late 21st-century (i.e., 2070-2099), the majority of land area is projected to lie more than 2 °C above this threshold (i.e., > 15.4°C) (Figure 3.5). For example, during the historical period (i.e., 1971-2000), the percentage (SD) of land area near the threshold was 65% (11%), 60%

(11%), and 66% (11%) for the GISS-E2-R, MPI-ESM, and MRI-CGCM3 GCMs, respectively. Towards the end of the 21st century (i.e., 2070-2099), the percentage (SD) of Alaskan land area projected to lie near this threshold decreases to 38% (12%), 13% (5%), and 37% (9%) for the same three GCMs.

Discussion

Our work highlights key uncertainties that accompany projections of ecosystem properties governed by threshold relationships. Focusing on fire regimes in arctic and boreal ecosystems, we used an existing set of statistical models to project fire activity outside of the observational record (i.e., 850-1850 CE) and quantified accuracy by comparing projections to estimated fire histories from paleofire records. Our results reveal spatially varying prediction error across Alaskan ecoregions, and a high sensitivity in prediction error to changes in the nature of observed fire-climate relationships. Overall, our findings highlight the importance of considering the presence of thresholds when projecting ecosystem properties, with important implications for understanding 21st-century ecosystem change.

Threshold impacts on ecological projections

Threshold relationships between climate and fire activity introduce significant uncertainty when projecting fire regimes beyond the observational record. Our findings highlight higher prediction errors in regions with summer temperatures close to the observed threshold to burning (e.g., Copper River Basin, Noatak River Watershed, and Kobuk Valley; Figure 3.3), a pattern related to heightened variability in ecological properties over a relatively narrow range of climate conditions (Figure 3.1). Increased ecosystem variability near

thresholds inherently decreases predictability, as slight changes in an ecosystem driver result in sudden changes in ecosystem states (Peters et al. 2004a; Figure 3.1), thereby increasing uncertainty for projections outside the observational record.

In this study, we evaluated the ability of a statistical model to predict fire regimes outside of the observational period. The resulting high prediction errors we observed could arise from several sources. First, poorly characterized fire-climate relationship or changing fire-climate relationships in the past (i.e., non-stationary dynamics) could both contribute to prediction errors. This possibility seems unlikely, however, given the strong cross-validation statistics in the original model, which indicate the ability to capture a wide range of fire-regime variability across Alaska (Young et al., 2017). Second, the paleofire records are also subject to uncertainty in their estimates of past fire activity (Higuera et al. 2010), with false positives or false negatives potentially contributing to prediction errors. However, given the standardization of our error metric (Eqn. 3.1), which minimizes the influence of individual records, and the high number of paleofire records used in this study (n = 29), it is unlikely that errors in the paleofire records account for the magnitude of observed prediction errors. Finally, we suggest that the most likely source of the high predictions errors is GCM-based temperatures that are lower than what likely occurred, as suggested by a number (n = 7) of independent paleoclimate records (Appendix C.6; Wilson et al. 2016). It is possible, although we deem unlikely, that lower mean temperatures were accompanied by higher interannual variability, such that the frequency of fire-conducive years could remain high, while the mean 30-yr temperatures were lower than the historical period. Past projections under such cool average temperatures would, as simulated by the GCMs, shift projections in many regions

below the 13.4 °C threshold to burning, causing significant underestimation of fire activity, relative to the paleofire records. For example, in the Kobuk Valley, large difference between the estimated mean fire return interval during the observational record (≈ 170 yr; Kasischke et al. 2010) and our projections during 850-1850 CE under the GISS-E2-R GCM (> 1300 yr) suggest a distinct fire-regime shift occurred between the two time periods. While fire regimes have certainly varied in the past, this order-of-magnitude difference is inconsistent with the independent paleo-fire records spanning this period. Overall, if the high prediction errors are due to cooler-than-actual GCM-based temperatures, then our model-paleodata comparisons demonstrate how relatively small differences in mean climate can lead to incorrect inferences about ecological regime shifts in threshold-governed systems.

This sensitivity of statistical predictions to small variations in input data, such as cooler GCM estimates, is further highlighted by our sensitivity analysis. Modified threshold values lead to significant variability in prediction error (Table 3.1 and Figure 3.4), particularly in regions near the summer temperature threshold. This implies that variables characterized by threshold relationships will be particularly sensitive to uncertainty in future projections when using different GCMs and/or emissions scenarios. Similar uncertainties are found when projecting species' range shifts, which is at least partly attributable to variability among GCMs and emissions scenarios (Diniz-Filho et al. 2009, Wenger et al. 2013, Watling et al. 2015). Given that species distributions are also governed by complex, nonlinear relationships (Thomas and Bovee 1993, Elith and Leathwick 2009), varying patterns of uncertainty in species range shifts may also be due in part to the presence of threshold relationships, although to our knowledge this has yet to be tested.

Heightened sensitivity of ecological projections in threshold-governed systems may also occur when ecological relationships change over time. In our sensitivity analysis, modifying observational relationships caused notable shifts in prediction error, particularly in regions closer to the observed summer temperature threshold to burning (Figure 3.4). There are several reasons why ecological relationships may differ in the past or future, relative to those specified during the observational record. First, differing relationships could reflect uncertainty in the data, such as missing observations (Barry and Elith 2006). In the context of our study, small fires are likely missing from the Alaska Large Fire Database (Kasischke et al. 2002) used to develop the statistical models (Young et al., 2017). If such small fires occurred near the observed temperature threshold, this could affect the shape of the modeled relationship between summer temperature and the probability of fire occurrence (e.g., Appendix C.4). Additionally, differences between past and future relationships could also arise from changing ecological dynamics (i.e., non-stationary relationships) under environmental conditions beyond the observational record. For example, projections of the spatial distributions in European tree species over the past 21,000 years had varied accuracy depending on the species, and the highest prediction errors occurred for species experiencing the largest shifts in their realized niche space (i.e., the set of ecological relationships defining where a species is present/absent) (Pearman et al. 2008, Veloz et al. 2012). In our study, the most linear fire-climate relationship (i.e., Shape 3, Figure C.7) results in the highest correspondence between the paleo-fire data and model projections for 850-1850 CE (Figure 3.4), suggesting that past fire-climate relationships may have differed from those characterizing the past 60 years. However, as noted earlier, we suggest that the discrepancy between the GCM-based and paleoclimate-inferred temperature (Appendix C.6) is the more

likely explanation for the poor correspondence between model predictions and the paleofire records.

Implications for projecting 21st-century change

Threshold-driven uncertainty in the future will be strongly dependent on the current climatological location of an ecosystem. Spatial variability in climate implies regionally varying proximity to climate-related thresholds, which will change as climate changes throughout the 21st century. We found that threshold-caused uncertainty in projections of Alaskan fire regimes is expected to lessen by the end of the 21st century, relative to the early 21st century (Figure 3.5). This pattern arises because most regions of Alaska are projected to exceed the climatic threshold to burning by the end of the 21st century, suggesting fire regimes across the state may become similar to those currently in the Yukon flats, the most flammable region of Alaska (Young et al. 2017).

Varying patterns in threshold-driven uncertainty may also hint at broader implications beyond the statistical projection of ecosystem change. Specifically, our results imply sudden ecosystem state changes may naturally exhibit significant variability across space and time. Given that many ecosystem properties are governed by threshold relationships, while also spanning large geographic regions (Scheffer et al. 2012), inherent spatial variability in state changes will likely have important ecological and human impacts, as different biological and natural resources have varying spatial distributions. For example, the spatial extent of the boreal forest biome is strongly determined by climate, and treeline itself is sensitive to climate-induced changes (Scheffer et al. 2012). A shift from a non-forested to forested states (or vice versa) in one location could have a larger impact on global carbon cycling, since

quantities of soil and aboveground carbon storage, as well as permafrost, follow distinct spatial patterns across the biome (Tarnocai et al. 2009). It is therefore critical to understand how much of the landscape resides near a threshold *and* the associated spatiotemporal dynamics, to assist land managers and policy makers in anticipating and planning for climate change impacts on ecosystems.

Limitations, future research needs, and conclusions

Our insights into the implications of threshold relationships for ecological predictions come with several important limitations. First, we focus on a relationship between a single explanatory (i.e., summer temperature) and response variable (i.e., fire presence/absence), while most ecological relationships are controlled by interactions among multiple factors. Since changes in one explanatory variable may affect changes in another (e.g., precipitation offsetting warmer temperatures), it is critical to understand how thresholds may occur in a multivariate setting under such interactions. In this study, interactions between temperature and precipitation may explain the low prediction error in the Yukon River Delta (Figure 3.3), which lies close to the temperature threshold but is also one of the wettest regions of our study area (Young et al., 2017); these wetter conditions at 30-yr timescales suggest burning is more likely to be limited by moisture in any given year, despite lying closer to the summer temperature threshold. Second, this work relies on a single modeled relationship from the observational record, and as such, we are unable to compare our results to a system that may exhibit a more linear relationship. A simulation modeling experiment, where the degree of linearity can be controlled, would aid in understanding the overall influence that differing

relationship shapes may have on predicting ecological change outside the observational record.

Despite these limitations, our findings highlight how threshold relationships can contribute significantly to uncertainty in ecological projections beyond the observational record. To our knowledge, few studies have highlighted or explored these threshold-related impacts on future projections, which we highlight as a critical source of projection uncertainty. Understanding the biophysical mechanisms and interactions underlying threshold relationships (Peters et al. 2004b) and identifying key ecological relationships that exhibit threshold responses in general (Groffman et al. 2006) are important next steps for anticipating the timing, location, and magnitude of future ecosystem change.

Acknowledgements

We thank M. Leonawicz for helpful comments and support in downscaling the climate data used in this research. Funding for this research was provided by NSF grants ARC-1023669 to PEH and PAD, ARC-1023477 to FSH, and a BLM Joint Fire Science Program GRIN Award (#14-3-01-7) and a NASA Earth and Space Science Fellowship (NNX14AK86H) to AMY.

References

Barry, S. and J. Elith. 2006. Error and uncertainty in habitat models. Journal of Applied Ecology **43**:413-423.

Bedia, J., S. Herrera, J. M. Gutierrez, A. Benali, S. Brands, B. Mota, and J. M. Moreno. 2015. Global patterns in the sensitivity of burned area to fire-weather: Implications for climate change. Agricultural and Forest Meteorology **214**:369-379.

Braconnot, P., S. P. Harrison, M. Kageyama, P. J. Bartlein, V. Masson-Delmotte, A. Abe-Ouchi, B. Otto-Bliesner, and Y. Zhao. 2012. Evaluation of climate models using palaeoclimatic data. Nature Climate Change **2**:417-424.

Buotte, P. C., J. A. Hicke, H. K. Preisler, J. T. Abatzoglou, K. F. Raffa, and J. A. Logan. 2016. Climate influences on whitebark pine mortality from mountain pine beetle in the Greater Yellowstone Ecosystem. Ecological Applications **26**:2505-2522.

Chipman, M. L., V. Hudspith, P. E. Higuera, P. A. Duffy, R. Kelly, W. W. Oswald, and F. S. Hu. 2015. Spatiotemporal patterns of tundra fires: Late-Quaternary charcoal records from Alaska. Biogeosciences **12**:4017-4027.

De'ath, G. 2007. Boosted trees for ecological modeling and prediction. Ecology **88**:243-251.

Diniz-Filho, J. A., L. M. Bini, T. F. Rangel, R. D. Loyola, C. Hof, D. Nogues-Bravo, and M. B. Araujo. 2009. Partitioning and mapping uncertainties in ensembles of forecasts of species turnover under climate change. Ecography **32**:897-906.

Elith, J. and J. R. Leathwick. 2009. Species distribution models: Ecological explanation and prediction across space and time. Annual Review of Ecology Evolution and Systematics **40**:677-697.

Giorgi, F. and L. O. Mearns. 1991. Approaches to the simulation of regional climate change - a review. Reviews of Geophysics **29**:191-216.

Grimm, N. B., F. S. Chapin, B. Bierwagen, P. Gonzalez, P. M. Groffman, Y. Q. Luo, F. Melton, K. Nadelhoffer, A. Pairis, P. A. Raymond, J. Schimel, and C. E. Williamson. 2013. The impacts of climate change on ecosystem structure and function. Frontiers in Ecology and the Environment **11**:474-482.

Groffman, P., J. Baron, T. Blett, A. Gold, I. Goodman, L. Gunderson, B. Levinson, M. Palmer, H. Paerl, G. Peterson, N. Poff, D. Rejeski, J. Reynolds, M. Turner, K. Weathers, and J. Wiens. 2006. Ecological thresholds: The key to successful environmental management or an important concept with no practical application? Ecosystems **9**:1-13.

Gunderson, L. H. 2000. Ecological resilience - in theory and application. Annual Review of Ecology and Systematics **31**:425-439.

Higuera, P. E., L. B. Brubaker, P. M. Anderson, F. S. Hu, and T. A. Brown. 2009. Vegetation mediated the impacts of postglacial climate change on fire regimes in the south-central Brooks Range, Alaska. Ecological Monographs **79**:201-219.

Higuera, P. E., M. L. Chipman, J. L. Barnes, M. A. Urban, and F. S. Hu. 2011. Variability of tundra fire regimes in Arctic Alaska: millennial scale patterns and ecological implications. Ecological Applications **21**:3211-3226.

Higuera, P. E., D. G. Gavin, P. J. Bartlein, and D. J. Hallett. 2010. Peak detection in sediment-charcoal records: impacts of alternative data analysis methods on fire-history interpretations. International Journal of Wildland Fire **19**:996-1014.

Hu, F. S., P. E. Higuera, J. E. Walsh, W. L. Chapman, P. A. Duffy, L. B. Brubaker, and M. L. Chipman. 2010. Tundra burning in Alaska: Linkages to climatic change and sea ice retreat. Journal of Geophysical Research-Biogeosciences **115**:G04002.

Hunsicker, M. E., C. V. Kappel, K. A. Selkoe, B. S. Halpern, C. Scarborough, L. Mease, and A. Amrhein. 2016. Characterizing driver-response relationships in marine pelagic ecosystems for improved ocean management. Ecological Applications **26**:651-663.

Johnson, E. A. and S. L. Gutsell. 1994. Fire frequency models, methods and interpretations. Advances in Ecological Research, Vol 25 **25**:239-287.

Kasischke, E. S., D. L. Verbyla, T. S. Rupp, A. D. McGuire, K. A. Murphy, R. Jandt, J. L. Barnes, E. E. Hoy, P. A. Duffy, M. Calef, and M. R. Turetsky. 2010. Alaska's changing fire regime - implications for the vulnerability of its boreal forests. Canadian Journal of Forest Research-Revue Canadienne De Recherche Forestiere **40**:1313-1324.

Kasischke, E. S., D. Williams, and D. Barry. 2002. Analysis of the patterns of large fires in the boreal forest region of Alaska. International Journal of Wildland Fire **11**:131-144.

Martínez-Meyer, E., A. Townsend Peterson, and W. W. Hargrove. 2004. Ecological niches as stable distributional constraints on mammal species, with implications for Pleistocene extinctions and climate change projections for biodiversity. Global Ecology and Biogeography **13**:305-314.

McAfee, S. A. 2013. Methodological differences in projected potential evapotranspiration. Climatic Change **120**:915-930.

Moreno-Amat, E., R. G. Mateo, D. Nieto-Lugilde, N. Morueta-Holme, J. C. Svenning, and I. Garcia-Amorena. 2015. Impact of model complexity on cross-temporal transferability in Maxent species distribution models: An assessment using paleobotanical data. Ecological Modelling **312**:308-317.

Moritz, M. A., M. A. Parisien, E. Batllori, M. A. Krawchuk, J. Van Dorn, D. J. Ganz, and K. Hayhoe. 2012. Climate change and disruptions to global fire activity. Ecosphere **3**.

Muggeo, V. M. R. 2003. Estimating regression models with unknown break-points. Statistics in Medicine **22**:3055-3071.

Nowacki, G., P. Spencer, T. Brock, M. Fleming, and T. Jorgenson. 2001. Ecoregions of Alaska and neighboring territories - US Geological Survey Open-File Report 02-297 (map). Online at http://agdc.usgs.gov/data/projects/fhm/#H, USGS, Reston, VA.

Pausas, J. G. and S. Paula. 2012. Fuel shapes the fire-climate relationship: evidence from Mediterranean ecosystems. Global Ecology and Biogeography **21**:1074-1082.

Pearman, P. B., C. F. Randin, O. Broennimann, P. Vittoz, W. O. van der Knaap, R. Engler, G. Le Lay, N. E. Zimmermann, and A. Guisan. 2008. Prediction of plant species distributions across six millennia. Ecology Letters **11**:357-369.

Peters, D. P. C., J. E. Herrick, D. L. Urban, R. H. Gardner, and D. D. Breshears. 2004a. Strategies for ecological extrapolation. Oikos **106**:627-636.

Peters, D. P. C., R. A. Pielke, B. T. Bestelmeyer, C. D. Allen, S. Munson-McGee, and K. M. Havstad. 2004b. Cross-scale interactions, nonlinearities, and forecasting catastrophic events. Proceedings of the National Academy of Sciences of the United States of America **101**:15130-15135.

Scheffer, M., S. Carpenter, J. A. Foley, C. Folke, and B. Walker. 2001. Catastrophic shifts in ecosystems. Nature **413**:591-596.

Scheffer, M., M. Hirota, M. Holmgren, E. H. Van Nes, and F. S. Chapin. 2012. Thresholds for boreal biome transitions. Proceedings of the National Academy of Sciences of the United States of America **109**:21384-21389.

Suding, K. N. and R. J. Hobbs. 2009. Threshold models in restoration and conservation: a developing framework. Trends in Ecology & Evolution **24**:271-279.

Tarnocai, C., J. G. Canadell, E. A. G. Schuur, P. Kuhry, G. Mazhitova, and S. Zimov. 2009. Soil organic carbon pools in the northern circumpolar permafrost region. Global Biogeochemical Cycles **23**.

Taylor, K. E., R. J. Stouffer, and G. A. Meehl. 2012. An overview of CMIP5 and the experiment design. Bulletin of the American Meteorological Society **93**:485-498.

Thomas, J. A. and K. D. Bovee. 1993. Application and Testing of a Procedure to Evaluate Transferability of Habitat Suitability Criteria. Regulated Rivers-Research & Management **8**:285-294.

Vaughan, D. G., J. C. Comiso, I. Allison, J. Carrasco, G. Kaser, R. Kwok, P. Mote, T. Murray, F. Paul, J. Ren, E. Rignot, O. Solomina, K. Steffen, and T. Zhang. 2013. Observations: Cryosphere.*in* T. F. Stocker, D. Qin, G.-K. Plattner, M. Tignor, S. K. Allen, J. Boschung, A. Nauels, Y. Xia, V. Bex, and P. M. Midgley, editors. Climate Change 2013: The Physical Science Basis. Contribution of Working Group I to the Fifth Assessment Report of the Intergovernmental Panel on Climate Change. Cambridge University Press, Cambridge, United Kingdom and New York, NY, USA.

Veloz, S. D., J. W. Williams, J. L. Blois, F. He, B. Otto-Bliesner, and Z. Y. Liu. 2012. No-analog climates and shifting realized niches during the late quaternary: Implications for 21st-century predictions by species distribution models. Global Change Biology **18**:1698-1713.

Walther, G. R., E. Post, P. Convey, A. Menzel, C. Parmesan, T. J. C. Beebee, J. M. Fromentin, O. Hoegh-Guldberg, and F. Bairlein. 2002. Ecological responses to recent climate change. Nature **416**:389-395.

Watling, J. I., L. A. Brandt, D. N. Bucklin, I. Fujisaki, F. J. Mazzotti, S. S. Romanach, and C. Speroterr. 2015. Performance metrics and variance partitioning reveal sources of uncertainty in species distribution models. Ecological Modelling **309**:48-59.

Wenger, S. J., N. A. Som, D. C. Dauwalter, D. J. Isaak, H. M. Neville, C. H. Luce, J. B. Dunham, M. K. Young, K. D. Fausch, and B. E. Rieman. 2013. Probabilistic accounting of uncertainty in forecasts of species distributions under climate change. Global Change Biology **19**:3343-3354.

Wilson, R., K. Anchukaitis, K. R. Briffa, U. Buntgen, E. Cook, R. D'Arrigo, N. Davi, J. Esper, D. Frank, B. Gunnarson, G. Hegerl, S. Helama, S. Klesse, P. J. Krusic, H. W. Linderholm, V. Myglan, T. J. Osborn, M. Rydval, L. Schneider, A. Schurer, G. Wiles, P. Zhang, and E. Zorita. 2016. Last millennium northern hemisphere summer temperatures from tree rings: Part I: The long term context. Quaternary Science Reviews **134**:1-18.

Young, A. M., P. E. Higuera, P. A. Duffy, and F. S. Hu. 2017. Climatic thresholds shape northern high-latitude fire regimes and imply vulnerability to future change. Ecography **40**:606-617.

Table 3.1. Summary of prediction errors for each ecoregion under the original (i.e., unmodified) and modified fire-climate relationships. Values for each ecoregion and modification summarize the median (IQR) prediction error. T1-T3 designates the three different temperature modifications (T1 = +0.50 °C, T2 = +1.00 °C, and T3 = +1.50 °C). In the three rightmost columns, Shape 1-Shape 3 designates the three modified shapes of the relationship between fire and July temperature (Appendix C.4).

	Orig.	**T1**	**T2**	**T3**	**Shape 1**	**Shape 2**	**Shape 3**
Yukon Flats	-28 (38)	-35 (31)	-41 (34)	-46 (49)	-27 (34)	-29 (31)	-28 (33)
Noatak River Watershed	148 (413)	49 (294)	2 (151)	-22 (68)	111 (281)	80 (226)	24 (106)
Kobuk Valley	158 (336)	63 (156)	17 (78)	-6 (48)	123 (224)	95 (164)	41 (86)
Copper River Basin	453 (203)	395 (210)	318 (216)	192 (237)	295 (144)	217 (109)	94 (69)
Brooks Foothills, Brooks Range, & Yukon Kusk. Delta	1 (25)	0 (24)	-6 (28)	-14 (34)	-20 (16)	-29 (20)	-46 (13)

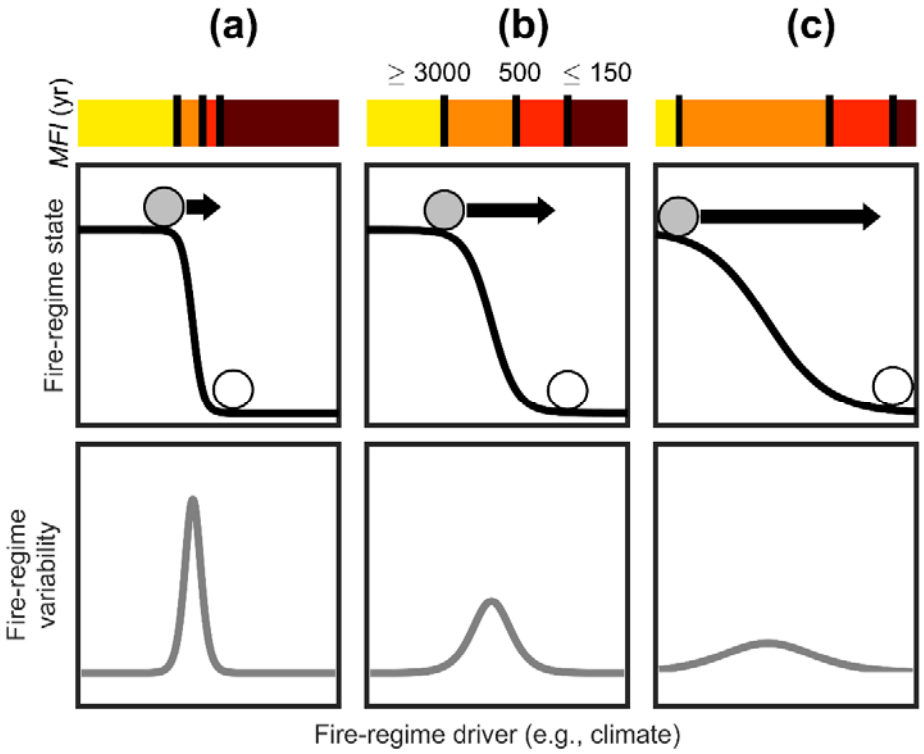

Figure 3.1. Conceptual framework of how differing fire-climate relationships may impact predictions of fire-regime shifts. (a) With a distinct threshold, significant fire-regime changes can occur over a relatively small change in climate (length of arrow). (b-c) Under more linear relationships, a larger change in climate is needed to drive a fire-regime shift of similar magnitude. Different levels of fire-regime variability in response to climatic change accompany each relationships, measured in terms of mean fire return intervals (*MFI*). For example, in (a) high variability immediately surrounding the distinct threshold.

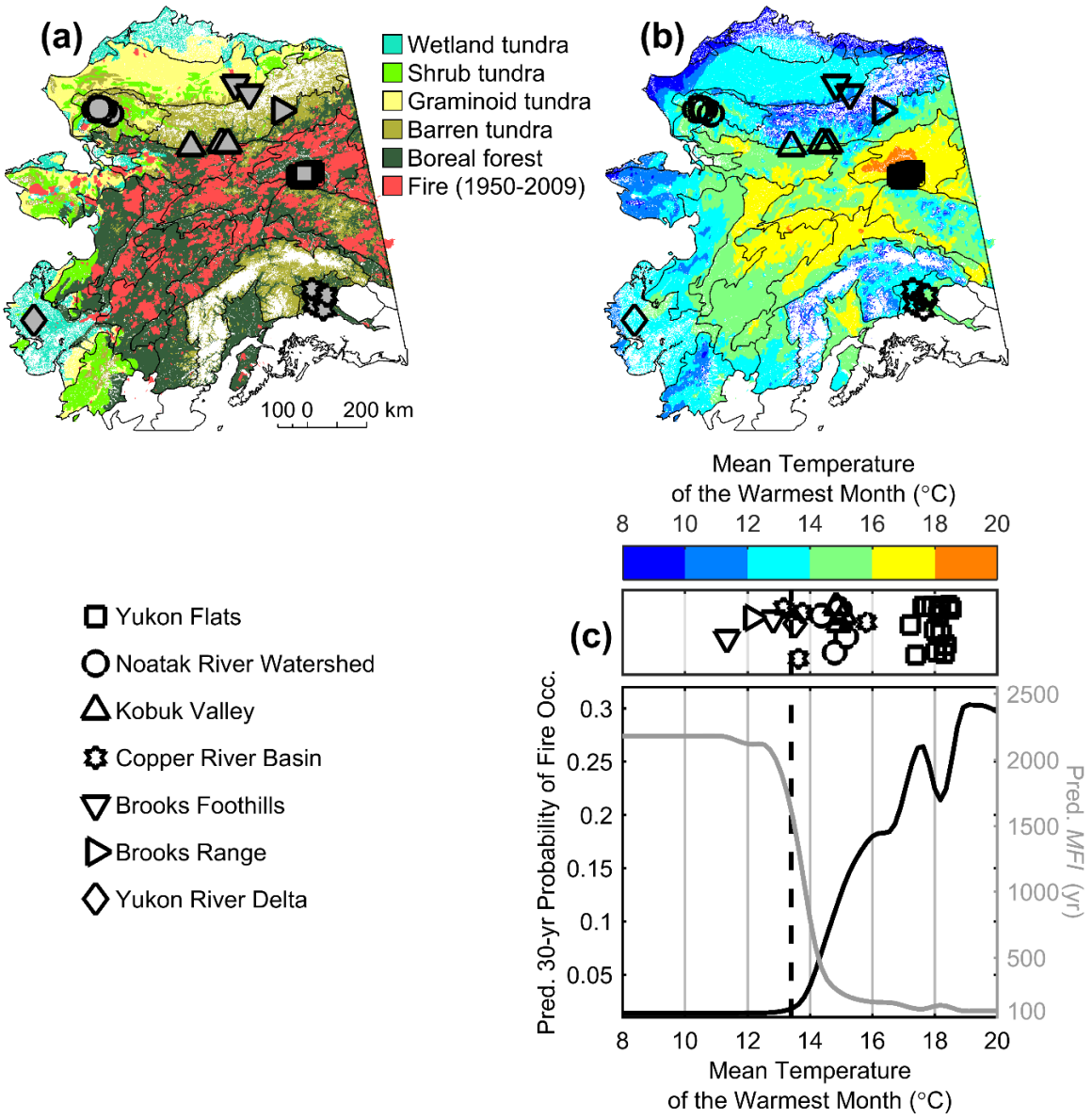

Figure 3.2. Alaskan study area (1950-2009), including vegetation, fire history, climate, and key modeled fire-climate relationship. (a) Spatial distribution of modern vegetation and recent fire occurrence (1950-2009) at 2-km resolution. Plotted symbols represent locations of individual fire-history reconstructions, and different symbols represent different ecoregions. (b) Mean temperature of the warmest month (°C) from 1950-2009, the most important control of fire occurrence in Alaska during the observational record (Young et al. 2017). (c) Modeled observational relationships between the probability of fire occurrence and mean temperature of the warmest month at a 30-yr timescale. The vertical line at 13.4 °C is the threshold value estimated in Young et al. (2017). The upper panel in (c) displays the distribution of lake locations in univariate climate space along July temperature (i.e., Mean Temperature of the Warmest Month). The plotting of lake locations includes a vertical "jittering" to reduce overlapping of symbols. For reference, the gray line is the inverse of the black line, approximating the predicted mean fire return interval (*MFI*), and is displayed due to the use of *MFI* as the measure for model-paleodata comparisons.

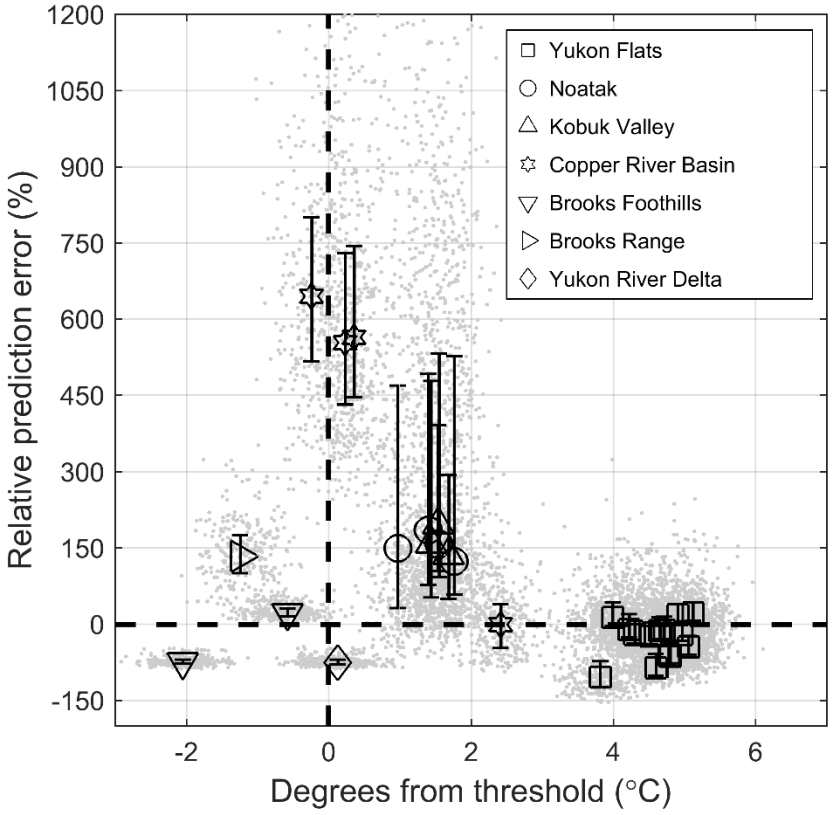

Figure 3.3. Relative prediction errors for each lake in the study area during 850-1850 CE. Dark-colored symbols represent the median prediction error from all 300 predictions for each lake (i.e., all BRTs [n = 100] and GCMs [n = 3]). Confidence bounds represent the 25th to 75th percentiles of prediction errors. Gray dots are prediction errors associated with an individual BRT, GCM, and paleo-record.

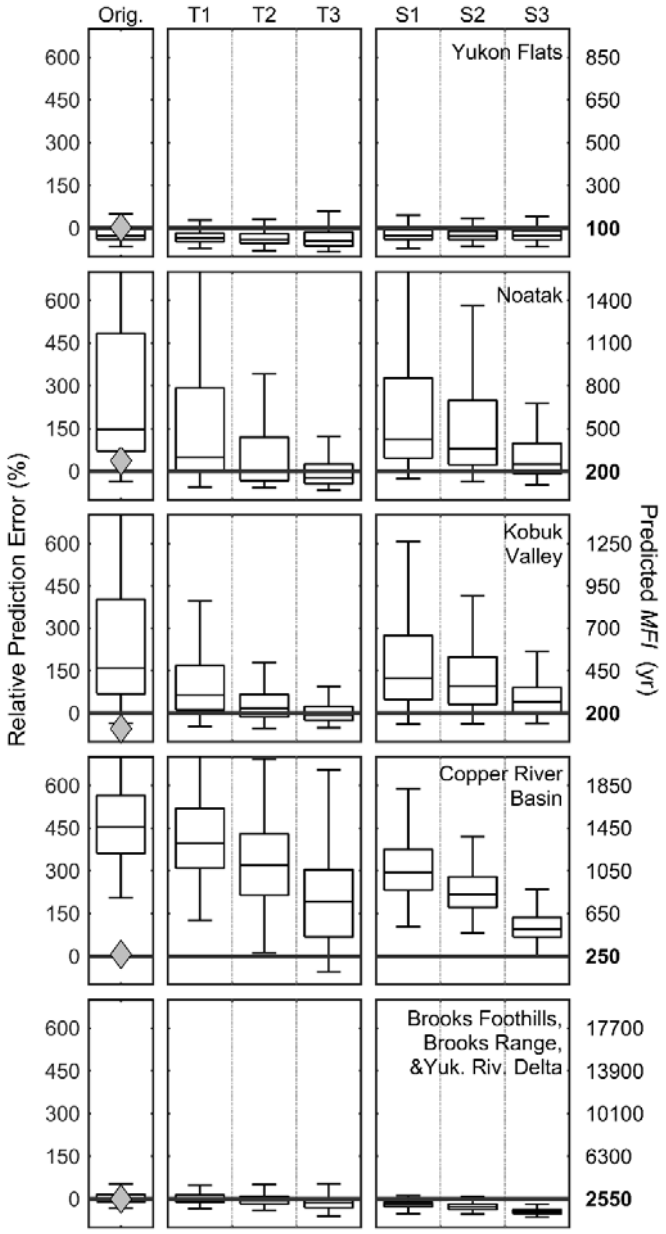

Figure 3.4. Impacts of modified relationships on prediction error for *MFI* for the 850-1850 CE period, stratified by ecoregion (rows). In the leftmost column, predictions are summarized by using the unmodified, original relationship between temperature and the probability of fire occurrence. For each ecoregion, relative prediction error was averaged across all lakes, and the boxplots display the distribution of this averaged prediction error for all BRTs and GCMs. In the middle column, boxplots display the distribution of prediction errors under three relationships that were modified by shifting the threshold value (T1 = +0.50 °C, T2 = +1.00 °C, and T3 = +1.50 °C). In the rightmost column, boxplots display the distribution of prediction errors under three scenarios where the shape of the relationship was modified (i.e., S1 = Shape 1, S2 = Shape 2, S3 = Shape 3). The right axis represents predicted *MFI*, with the bold value and horizontal line highlighting the observed *MFI* in each ecoregion (rounded to the nearest 50 yr). As a reference, the gray diamond represents the median of the observed prediction error for the original 100 BRTs during the historical period (1950-2009).

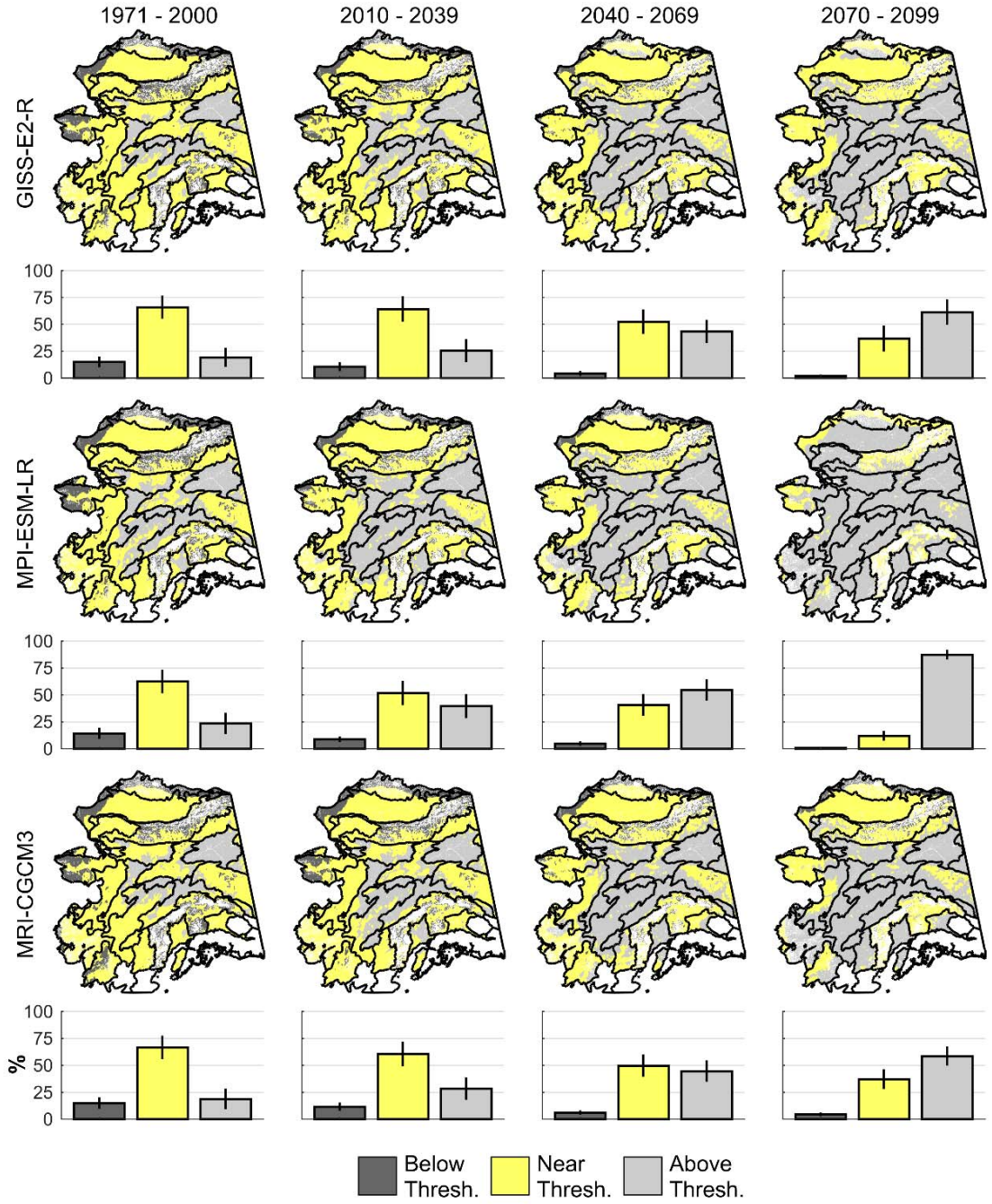

Figure 3.5. Historical and future distribution of locations in Alaska classified as occurring below, near, or above the 13.4 °C threshold (i.e., within ±2 °C). Bar heights indicate the proportion of Alaska occurring under each classification. Standard deviations (vertical lines) account for potential uncertainty in the value of the temperature threshold. Specifically, the lower and upper limits to the classification conditions (i.e., 13.4 ± 2 °C) were modified 100 times by adding a random value from a uniform distribution (parameters a = -1 and b = 1). For each random modification, the distribution of the Alaskan landscape occurring below, near, or above the July temperature threshold was reclassified, and the standard deviation was calculated from these 100 reclassifications.

Appendix A: Supplementary information for Chapter 1

Appendix A.1. Supplementary methods

Boosted regression tree modeling

To construct our boosted regression trees (BRTs), we used a Bernoulli distribution to characterize the binary response variable of fire presence/absence. We set our bagging fraction of 0.5, and used a 5-fold cross validation to identify the optimal number iterations from a maximum of 5000. Since we used a small pre-selected subset of 2-km pixels to train each BRT, we set the training fraction to 1.0. The minimum number of observations allowed in each regression tree node was set to 1. Our interaction depth was set at 2, to capture pairwise potential interactions among explanatory variables. The learning rate (i.e., shrinkage) was 0.01 for each model, and was chosen to ensure deviance of the predicted response reached a minimum within the maximum number of trees (i.e., 5000) (Supplementary material Appendix A.2, Figure A.1).

Landscape sampling of Alaskan wildfire occurrence

To prevent overfitting of historical fire-climate relationships and to account for potential spatial autocorrelation in our analyses, we sampled a small subset of all available 2-km pixels from the spatial domain of each model (AK, BOREAL, and TUNDRA). The total number of pixels from each spatial domain (i.e., sampling rate) used to train our boosted regression tree models (BRTs) was determined by evaluating the predictive performance of BRTs built at different sampling rates. Specifically, we increased the sampling rate until subsequent increases resulted in model improvement < 5% for both the mean AUC and

median Pearson correlation value. We tested eight different sampling rates, based on the 50th, 60th, 75th, 80th, 85th, 90th, 95th, and 99th percentiles of the size distribution of fires from 1950-2009. For example, in the BOREAL domain, the 85th percentile fire size is 121.6 km^2, and the total study area is 125,470 pixels (i.e., 501,880 km2); therefore there are 501,880 km^2 / 121.6 km_2 ≈ 4127 observations available, corresponding to a sampling rate of 4127 pixels / 125,470 pixels = 3.29% (Supplementary material Appendix A.2, Table A.3). This sampling rate is comparable to randomly selecting a single 2-km pixel every 122 km^2. For each spatial domain and sampling rate, we trained a set of 15 BRTs, which was used to predict fire presence/absence. To evaluate model performance, we recorded AUC values and Pearson correlations between predicted and observed fire rotation periods (FRPs) for ecoregions. If needed, the number of iterations and the shrinkage parameters for the BRTs were adjusted for different sampling rates. Finally, we selected the lowest sampling rate that met our criteria for all three sampling domains. Based on our criteria, we used sampling rates associated with the 85th percentile of fire sizes, or 3.52%, 3.29%, and 5.43% of the available pixels for the AK, BOREAL, and TUNDRA models, respectively (Supplementary material Appendix A.2, Table A.3).

This sampling design has several advantages compared to using all available pixels in each sampling domain. First, our approach helps to guard against overfitting, as relationships derived from a subsample of points are likely more generalizable to new observations than relationships fit using all available pixels. Second, our design helps account for spatial autocorrelation, which is particularly important when modeling variability in fire occurrence, because the process of fire spread is highly autocorrelated in space. Using all available pixels

runs the risk of over-estimating the predictive power of explanatory variables. Finally, using different subsampling rates for each spatial domain helps account for significant fire-regime differences among study domains (e.g., boreal forest fire are generally larger than tundra fires).

Identifying climatic thresholds to fire occurrence with segmented regression models

To quantify potential thresholds we used a piecewise linear regression using the "segmented" package in R (Muggeo 2003, Muggeo 2008). We used the median predicted probability of fire occurrence for each climate explanatory variable and restricted the segmented regression to climate values immediately surrounding a visually identified threshold. Specifically, we sampled BRT predictions (n = 100) with replacement 2000 times, calculated the median predicted probability from the 100 BRTs each time, performed piecewise regression on each sample, and recorded threshold estimates from each bootstrap sample. We report the mean threshold estimate and the 2.5th and 97.5th percentiles as 95% confidence intervals from the 2000 bootstrapped samples.

Appendix A.2 Supplementary results

Table A.1. List of the 13 continuous candidate explanatory variables originally considered in the boosted regression tree (BRT) analysis and their predictive performance when each is used individually to model the 30-yr probability of fire occurrence. Values for each candidate climate variable are the 30-yr average. For each explanatory variable, 100 BRTs were constructed and used to predict the presence/absence of fire. AUC mean and SD values are calculated from the predictions of these 100 BRTs.

Variable	Units	Description	AUC Mean (SD)
GDD_{ANN}	°C	Total Growing Degree Days	0.74 (0.01)
P_{ANN}	mm	Total Annual Precipitation	0.64 (0.03)
P_{DJF}	mm	Total Winter Precipitation	0.60 (0.06)
P_{JJA}	mm	Total Summer Precipitation	0.65 (0.02)
P_{MAM}	mm	Total Spring Precipitation	0.62 (0.02)
P_{RANGE}	mm	Annual Precipitation Range	0.60 (0.03)
$P\text{-}PET_{ANN}$	mm	Annual Moisture Availability	0.70 (0.02)
$P\text{-}PET_{JJA}$	mm	Summer Moisture Availability	0.60 (0.02)
T_{ANN}	°C	Mean Annual Temperature	0.62 (0.02)
T_{JJA}	°C	Mean Summer Temperature	0.73 (0.01)
T_{RANGE}	°C	Annual Temperature Range	0.59 (0.02)
T_{WARM}	°C	Mean Temp. of the Warmest Month	0.78 (0.01)
TR	m	Topographic Ruggedness	0.57 (0.01)

Table A.2. Median Spearman rank correlations among candidate explanatory variables. Correlations were calculated using 5% of the data randomly sampled across space 100 times using 1950-2009 averages.

ID	1	2	3	4	5	6	7	8	9	10	11	12	13
1 GDD_{ANN}	1.00												
2 P_{ANN}	0.06	1.00											
3 P_{DJF}	-0.04	0.93	1.00										
4 P_{JJA}	0.15	0.92	0.75	1.00									
5 P_{MAM}	0.00	0.96	0.93	0.83	1.00								
6 P_{RANGE}	0.06	0.96	0.83	0.95	0.89	1.00							
7 $P\text{-}PET_{ANN}$	-0.19	0.96	0.92	0.85	0.94	0.92	1.00						
8 $P\text{-}PET_{JJA}$	0.08	0.92	0.79	0.94	0.85	0.91	0.90	1.00					
9 T_{ANN}	0.69	0.54	0.44	0.56	0.51	0.50	0.40	0.64	1.00				
10 T_{JJA}	0.96	-0.09	-0.19	0.03	-0.15	-0.08	-0.34	-0.10	0.51	1.00			
11 T_{RANGE}	0.02	-0.71	-0.67	-0.64	-0.70	-0.67	-0.75	-0.82	-0.66	0.23	1.00		
12 T_{WARM}	0.91	-0.17	-0.26	-0.06	-0.22	-0.15	-0.42	-0.21	0.40	0.98	0.34	1.00	
13 TR	-0.22	0.37	0.31	0.43	0.32	0.38	0.38	0.34	-0.06	-0.22	-0.16	-0.24	1.00

Table A.3. Results from evaluating models built at different sampling rates. AUC and Pearson correlation values are calculated from the predictions of the 15 boosted regression trees models trained for each spatial domain and sampling rate. An example of how the "Number of pixels" and "Sampling rate" values are calculated is given in Appendix A.1.

Percentile	Model/ Spatial domain	Fire size (km^2)	Number of pixels	Sampling rate (%)	AUC Mean (SD)	Median Pearson correlation
99	AK	1434	707	0.28	0.78 (0.03)	0.61
	BOREAL	1489	337	0.27	0.63 (0.05)	0.61
	TUNDR	1070	381	0.37	0.61 (0.16)	0.41
95	AK	416	2435	0.96	0.78 (0.02)	0.65
	BOREAL	427	1177	0.94	0.63 (0.04)	0.64
	TUNDR	348	1170	1.15	0.69 (0.08)	0.47
90	AK	199	5093	2.01	0.78 (0.02)	0.66
	BOREAL	205	2443	1.95	0.63 (0.03)	0.62
	TUNDR	130	3126	3.07	0.70 (0.08)	0.50
85	AK	114	8930	3.52	0.78 (0.02)	0.74
	BOREAL	122	4127	3.29	0.63 (0.03)	0.63
	TUNDR	74	5526	5.43	0.71 (0.07)	0.59
80	AK	75	13496	5.33	0.78 (0.02)	0.80
	BOREAL	80	6297	5.02	0.62 (0.03)	0.67
	TUNDR	50	8665	8.51	0.72 (0.05)	0.60
75	AK	50	19991	7.89	0.78 (0.02)	0.81
	BOREAL	53	9381	7.48	0.62 (0.02)	0.70
	TUNDR	35	11770	11.56	0.72 (0.06)	0.57
60	AK	19	53193	21.28	0.77 (0.01)	0.79
	BOREAL	20	25606	20.41	0.62 (0.03)	0.67
	TUNDR	15	27510	26.67	0.72 (0.07)	0.55
50	AK	11	94725	37.38	0.77 (0.01)	0.82
	BOREAL	11	45214	36.04	0.62 (0.03)	0.68
	TUNDR	8	50907	50.00	0.71 (0.06)	0.54

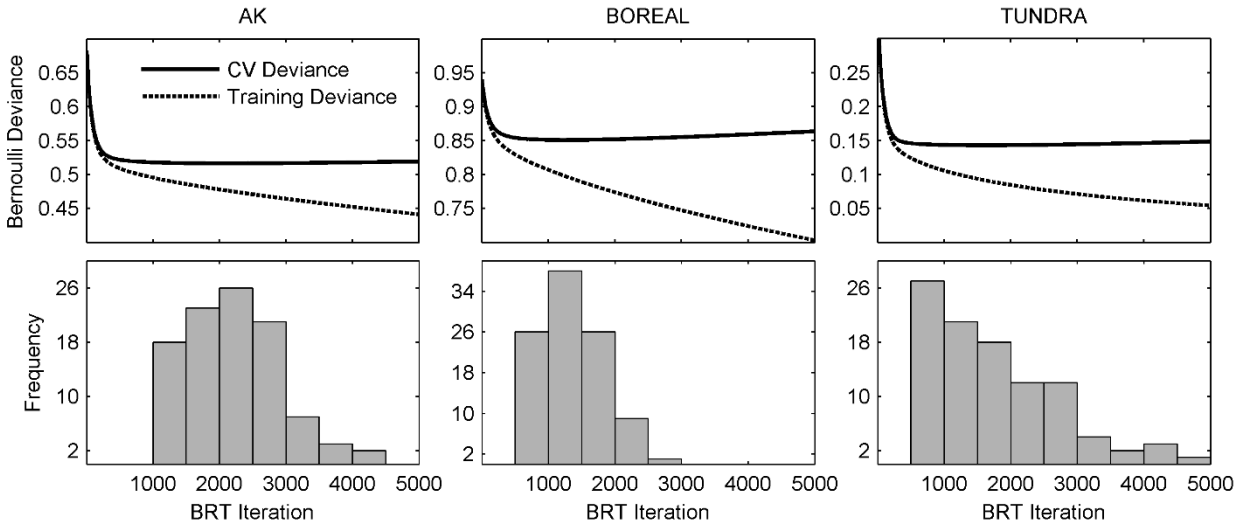

Figure A.1. Boosted regression tree (BRT) diagnostic information for each modeling domain. The top row displays the training and testing deviance averaged from the 100 BRTs for each of the three models. The bottom row displays the distribution of the optimal number of iterations selected for each of the 100 BRTs.

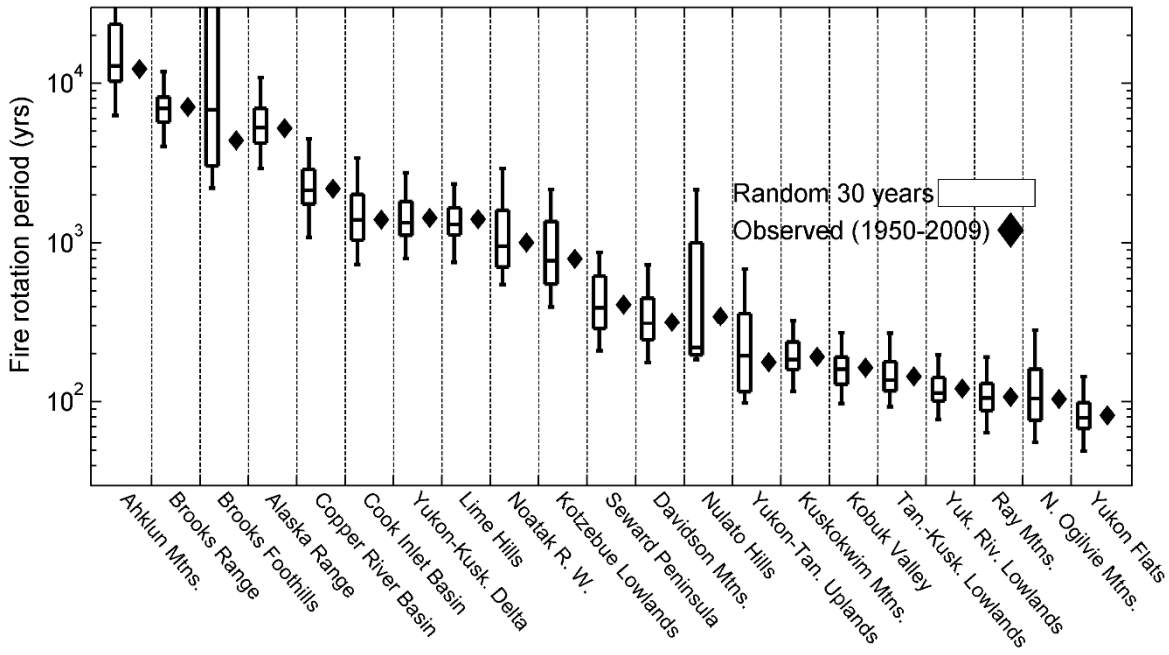

Figure A.2. Observed fire rotation periods (FRPs) for Alaskan ecoregions calculated using 30 non-continuous, randomly sampled years compared with the FRP of each ecoregion using all sixty years of available data (1950-2009).

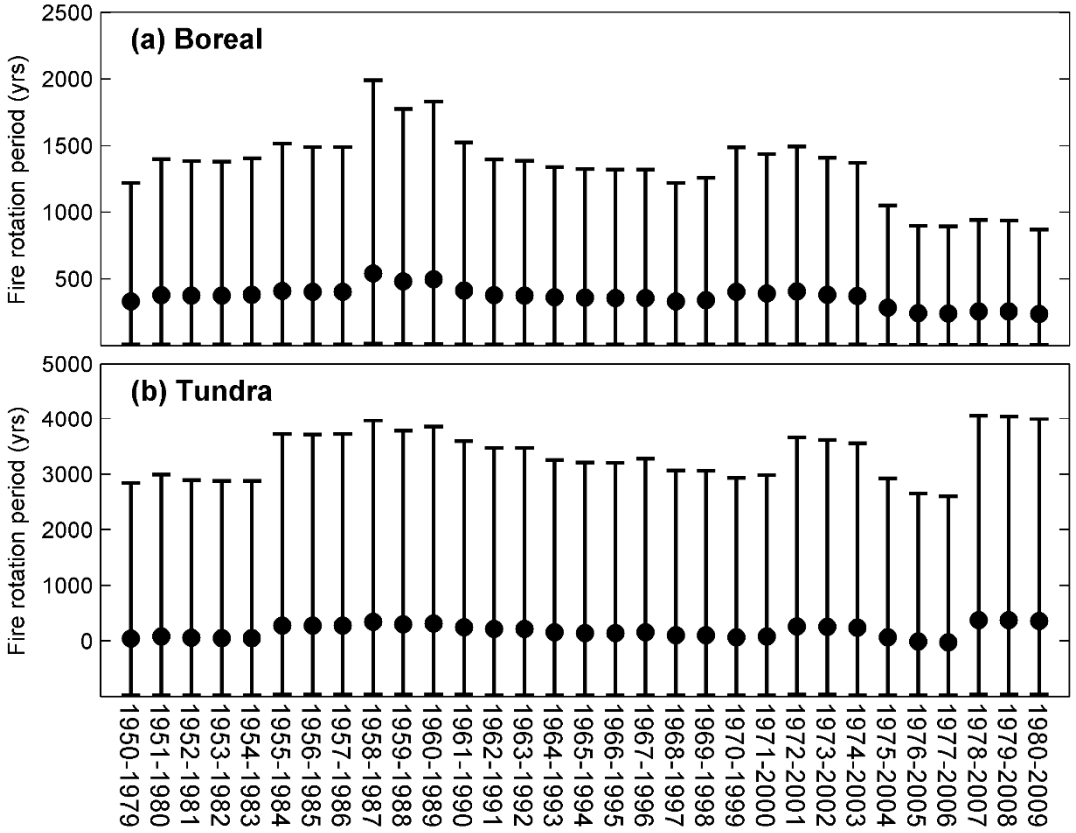

Figure A.3. Thirty-year fire rotation periods (FRPs) for continuous time periods from 1950 through 2009 for the (a) boreal forest and (b) tundra spatial domains. The solid point is the calculated FRP for each thirty year time period. Confidence bounds are the 2.5^{th} and 97.5^{th} quantiles assuming FRP is an exponential random variable with the rate parameter equal to the inverse FRP (e.g., Chipman et al. 2015).

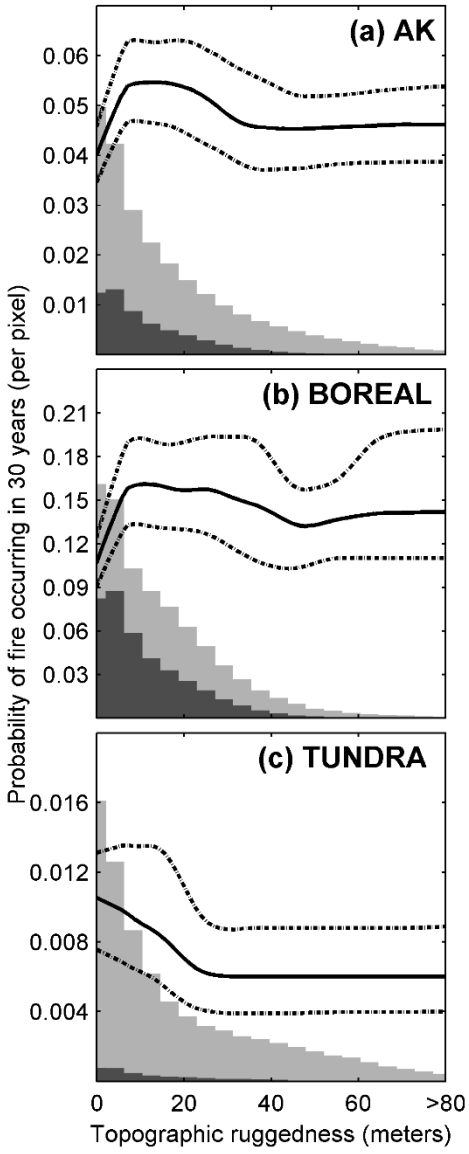

Figure A.4. Partial dependence plots illustrating the relationships between topographic ruggeddness and the predicted probability of fire occurrence from the (a) AK, (b) BOREAL, and (c) TUNDRA models, as in Figure 1.4 in the main text. The solid black lines represent the median predicted probability of fire occurrence, and the dashed lines represent the interquartile range from 100 boosted regression tree models. A lowess function (span = 0.1) was used to smooth the plotted predicted median and interquartile lines. As a reference, lighter (darker) colored histograms represent the historical distribution of topographic ruggedness among unburned (burned) pixels from 1950 to 2009. Histograms heights were scaled individually and are not associated with y-axis values.

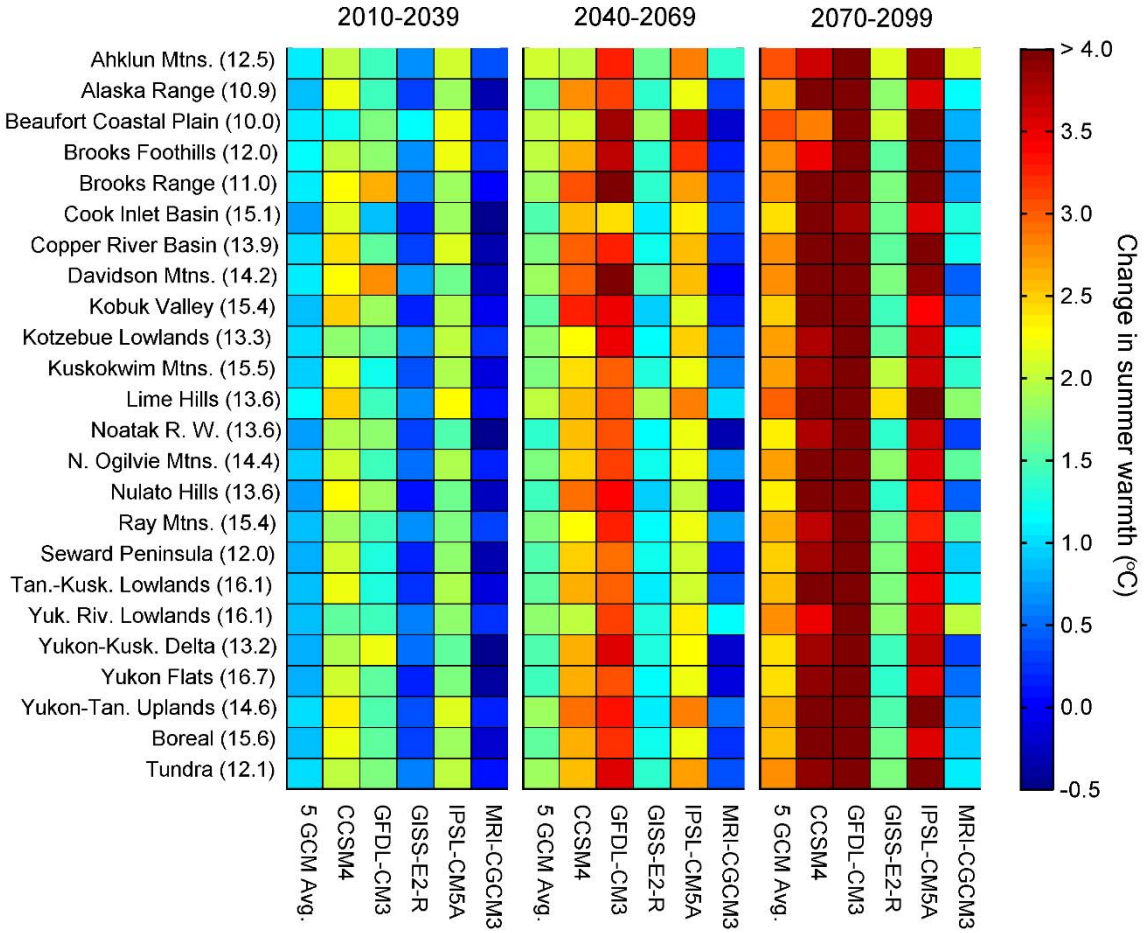

Figure A.5. Projected changes in summer warmth (i.e., mean temperature of the warmest month) for Alaskan ecoregions and the boreal forest and tundra spatial domains. Values in parentheses next to ecoregion names are the 1950-2009 averages, while colors indicate the magnitude of projected change for the five-GCM average and each GCM individually. Projected changes were calculated by taking the difference in projected climate for each 2-km pixel and then averaging this difference across each region and time period.

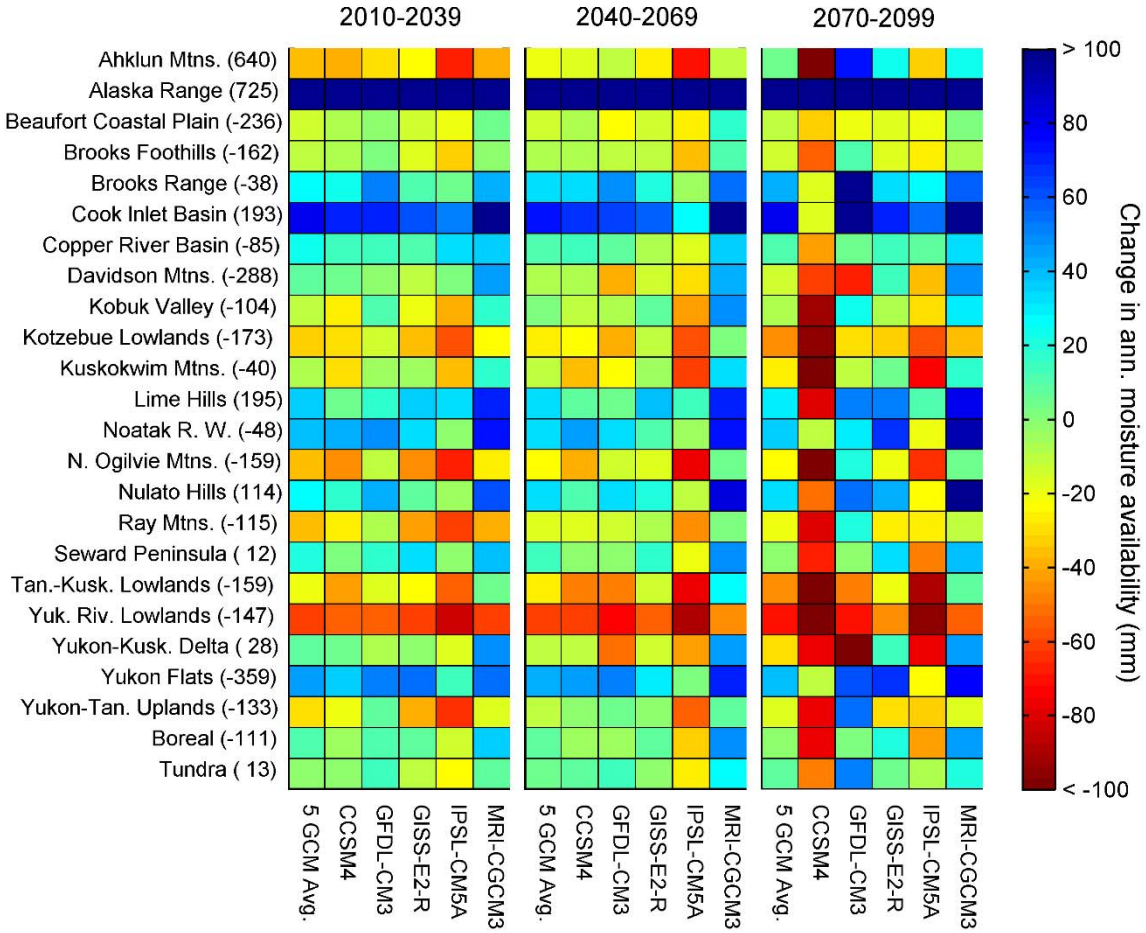

Figure A.6. Projected changes in annual moisture availability for Alaskan ecoregions and the boreal forest and tundra spatial domains. Values in parentheses next to ecoregion names are the 1950-2009 averages, while colors indicate the magnitude of projected change for the five-GCM average and each GCM individually. Projected changes were calculated by taking the difference in projected climate for each 2-km pixel and then averaging this difference across each region and time period.

Appendix A.3: References

Chipman, M. L., V. Hudspith, P. E. Higuera, P. A. Duffy, R. Kelly, W. W. Oswald, and F. S. Hu. 2015. Spatiotemporal patterns of tundra fires: Late-Quaternary charcoal records from Alaska. Biogeosciences **12**:4017-4027.

Muggeo, V. M. R. 2003. Estimating regression models with unknown break-points. Statistics in Medicine **22**:3055-3071.

Muggeo, V. M. R. 2008. segmented: an R Package to Fit Regression Models with Broken-Line Relationships. R News:20-25.

Appendix B: Supplementary information for Chapter 2

Appendix B.1: Supplementary figures and tables

Table B.1. AUC values characterizing goodness of fit for the boosted regression tree models. Mean and SD are for all 50 individual BRTs within each set. There were five different sets, one for each climate variable (denoted in second column). Note, for models that used DC_{JJA} and FWI_{90} we ran two sets of models, one based on MERRA2 data and one based on ERA-Interim (ERAI) data. **$P\text{-}PET_{JJA}$** = total summer (JJA) precipitation minus potential evapotranspiration; **DC_{JJA}** = average summer drought code; **FWI_{90}** = 90th-percentile of the daily fire weather index

Model #	Climate variable	AUC (mean ± SD)	
1	$P\text{-}PET_{JJA}$	0.75 ± 0.01	
		MERRA2	ERAI
2 and 3	DC_{JJA}	0.78 ± 0.01	0.79 ± 0.01
4 and 5	FWI_{90}	0.77 ± 0.01	0.80 ± 0.01

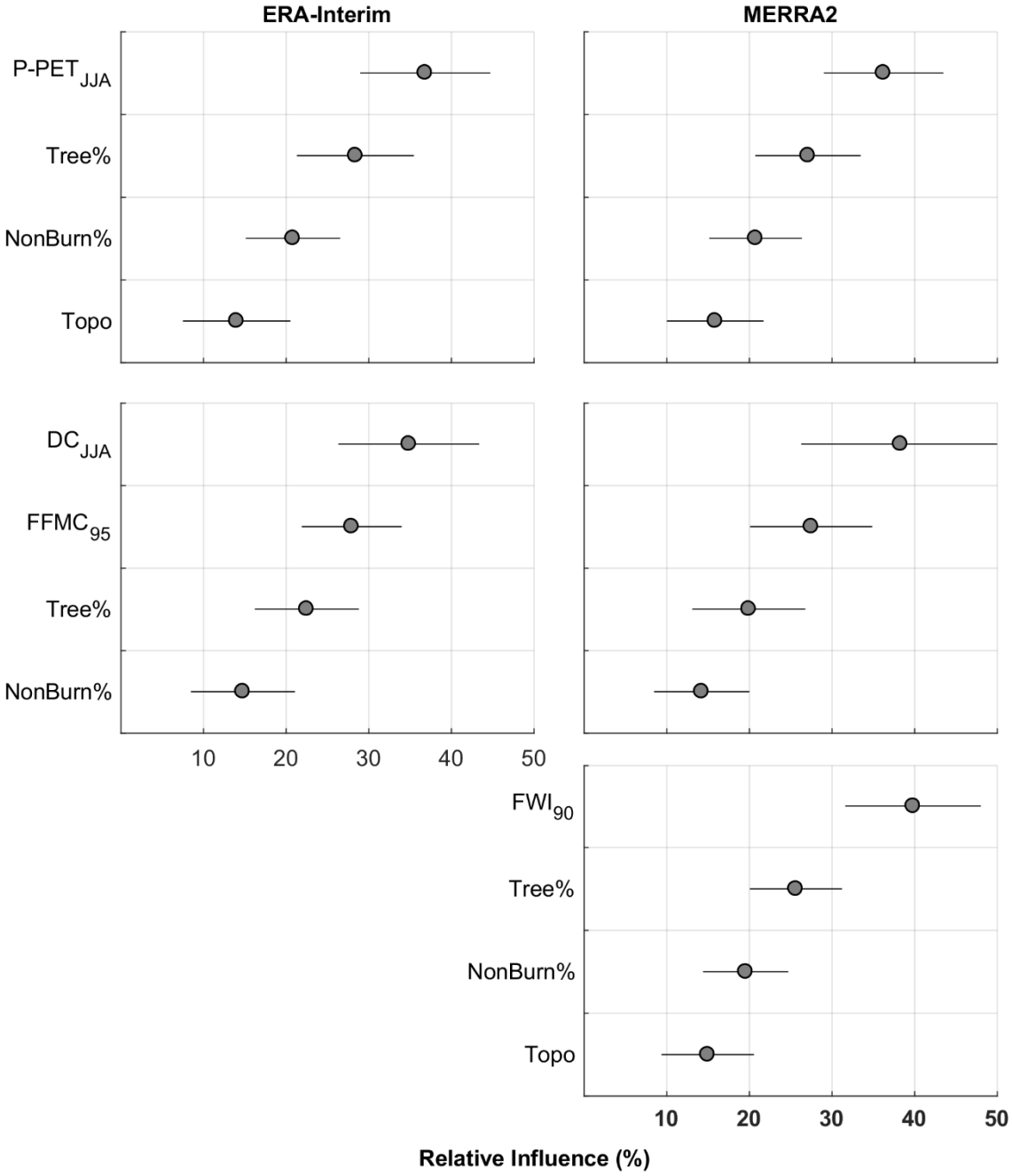

Figure B.1. Relative influence plots for different sets of explanatory variables in our Boosted Regression Tree analysis. Gray circles represent the average relative influence for 50 BRTs (±2 SD). **P-PET$_{JJA}$** = total summer (JJA) precipitation minus potential evapotranspiration; **DC$_{JJA}$** = average summer drought code; **FWI$_{90}$** = 90th-percentile of the daily fire weather index. The MERRA2 and ERAI designations (titles in each column) are only for DC$_{JJA}$ and FWI$_{90}$ variables. P-PET$_{JJA}$ were calculated using CRU TS4.01 climate data. Each row depicts results for a different climate variable.

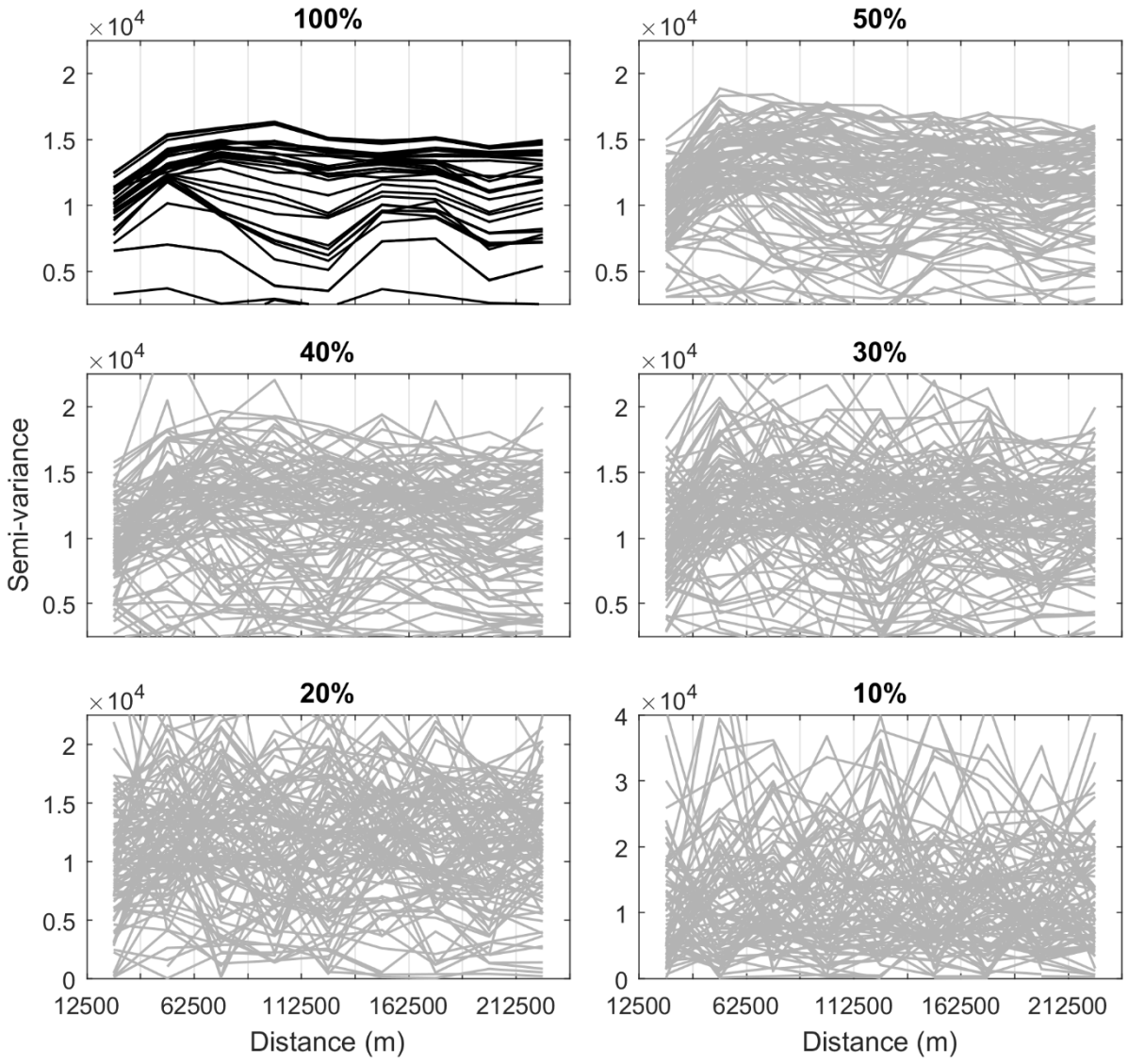

Figure B.2. Empirical semi-variograms depicting spatial covariance among hexel burned areas for individual years. The title to each panel represents different randomized sub-sampling rates. For the 100% subsampling rate, we used all available hexels in each year, with each year represented by a different black line (n = 36 yr). For the different subsampling rates, we randomly selected hexels without replacement from the entire population, recalculating and recording the empirical semi-variance for each sample. Results depicted here represent 100 randomized samples. Gray lines depict individual year from the random samples.

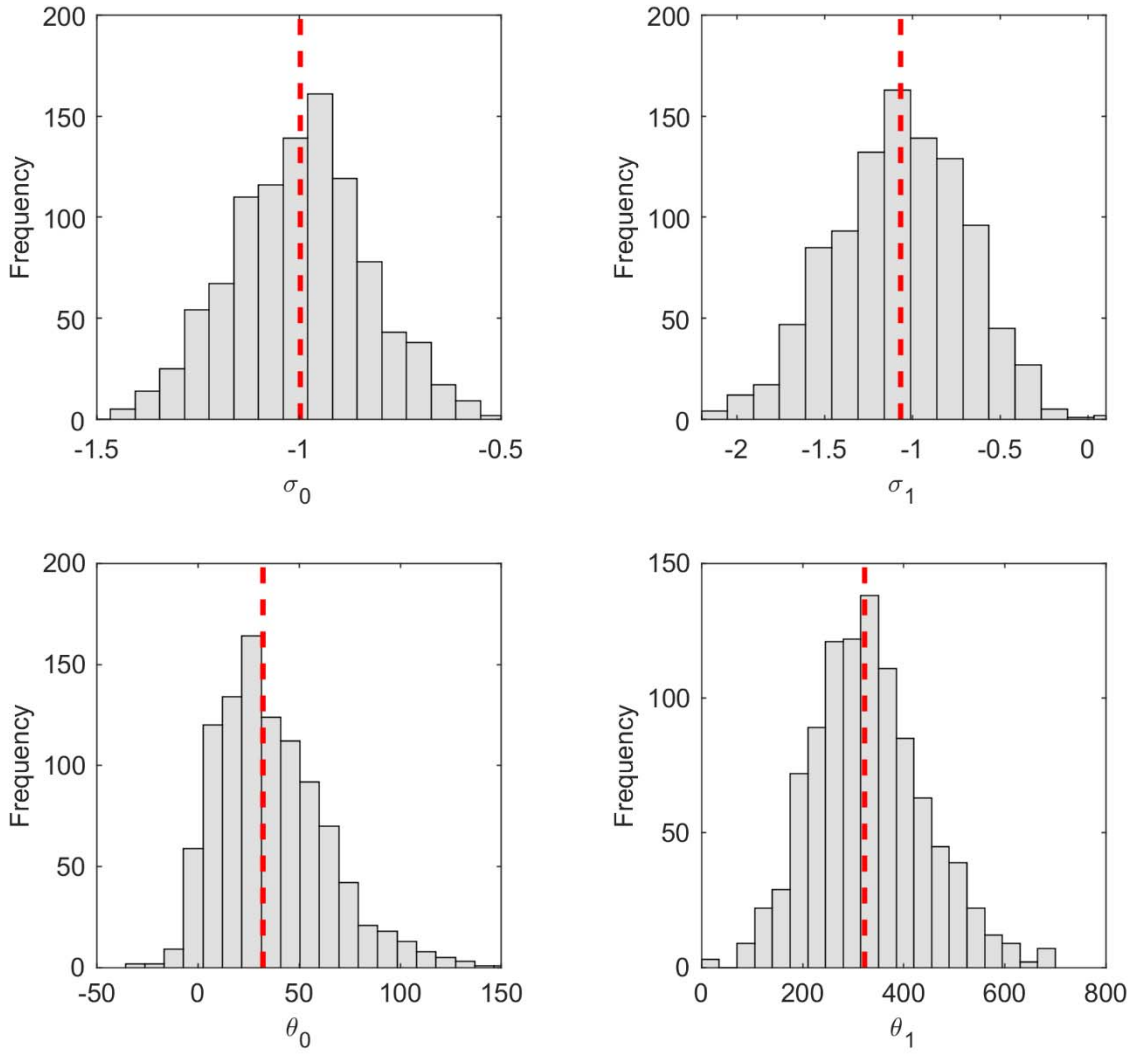

Figure B.3. Sampling distribution for the truncated-tapered Pareto parameters, defined in Eqns. 2.2 and 2.3. Parameter estimates were obtained using MLE 1000 times for different subsets of randomly sampled single-burned hexels. Horizontal red lines indicate the median of each sampling distribution, the value used when applying the truncated-tapered Pareto model to predict distributions of area burned.

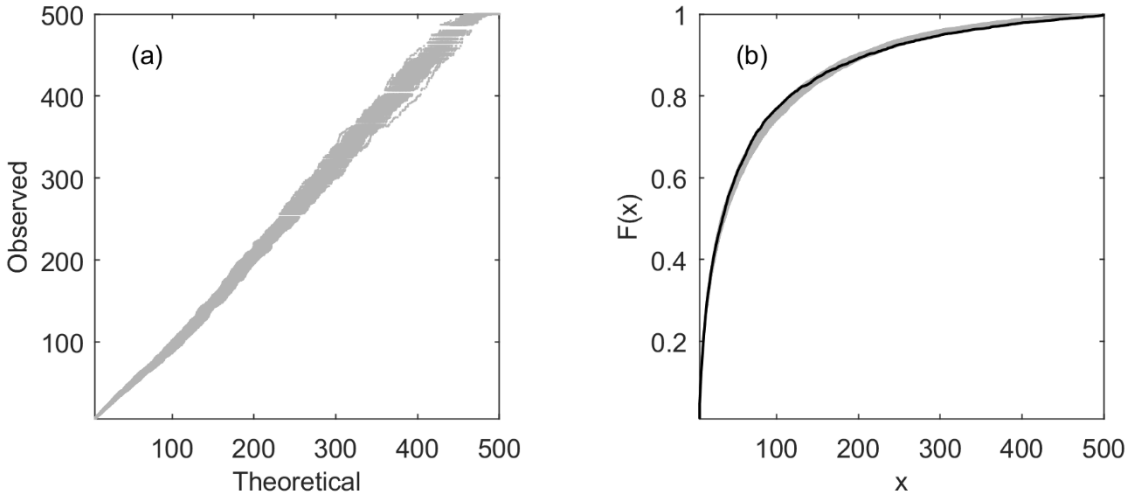

Figure B.4. Goodness of fit evaluation for the truncated-tapered Pareto distribution. (a) QQ-plots between the distribution of observed single-burned hexels (n = 4557, the entire dataset when using the 99th-percentile lower cutoff value), and 100 individual sets of randomly sampled realizations from a truncated-tapered Pareto distribution (gray dots). Each of these random samples was of size n. (b) Same data used in (a), but using CDFs to visualize goodness of fit (black lines = observed, gray lines = simulated).

Appendix C: Supplementary information for Chapter 3

Appendix C.1: Ranking Global Climate Model (GCM) performance in Alaska

GCM and observational data

The goal of this ranking analysis was to select global climate models (GCMs) that most credibly simulated July temperature and total annual precipitation in mainland Alaska. GCM credibility was assessed by comparing model output to observational data from 1951-2000 CE. The GCMs considered in this ranking analysis were chosen from the Earth System Grid Federation (https://www.earthsystemcog.org/projects/cog/) under the following criteria, they: (1) provided estimates for surface air temperature (tas) and precipitation (pr), (2) were at a monthly time frequency, and (3) were available for scenarios that covered the past millennium (850 – 1850 CE), the historical period (1851 – 2005 CE), and 21st-century projections under the Representative Concentration Pathway (RCP 8.5) (2006-2100 CE).

Observed monthly climate data were obtained from three sources: (1) Climate Research Unit time series data version 3.23 (CRUTS323, Harris et al. 2014), (2) Matsuura and Willmott (2012), and (3) the ECMWF 20th-Century Reanalysis (ERA20C; Poli et al. 2016). Additional details for these observed data are listed in Table C.1.

Quantifying GCM performance

We evaluated GCMs over a set of performance metrics (Table C.2) following Rupp et al. (2013), designed to evaluate how well GCMs simulated: (1) spatial patterns, (2) seasonal climate, (3) climatic trends, and (4) temporal variability. Prior to evaluating these metrics, we first resampled each GCM and observed dataset using bilinear interpolation to a common

spatial resolution of 2°×2°. To evaluate spatial patterns, we took 50-yr climatological normals (i.e., 1951-2000) for each individual grid cell and calculated the linear correlations between each GCM and observed dataset, treating each pixel as an observation. To evaluate seasonal climate, we calculated the root mean square error (*RMSE*, Eqn. C.1) between observed and predicted monthly climatological normals. Here, we averaged across all pixels in mainland Alaska and all 50 yr, thus providing a single value for each month and variable in Alaska. Specifically, for the j^{th} GCM, the *RMSE* was defined as

$$RMSE_j = \sqrt{n^{-1}\sum_{i=1}^{n}\left(x_{i,j} - x_{i,obs}\right)^2} \tag{C.1}$$

Here, n is equal to the number of months, $x_{i\,j}$ is the GCM-derived estimate for the i^{th} month, and $x_{i,obs}$ is the observed. Prior to calculating *RMSE*, monthly climatic averages were standardized by subtracting (dividing) the 1951-2000 12-month average for temperature (total precipitation). Trends for 1951-2000 were calculated by averaging across all months and grid points for each individual year from 1950-1999, and then estimating the slope parameter from a simple linear regression between year and climate. Finally, to measure temporal variability, we calculated two different metrics: standard deviation (*SD*) for temperature and the coefficient of variation (i.e., $CV = SD/\bar{x}$) for precipitation, at two different timescales: annual and decadal.

To quantify GCM performance, we used a relative error metric (Eqn. C.2; defined in Rupp et al. [2013]). This metric normalizes a measure of absolute error between GCM and observed estimates. To calculate relative error for a given metric, first, absolute error is calculated

$$e_{i,j} = \left| x_{i,j} - x_{i,obs} \right|$$

Here, $x_{i,j}$ is the j^{th} GCM-estimate for the i^{th} of ten metrics (Table C.2), and $x_{i,obs}$ is the estimate for a given observed dataset. This absolute error is normalized

$$e^{*}_{i,j} = \frac{e_{i,j} - \min(E)}{\max(E) - \min(E)} \tag{C.2}$$

Here, E is a set of the n absolute error values from all performance metrics (i.e., $E = \{e_{1,j}, e_{2,j}, \ldots, e_{n,j}\}$). For each observed dataset, each GCM was given a total relative error score, equal to the total summation across of ten performance metrics

$$E_{tot,j} = \sum_{i=1}^{10} e^{*}_{i,j}$$

Finally, the average relative error was calculated summed across all observed datasets (i.e., $n = 3$), proving a single metric of relative performance for each GCM (Table C.3).

Summary of ranking results

From our ranking analysis, the GISS-E2-R had the best overall performance, with an average (SD) total relative error score of 3.24 (0.71) (Table C.3). Comparatively, the GCMs with the next-best performances were the MPI-ESM-P and MRI-CGCM3, with average (SD) total relative error scores of 3.79 (1.34) and 4.38 (0.63), respectively (Table C.3). The MIROC-ESM appeared to have the lowest overall performance among all five GCMs, with an average (SD) total relative error score of 6.85 (0.65) (Table C.3). To aid in evaluation of the relative performance of each GCM, we provide visualizations depicting GCM- and

observationally derived estimates for climatic spatial patterns (Figures C.1 & C.2), seasonal climate (Figure C.3), annual trends (Figure C.4), temporal variability (Figure C.5), as well as the relative error score for each of these metrics (Figure C.6).

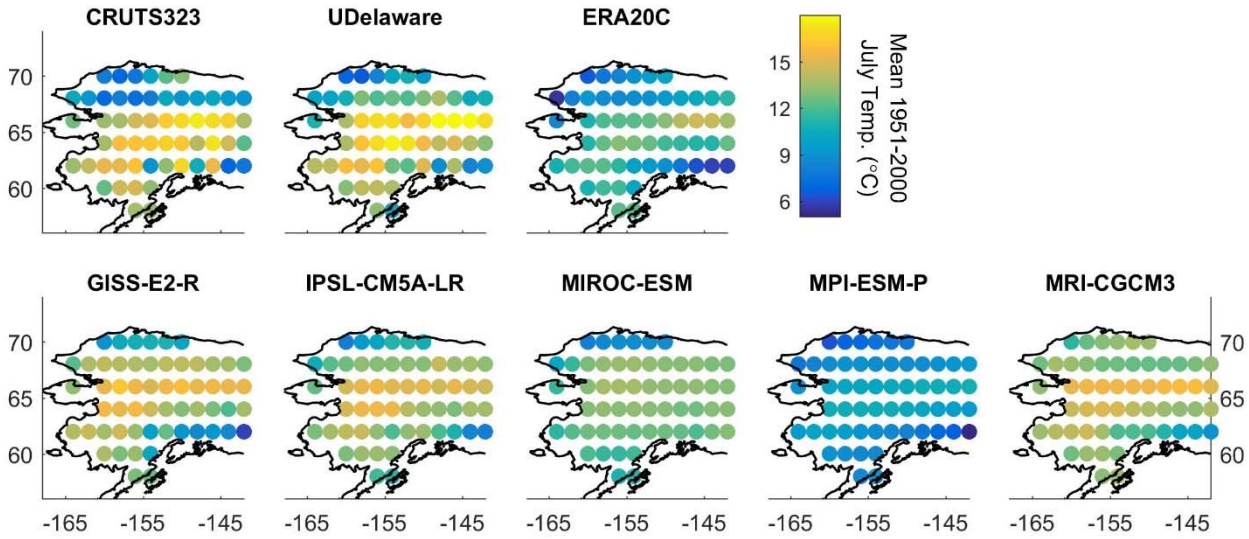

Figure C.1. Spatial patterns in mean July temperature (1951-2000) obtained from observed (first row) and GCM (second row) estimates.

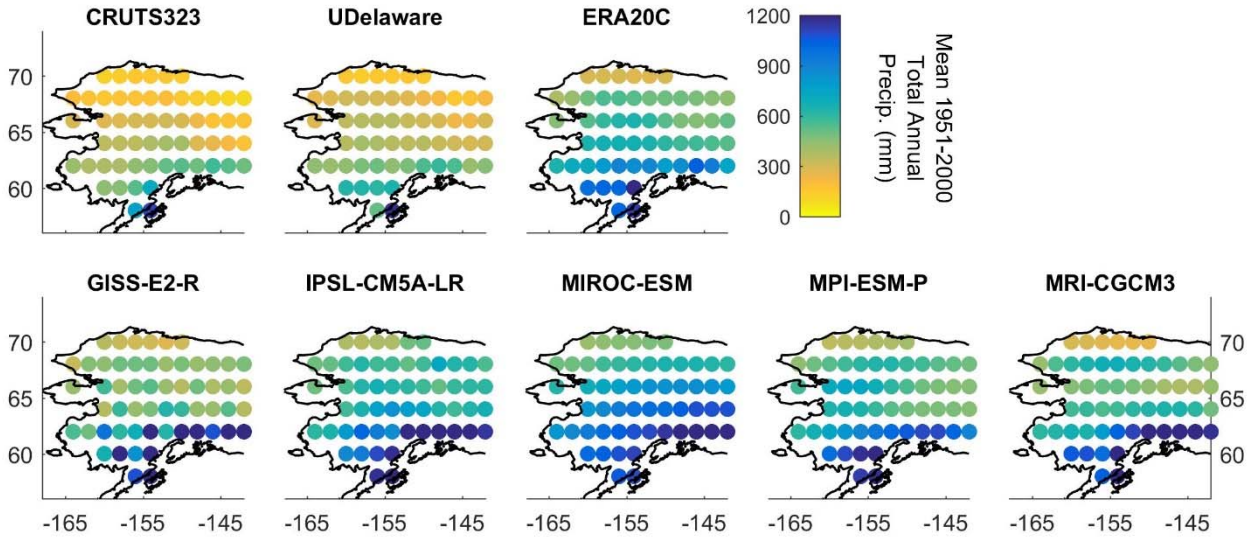

Figure C.2. Spatial patterns in mean total annual precipitation (1951-2000) obtained from observed (first row) and GCM (second row) estimates.

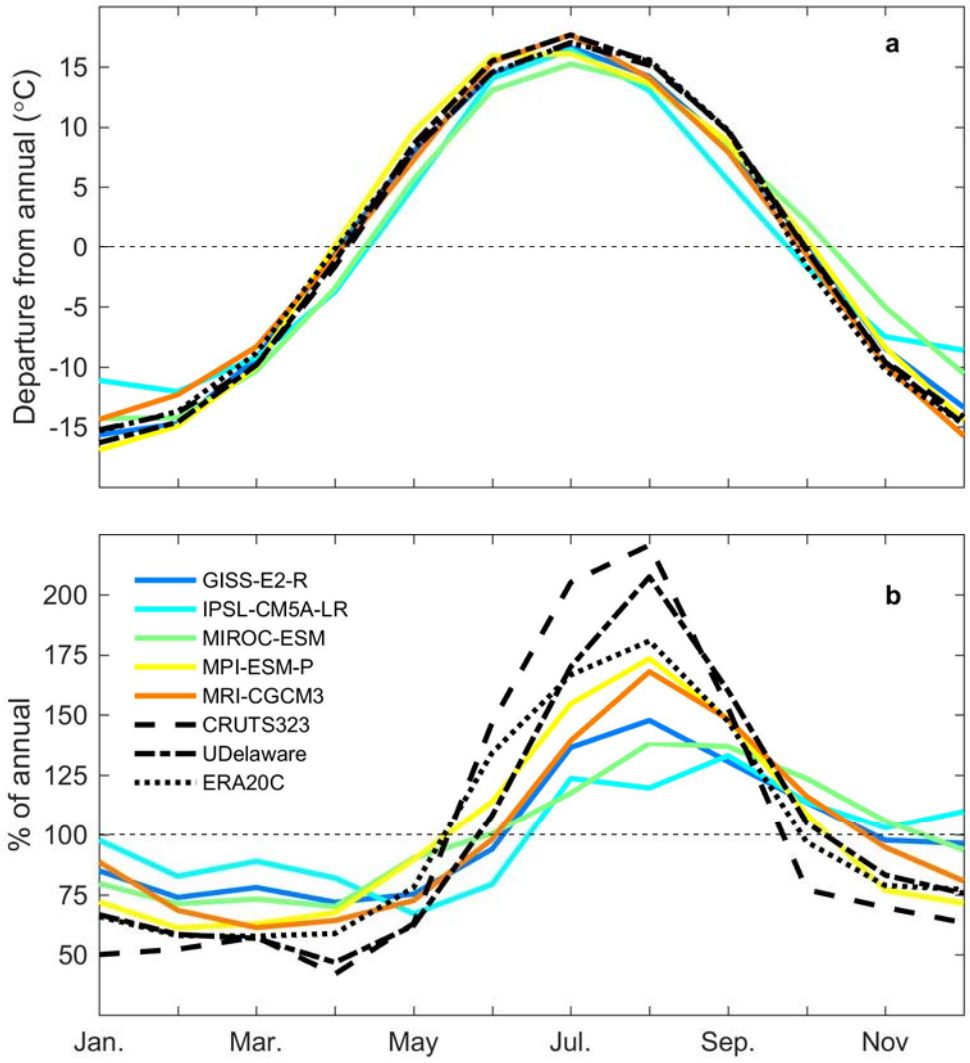

Figure C.3. Average seasonal climatological patterns of (a) monthly mean temperature and (b) total precipitation (1951-2000).

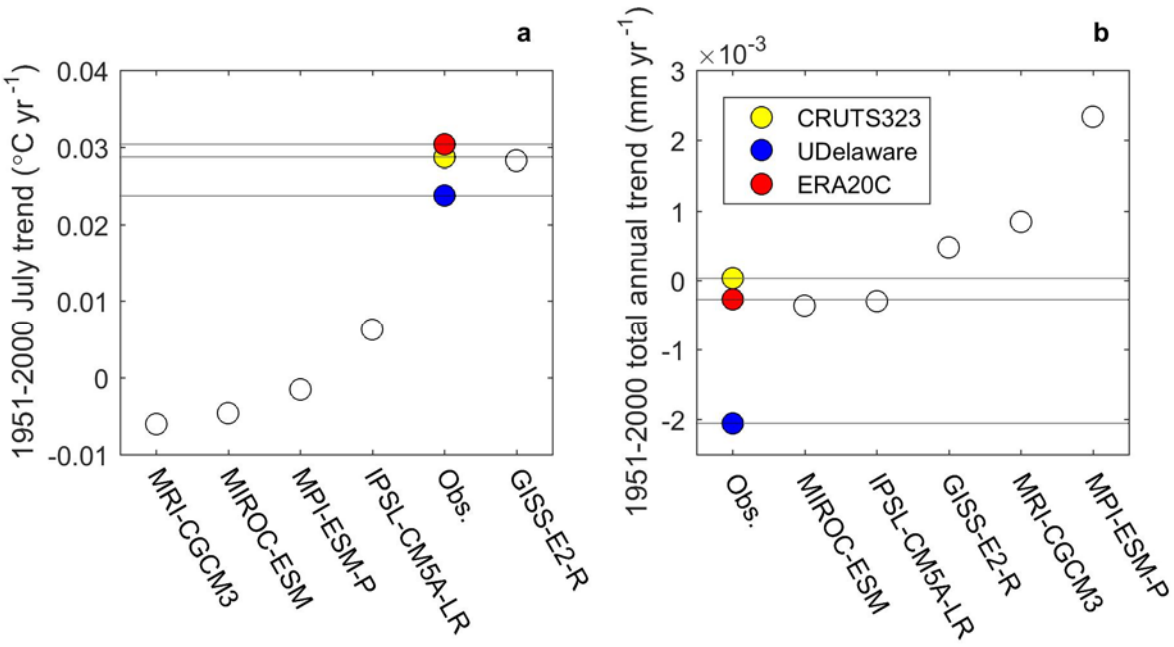

Figure C.4. Fifty-year linear trends for (a) July temperature and (b) total annual precipitation.

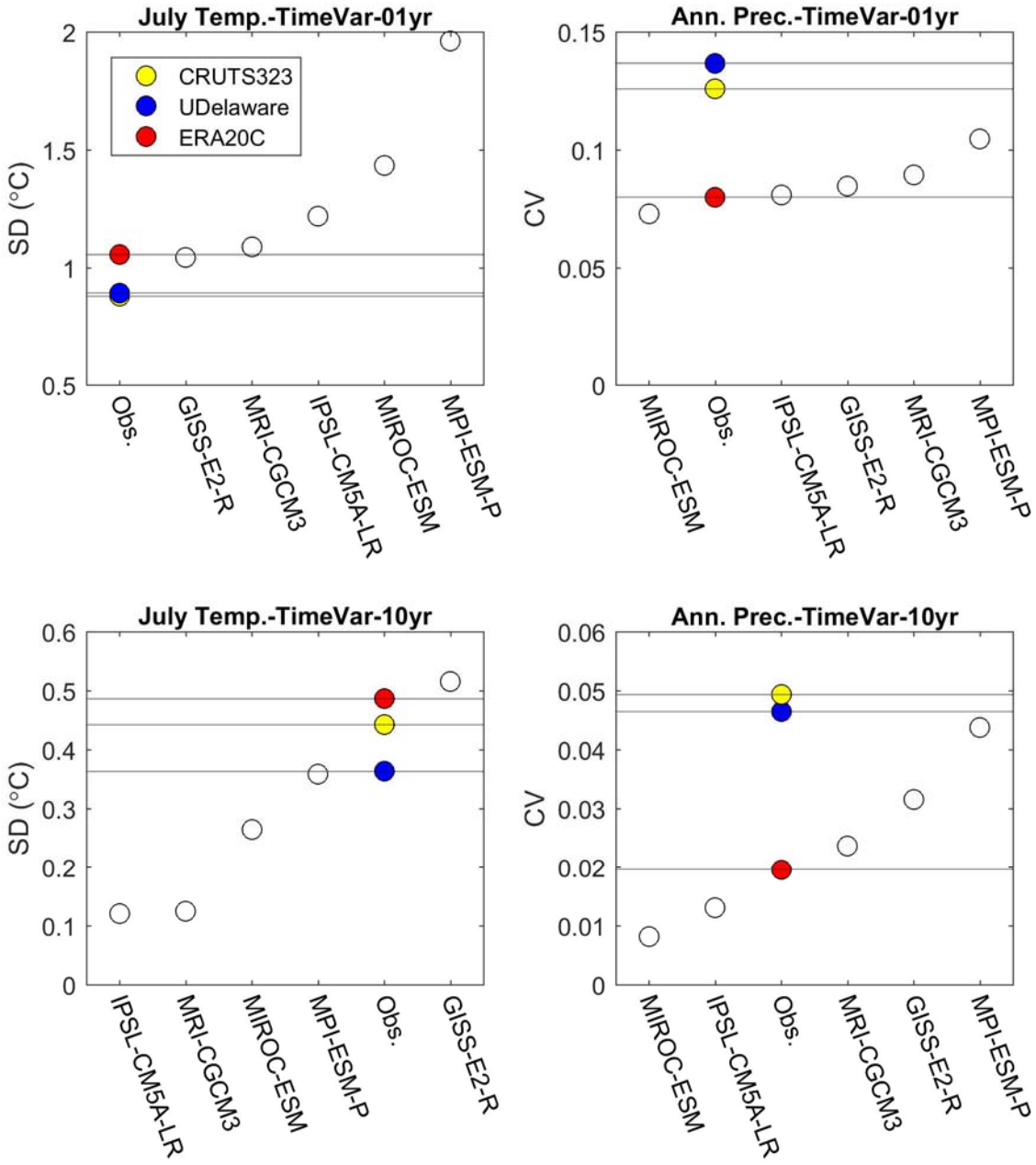

Figure C.5. Annual (top row) and decadal (bottom row) variability for July temperature (left column) and total annual precipitation (right column), 1951-2000.

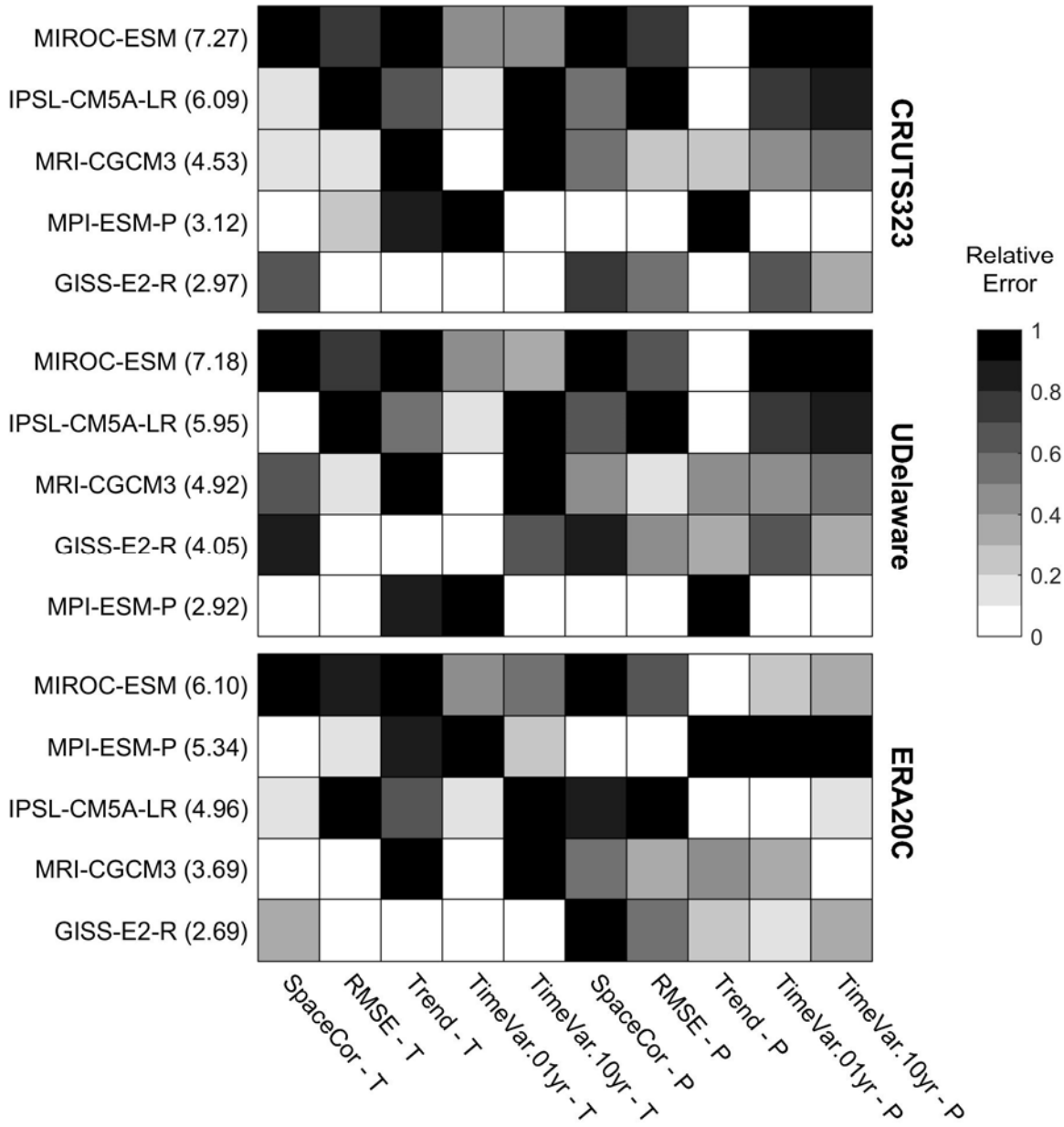

Figure C.6. Relative error for each metric and GCM among all three observational datasets. The relative error for each metric is unitless and on a scale from 0-1. For each observational dataset, GCMs are listed in the rows in descending order from least-to-most skillful, according to the total relative error (highlighted in parentheses).

Table C.1. Details for the five GCMs used in our ranking analysis and the 3 observed datasets. All GCMs are under the first ensemble member (i.e., r1i1p1), except GISS-E2-R (r1i1p124).

	Dataset name	Source	Spatial resolution (Lon. × Lat.)	Temporal coverage past1000/historical (yyyymm)
Observed	CRUTS323	Climate Research Unit Time Series version 3.23, University of East Anglia	0.5 × 0.5	NA/ 190101-201412
	UDelaware	Gridded Monthly Time Series Data from Matsuura & Willmott (2012), University of Delaware	0.5 × 0.5	NA/ 190001-201412
	ERA20C	European Centre for Medium-Range Weather Forecasts	1.0 × 1.0	NA/ 190001-201012
GCM	GISS-E2-R	NASA Goddard Institute for Space Studies, USA	2.5 × 2.0	085001-185012/ 185101-200512
	IPSL-CM5A-LR	Institut Pierre Simon Laplace, France	3.8 × 1.9	085001-185012/ 185001-200512
	MIROC-ESM	Japan Agency for Marine-Earth Science and Technology, Atmosphere and Ocean Research Institute (The Univ. of Tokyo), and National Institute for Environmental Studies	2.8 × 2.8	085001-184912/ 185001-200512
	MPI-ESM-P & MPI-ESM-LR†	Max Planck Institute for Meteorology, Germany	1.88 × 1.87	085001-184912/ 185001-200512
	MRI-CGCM3	Meteorological Research Institute, Japan	1.1 × 1.1	085001-185012/ 185001-200512

† MPI-ESM-P was used to obtain projections for the past1000 (850-1850 CE) and historical experiments (1850-2000 CE). The MPI-ESM-LR GCM was used for future projections (e.g., RCP 8.5, 2006-2100).

Table C.2. Performance metrics to evaluate GCM skill in Alaska from 1951-2000. *V*: Climate variable (P = Total annual precipitation, T = Mean July temperature).

Performance metric	Description
SpaceCor. – *V*	Spatial correlation between observed and GCM climatological normals (1951-2000)
RMSE – *V*	Root Mean Squared Error of monthly climate averages (Eq. 1)
Trend – *V*	Annual trend (1951-2000)
TimeVar.01yr. – *V*	Annual temporal variability (*SD* for T; *CV* for P)
TimeVar.10yr. – *V*	Decadal temporal variability (*SD* for T; *CV* for P)

Table C.3. Summary of total relative errors for each GCM and observational dataset. Mean and SD indicate total relative error averages and standard deviations among all three observational datasets for each GCM.

		Observed				
		CRUTS323	UDelaware	ERA20C	**Mean**	**SD**
GCM	GISS-E2-R	2.97	4.05	2.69	3.24	0.71
	IPSL-CM5A-LR	6.09	5.95	4.96	5.67	0.62
	MIROC-ESM	7.27	7.18	6.10	6.85	0.65
	MPI-ESM-P	3.12	2.92	5.34	3.79	1.34
	MRI-CGCM3	4.53	4.92	3.69	4.38	0.63

Appendix C.2: Bias-correcting and downscaling GCM data in Alaska

We bias-corrected coarse resolution (i.e., >1°) GCM output to the native 2-km resolution of the modern climate data using the delta-change method (Giorgi and Mearns, 1991). This method bilinearly interpolates monthly GCM anomalies (differences for temperature, ratios for precipitation, relative to a 1961-1990 baseline) to gridded 2-km observational climate normals for 1961-1990. Here, we use the Parameter-elevation Regressions on Independent Slopes Model (PRISM) as our observational dataset in the downscaling process (Daly et al. 2008; PRISM Climate Group, Oregon State University, http://prism.oregonstate.edu, accessed September 4, 2011). We chose to use this downscaling method and observational dataset as they are identical to methods used by the Scenarios Network for Alaska and Arctic Planning (2015a,b), and thus also used in Young et al. (2017). Alternative bias-correcting methods that correct for the cumulative distribution of data (e.g., Wood et al. 2002; Pierce et al. 2015) were not selected given our interest in only capturing low-frequency (>30 year) changes in climate normals, rather than aspects of interannual and higher-frequency variability.

Appendix C.3: Metadata and additional details for Alaskan paleo-fire-history records

Table C.4 Details for each of the 29 paleo-fire-history reconstructions used for model validation.

Site name	Lat., Lon. (decimal deg.)	Ecoregion	Oldest fire in analysis (yr CE)	Fire freq. 850-1850 CE (#/1000 yr)	Source
Chopper	66.00N, 156.28W	Yukon Flats	958	9	Kelly et al. 2013
Epilobium	65.97N, 145.57W	Yukon Flats	1039	6	Kelly et al. 2013
Granger	66.06N, 145.65W	Yukon Flats	878	13	Kelly et al. 2013
Jonah	66.07N, 145.09W	Yukon Flats	868	15	Kelly et al. 2013
Landing	65.90N, 145.78W	Yukon Flats	1048	4	Kelly et al. 2013
Latitude	65.93N, 146.14W	Yukon Flats	968	11	Kelly et al. 2013
Lucky	66.02N, 145.53W	Yukon Flats	998	9	Kelly et al. 2013
Noir	66.00N, 145.93W	Yukon Flats	1018	5	Kelly et al. 2013
Picea	65.88N, 145.59W	Yukon Flats	858	8	Kelly et al. 2013
Reunion	66.02N, 146.12W	Yukon Flats	879	8	Kelly et al. 2013
Robinson	65.97N, 145.70W	Yukon Flats	859	9	Kelly et al. 2013
Screaming Lynx	66.07N, 145.40W	Yukon Flats	1377	7	Kelly et al. 2013
West Crazy	65.89N, 145.62W	Yukon Flats	1127	7	Kelly et al. 2013
Windy	66.04N, 145.76W	Yukon Flats	868	6	Kelly et al. 2013
Crater	62.10N, 146.24W	Copper River Basin	1331	3	Barrett et al. 2013
Hudson	61.88N, 145.67W	Copper River Basin	986	3	Barrett et al. 2013
Minnesota Plateau	62.54N, 146.24W	Copper River Basin	881	6	Barrett et al. 2013
Super Cub	62.30N, 145.35W	Copper River Basin	896	3	Barrett et al. 2013
Code	67.16N, 151.86W	Kobuk Valley	936	7	Higuera et al. 2009
Ruppert	67.07N, 154.25W	Kobuk Valley	967	4	Higuera et al. 2009
Wild Tussock	67.13N, 151.38W	Kobuk Valley	937	6	Higuera et al. 2009
Little Isac	67.94N, 160.80W	Noatak	912	3	Higuera et al. 2011
Poktovik	68.03N, 161.38W	Noatak	897	5	Higuera et al. 2011
Raven	68.01N, 162.04W	Noatak	957	5	Higuera et al. 2011
Uchugrak	68.05N, 161.73W	Noatak	987	7	Higuera et al. 2011
Keche	68.02N, 146.92W	Brooks Range	1068	1	Chipman et al. 2015
Perch	68.94N, 150.50W	Brooks Foothills	-4586	0	Hu et al. 2010, Chipman et al. 2015
Upper Capsule	68.63N, 149.41W	Brooks Foothills	-4550	0	Chipman et al. 2015
Tungak	61.43N, 164.20W	Yukon-Kusk. Delta	-5019	0	Chipman et al. 2015

Appendix C.4: Modifying the shape of fire-temperature relationships

To modify the shape of the original fire-temperature relationship in Alaska (Figure 3.2c), we artificially increased the number of fire occurrences over a pre-specified temperature range. Specifically, our goal was to incrementally linearize this relationship, so we chose a temperature range that spanned the threshold response at 13.4 °C, here 7-15 °C. Across this range, we selected all available observations where fire had not occurred (i.e., fire absence), and then randomly selected a given number of these absences and "switched" them to fire occurrences. The number of switches was done at three different levels to proportionally increase the total number of fire occurrences in Alaska by 5%, 10%, and 25%. Across the 7-15 °C temperature range, the number of absences switched to occurrences was not uniformly distributed, but rather weighted to switch more observations under warmer temperatures and less under cooler temperatures. This weighting was accomplished by employing a Beta probability density function. We set Beta parameters to $\alpha = 3$ and $\beta = 1$, and under this setting we rescaled Beta quantiles (naturally spanning 0-to-1) to the scale of the temperature range (7-15 °C). Under this rescaling, probability density values were associated with a given temperature and used as the weights for random selection of fire absence. The three modified fire-temperature relationships were created by increasing total fire occurrences in Alaska by 5%, 10%, and 25% are designated by Shape 1-Shape 3 (Figure C.7).

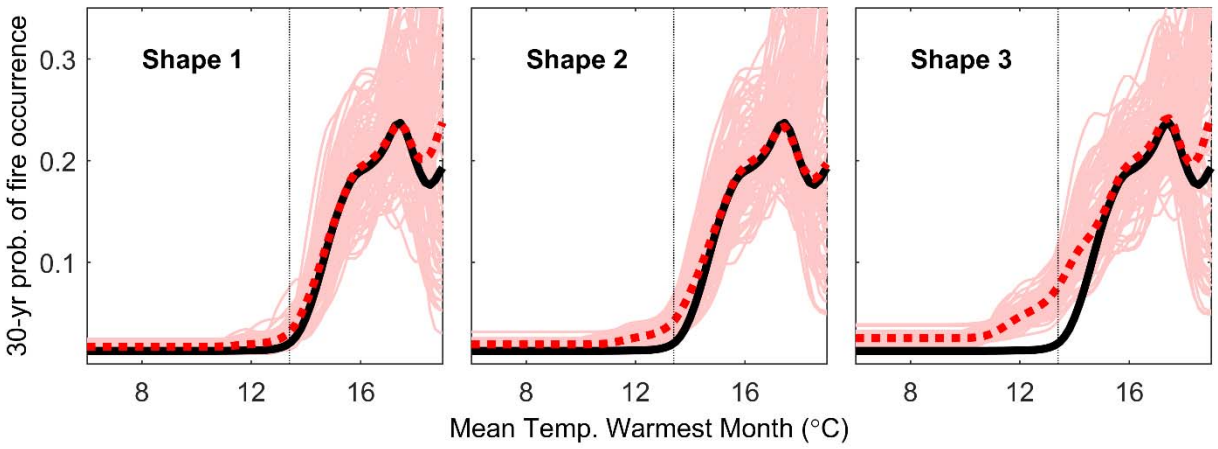

Figure C.7. Three modified relationships (Shape 1 - Shape 3) used in the sensitivity analysis. The black line is the median prediction of the 100 BRTs from the original relationship (i.e., unmodified). The dashed red line is the median prediction for the modified relationship, and the light pink lines are the predictions for individual, modified BRTs. The vertical line indicates the estimated threshold value under the original fire-temperature relationship (i.e., 13.4 °C).

Appendix C.5: GCM output for the past 1000 years

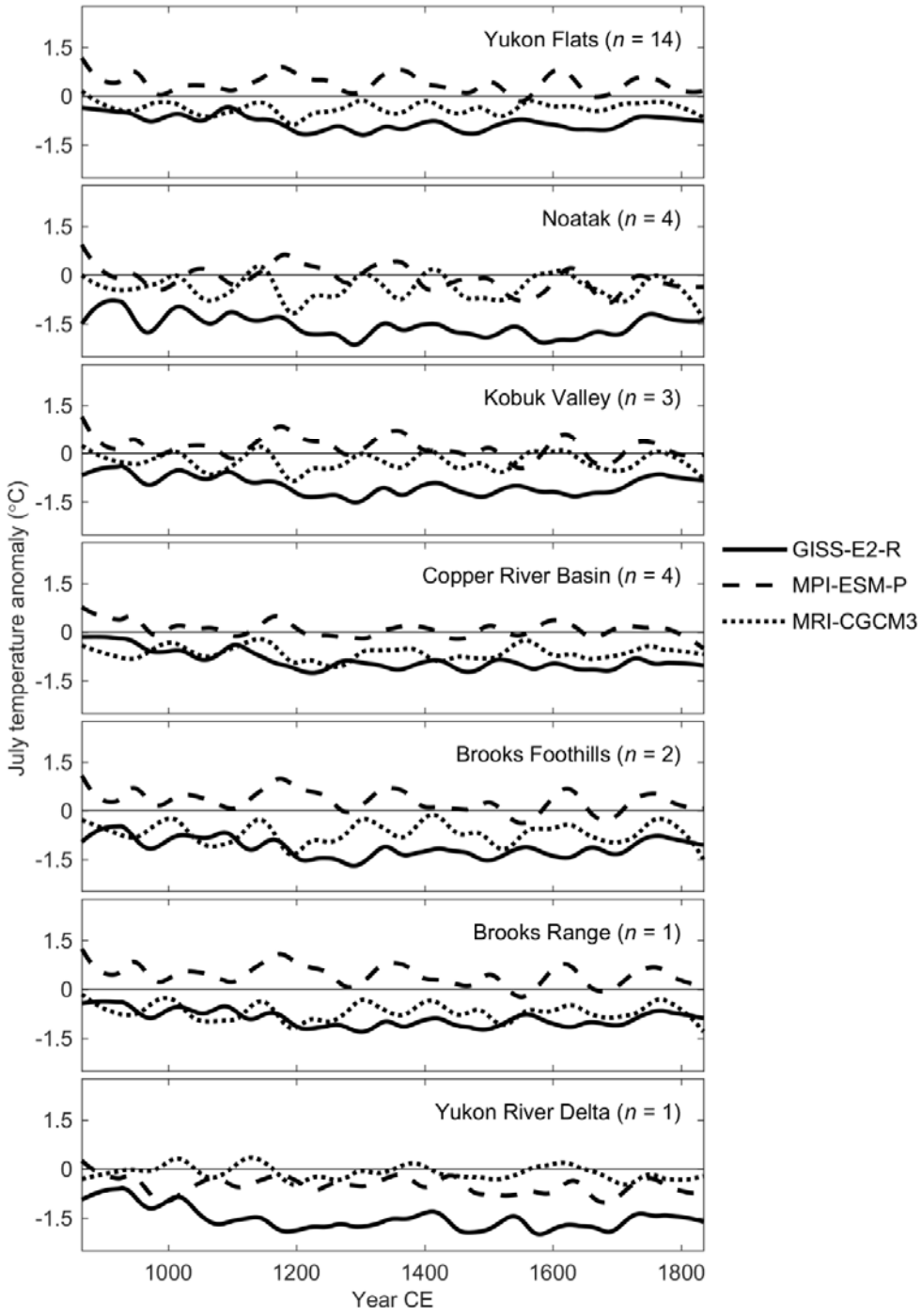

Figure C.8. July temperature anomalies from 850-1850 CE for each GCM, relative to a 1971-2000 baseline period. Values for each GCM are the average from among all lakes in each ecoregion, where the number of lakes in each ecoregion is displayed in parentheses. Time series are smoothed using a locally weighted regression (span = 0.15, approximately 150 yr).

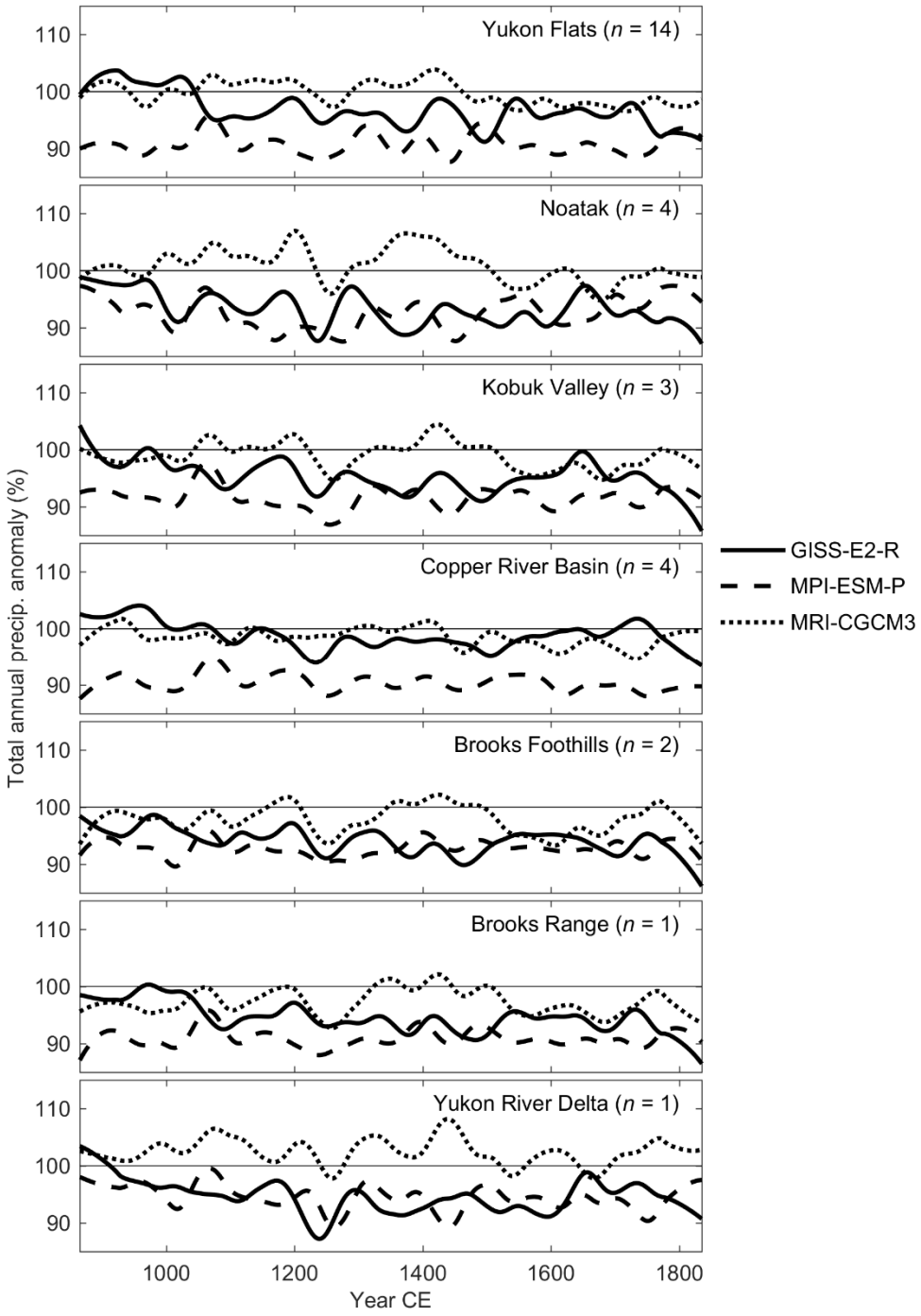

Figure C.9. Total annual precipitation anomalies (%) from 850-1850 CE for each GCM, relative to a 1971-2000 baseline period. Values for each GCM are the average from among all lakes in each ecoregion, where the number of lakes in each ecoregion is displayed in parentheses. Time series are smoothed using a locally weighted regression (span = 0.15, approximately 150 yr).

Appendix C.6: Comparing GCM and paleo-proxy temperatures, 850-1850 CE

To identify potential biases in past-millennium GCM projections, we compared our downscaled GCM temperature estimates for 850-1850 CE (Appendix C.2) with paleo-climate reconstructions. To conduct these comparisons, we selected seven paleo-temperature reconstructions from Alaska (Table C.5), bias-correcting each of these records relative to downscaled CRU Time Series temperature data for 1901-2005 (Harris et al., 2014; Scenarios Network for Alaska and Arctic Planning 2015a). Specifically, we added the average temperature difference between observed and proxy temperatures for 1901-2005 CE to the original paleo-temperature estimates. Tree-ring-based records provide reconstructions for average May-August temperature, while midge-based records provide reconstructions for July temperature. Additionally, for midge-based temperature reconstructions (Table C.5), we linearly interpolated temperature estimates between individual samples in the paleo-record to an annual timescale. Annual differences were subsequently taken between paleo-reconstructed and GCM-derived temperatures and summarized for 850-1850 CE (Table C.6). These GCM- and paleo-derived temperatures are further visualized in Figure C.10.

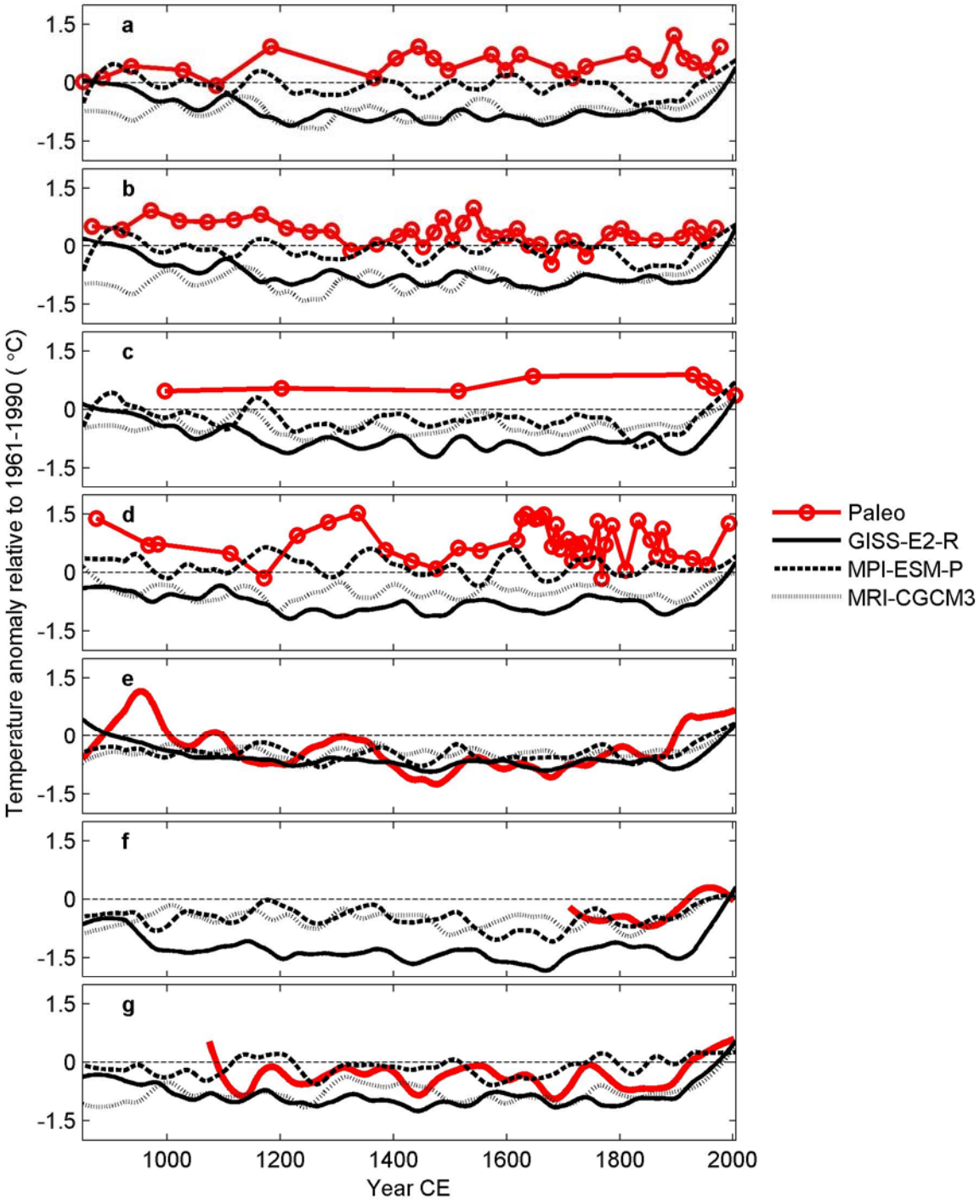

Figure C.10. Time-series for paleo- and GCM-derived temperatures for the (a) Hudson, (b) Moose, (c) Rainbow, (d) Screaming Lynx, (e) Gulf of Alaska, (f) Seward Peninsula, and (g) Firth River sites. GCM temperatures were smoothed using locally weighted regression (loess) with a span of 0.13 (≈150 yr), and tree-ring temperatures (e-g) were similarly smoothed. For midge-based reconstructions (a-d), the locations of individual samples in the records are indicated by open circles.

Table C.5. Details for the seven paleo-proxy climate records used to assess potential GCM temperature biases from 850-1850 CE. All midge-based records were downloaded from the NOAA National Centers for Environmental Information (https://www.ncdc.noaa.gov/data-access/paleoclimatology-data). Tree-ring records were downloaded from the Northern Hemisphere Tree-Ring Network Development (N-TREND) consortium (Wilson et al., 2016; https://ntrenddendro.wordpress.com/).

Site name	Lat., Lon. (decimal degrees)	Method	Time period covered	Source
Hudson	61.90N, 145.67W	Midge	7624 BCE to 1978 CE	Clegg et al. (2011)
Moose	61.37N, 143.60W	Midge	4508 BCE to 1970 CE	Clegg et al. (2010)
Rainbow	60.72N, 150.80W	Midge	11556 BCE to 2004 CE	Clegg et al. (2011)
Screaming Lynx	66.07N, 145.40W	Midge	8661 BCE to 1993 CE	Clegg et al. (2011)
Gulf of Alaska	Multiple locations[a]	Tree ring	800 to 2010 CE	Wiles et al. (2014)
Seward Peninsula	Multiple locations[b]	Tree ring	1710 to 2001 CE	D'Arrigo et al. (2004)
Firth River	68.39N, 141.38W	Tree ring	1073 to 2011 CE	Anchukaitis et al. (2013)

[a]Bounding box: NW corner = 61.11N, 149.00W, SE corner = 60.00N, 141.68W.
[b]Bounding box: NW corner = 65.22N, 162.27W, SE corner = 65.11N, 162.18W.

Table C.6. Temperature differences between paleo- and GCM-derived temperatures (i.e., paleo minus GCM estimates) averaged over the time period of 850-1850 CE.

Site name	GCM	Paleo – GCM temperature differences Mean ± SD (°C)
Hudson	GISS-E2-R	1.20 ± 1.21
	MPI-ESM-P	0.55 ± 1.97
	MRI-CGCM3	1.21 ±1.36
Moose	GISS-E2-R	1.11 ± 1.22
	MPI-ESM-P	0.46 ± 2.00
	MRI-CGCM3	1.28 ± 1.53
Rainbow	GISS-E2-R	1.45 ± 1.19
	MPI-ESM-P	0.93 ± 2.00
	MRI-CGCM3	1.06 ± 1.15
Screaming Lynx	GISS-E2-R	1.51 ± 1.32
	MPI-ESM-P	0.56 ± 1.95
	MRI-CGCM3	1.22 ± 1.47
Gulf of Alaska	GISS-E2-R	0.23 ± 1.11
	MPI-ESM-P	0.10 ± 1.41
	MRI-CGCM3	0.08 ± 1.22
Seward Peninsula	GISS-E2-R	0.78 ± 1.44
	MPI-ESM-P	0.06 ± 1.66
	MRI-CGCM3	0.18 ± 1.36
Firth River	GISS-E2-R	0.54 ± 1.55
	MPI-ESM-P	-0.25 ± 1.59
	MRI-CGCM3	0.41 ± 1.60

Appendix C.7: References

Anchukaitis, K. J., R. D. D'Arrigo, L. Andreu-Hayles, D. Frank, A. Verstege, A. Curtis, B. M. Buckley, G. C. Jacoby, and E. R. Cook. 2013. Tree-ring-reconstructed summer temperatures from northwestern North America during the last nine centuries. Journal of Climate **26**:3001-3012.

Barrett, C. M., R. Kelly, P. E. Higuera, and F. S. Hu. 2013. Climatic and land cover influences on the spatiotemporal dynamics of Holocene boreal fire regimes. Ecology **94**:389-402.

Chipman, M. L., V. Hudspith, P. E. Higuera, P. A. Duffy, R. Kelly, W. W. Oswald, and F. S. Hu. 2015. Spatiotemporal patterns of tundra fires: Late-Quaternary charcoal records from Alaska. Biogeosciences **12**:4017-4027.

Clegg, B. F., G. H. Clarke, M. L. Chipman, M. Chou, I. R. Walker, W. Tinner, and F. S. Hu. 2010. Six millennia of summer temperature variation based on midge analysis of lake sediments from Alaska. Quaternary Science Reviews **29**:3308-3316.

Clegg, B. F., R. Kelly, G. H. Clarke, I. R. Walker, and F. S. Hu. 2011. Nonlinear response of summer temperature to Holocene insolation forcing in Alaska. Proceedings of the National Academy of Sciences of the United States of America **108**:19299-19304.

D'Arrigo, R., E. Mashig, D. Frank, G. Jacoby, and R. Wilson. 2004. Reconstructed warm season temperatures for Nome, Seward Peninsula, Alaska. Geophysical Research Letters **31**: L09202.

Daly, C., M. Halbleib, J. I. Smith, W. P. Gibson, M. K. Doggett, G. H. Taylor, J. Curtis, and P. P. Pasteris. 2008. Physiographically sensitive mapping of climatological temperature and precipitation across the conterminous United States. International Journal of Climatology **28**:2031-2064.

Giorgi, F. and L. O. Mearns. 1991. Approaches to the simulation of regional climate change - a review. Reviews of Geophysics **29**:191-216.

Harris, I., P. D. Jones, T. J. Osborn, and D. H. Lister. 2014. Updated high-resolution grids of monthly climatic observations - the CRU TS3.10 Dataset. International Journal of Climatology **34**:623-642.

Higuera, P. E., L. B. Brubaker, P. M. Anderson, F. S. Hu, and T. A. Brown. 2009. Vegetation mediated the impacts of postglacial climate change on fire regimes in the south-central Brooks Range, Alaska. Ecological Monographs **79**:201-219.

Higuera, P. E., M. L. Chipman, J. L. Barnes, M. A. Urban, and F. S. Hu. 2011. Variability of tundra fire regimes in Arctic Alaska: millennial scale patterns and ecological implications. Ecological Applications **21**:3211-3226.

Hu, F. S., P. E. Higuera, J. E. Walsh, W. L. Chapman, P. A. Duffy, L. B. Brubaker, and M. L. Chipman. 2010. Tundra burning in Alaska: Linkages to climatic change and sea ice retreat. Journal of Geophysical Research-Biogeosciences **115**:G04002.

Kelly, R., M. L. Chipman, P. E. Higuera, I. Stefanova, L. B. Brubaker, and F. S. Hu. 2013. Recent burning of boreal forests exceeds fire regime limits of the past 10,000 years. Proceedings of the National Academy of Sciences of the United States of America **110**:13055-13060.

Matsuura, K. and C. J. Willmott. 2012. Terrestrial Air Temperature and Precipitation: Monthly Time Series (1900 - 2010). Precipitation: http://climate.geog.udel.edu/~climate/html_pages/Global2011/README.GlobalTsP2011.html. Temperature: http://climate.geog.udel.edu/~climate/html_pages/Global2011/README.GlobalTsT2011.html

Pierce, D.W., D. R. Cayan, E. P. Maurer, J. T. Abatzoglou, and K. C. Hegewisch. 2015. Improved Bias Correction Techniques for Hydrological Simulations of Climate Change. Journal of Hydrometeorology **16**:2421-2442.

Poli, P., H. Hersbach, D. P. Dee, P. Berrisford, A. J. Simmons, F. Vitart, P. Laloyaux, D. G. H. Tan, C. Peubey, J. N. Thepaut, Y. Tremolet, E. V. Holm, M. Bonavita, L. Isaksen, and M. Fisher. 2016. ERA-20C: an atmospheric reanalysis of the twentieth century. Journal of Climate **29**:4083-4097.

Rupp, D. E., J. T. Abatzoglou, K. C. Hegewisch, and P. W. Mote. 2013. Evaluation of CMIP5 20th century climate simulations for the Pacific Northwest USA. Journal of Geophysical Research-Atmospheres **118**:10884-10906.

Scenarios Network for Alaska and Arctic Planning, University of Alaska. 2015a. Historical Monthly Temperature and Precipitation - 2 km CRU TS. Retrieved January 2015 from https://www.snap.uaf.edu/tools/data-downloads.

Scenarios Network for Alaska and Arctic Planning, University of Alaska. 2015b. Projected Monthly Temperature and Precipitation - 2 km CMIP5/AR5. Retrieved January 2015 from https://www.snap.uaf.edu/tools/data-downloads.

Wiles, G. C., R. D. D'Arrigo, D. Barclay, R. S. Wilson, S. K. Jarvis, L. Vargo, and D. Frank. 2014. Surface air temperature variability reconstructed with tree rings for the Gulf of Alaska over the past 1200 years. Holocene **24**:198-208.

Wilson, R., K. Anchukaitis, K. R. Briffa, U. Buntgen, E. Cook, R. D'Arrigo, N. Davi, J. Esper, D. Frank, B. Gunnarson, G. Hegerl, S. Helama, S. Klesse, P. J. Krusic, H. W. Linderholm, V. Myglan, T. J. Osborn, M. Rydval, L. Schneider, A. Schurer, G. Wiles, P. Zhang, and E. Zorita. 2016. Last millennium northern hemisphere summer temperatures from tree rings: Part I: The long term context. Quaternary Science Reviews **134**:1-18.

Wood, A.W., E. P. Maurer, A. Kumar, and D. P. Lettenmaier. 2002. Long-range experimental hydrologic forecasting for the eastern United States. Journal of Geophysical Research-Atmospheres **107**(D20):4429.

Young, A. M., P. E. Higuera, P. A. Duffy, and F. S. Hu. 2017. Climatic thresholds shape northern high-latitude fire regimes and imply vulnerability to future change. Ecography **40**:606-617.

Appendix D: Copyright for Ecography

Copyright statement

The inclusion of Chapter 1 (Young et al. 2017) within this dissertation is consistent with the authors' copyright agreement with the publisher (p. 160-161). Third-party use of Chapter 1, in part or entirety, must include explicit permission from the publisher. The definitive version of Young et al. (2017) is available at https://onlinelibrary.wiley.com/. Signatures have been redacted from the copyright letter for security purposes.

When referencing Chapter 1, please use the following citation:

Young, A. M., P. E. Higuera, P. A. Duffy, and F. S. Hu. 2017. Climatic thresholds shape northern high-latitude fire regimes and imply vulnerability to future climate change. Ecography **40**:606-617. doi: 10.1111/ecog.02205.

Copyright letter

Blackwell Publishing

Ecography - Exclusive Licence Form

Author's name: Philip Higuera

Author's address: Dep. of Ecosystem & Conservation Sciences
Univ. of Montana, Missoula, MT 59812-0004

Title of article ("Article"): Climatic thresholds shape northern high-latitude fire regimes and imply vulnerability to future climate change

Manuscript no. (if known): 39: 001-012; 2006

Names of all authors in the order in which they appear in the Article: Adam M. Young, Philip E. Higuera, Paul A. Duffy, Feng Sheng Hu

In order for your Article to be distributed as widely as possible in Ecography (the Journal) you grant Nordic Ecological Society and Blackwell Publishing Ltd (Blackwell Publishing) an exclusive licence to publish the above Article including the abstract in printed and electronic form, in all languages, and to administer subsidiary rights agreements with third parties for the full period of copyright and all renewals, extensions, revisions and revivals. The Article is deemed to include all material submitted for publication with the exception of Letters, and includes the text, figures, tables, author contact details and all supplementary material accompanying the Article.

Please read this form carefully, sign at the bottom (if your employer owns copyright in your work, arrange for your employer to sign where marked), and return the ORIGINAL to the address below as quickly as possible. As author, *you remain the copyright owner of the Article*, unless copyright is owned by your employer. (US Federal Government authors please note: your Article is in the public domain.)

Your Article will not be published unless an Exclusive Licence Form (ELF) has been signed and received by Blackwell Publishing.

Please note: You retain the following rights to re-use the Article, as long as you do not sell or reproduce the Article or any part of it for commercial purposes (i.e. for monetary gain on your own account or on that of a third party, or for indirect financial gain by a commercial entity). These rights apply without needing to seek permission from Blackwell Publishing.

- **Prior to acceptance:** Provided that you acknowledge that the Article has been submitted for publication in the Journal by *Nordic Ecological Society* and *Blackwell Publishing Ltd.* you may use the unpublished Article, in form and content as submitted for publication in the Journal, in the following ways:
  - you may share print or electronic copies of the Article with colleagues;
  - you may post an electronic version of the Article on your own personal website, on your employer's website/repository and on free public servers in your subject area.
- **After acceptance:** Provided that you give appropriate acknowledgement to the Journal, and Blackwell Publishing, and full bibliographic reference for the Article when it is published, you may use the accepted version of the Article as originally submitted for publication in the Journal, and updated to include any amendments made after peer review, in the following ways:
  - you may share print or electronic copies of the Article with colleagues;
  - you may use all or part of the Article and abstract, without revision or modification, in personal compilations or other publications of your own work;
  - you may use the Article within your employer's institution or company for educational or research purposes, including use in course packs;
  - 12 months after publication you may post an electronic version of the Article on your own personal website, on your employer's website/repository and on free public servers in your subject area. Electronic versions of the accepted Article must include a link to the published version of the Article together with the following text: 'The definitive version is available at www.blackwell-synergy.com'.

Please note that you are not permitted to post the Blackwell Publishing PDF version of the Article online.

All requests by third parties to re-use the Article in whole or in part will be handled by Blackwell Publishing. Any permission fees will be retained by the Journal. All requests to adapt substantial parts of the Article in another publication (including publication by Blackwell Publishing) will be subject to your approval (which is deemed to be given if we have not heard from you within 4 weeks of your approval being sought by us writing to you at your last notified address). Please address any queries to journalsrights@oxon.blackwellpublishing.com.

In signing this Agreement:

1. You hereby warrant that this Article is an original work, has not been published before and is not being considered for publication elsewhere in its final form either in printed or electronic form;
2. You hereby warrant that you have obtained permission from the copyright holder to reproduce in the Article (in all media including print and electronic form) material not owned by you, and that you have acknowledged the source;
3. You hereby warrant that this Article contains no violation of any existing copyright or other third party right or any material of an obscene, indecent, libellous or otherwise unlawful nature and that to the best of your knowledge this Article does not infringe the rights of others;

4. You hereby warrant that in the case of a multi-authored Article you have obtained, in writing, authorization to enter into this Agreement on their behalf and that all co-authors have read and agreed the terms of this Agreement;
5. You warrant that any formula or dosage given is accurate and will not if properly followed injure any person;
6. You will indemnify and keep indemnified the Editors and Blackwell Publishing against all claims and expenses (including legal costs and expenses) arising from any breach of this warranty and the other warranties on your behalf in this Agreement.

By signing this Agreement you agree that Blackwell Publishing may arrange for the Article to be:

- Published in the above Journal, and sold or distributed, on its own, or with other related material;
- Published in multi-contributor book form or other edited compilations by Blackwell Publishing;
- Reproduced and/or distributed (including the abstract) throughout the world in printed, electronic or any other medium whether now known or hereafter devised, in all languages, and to authorize third parties (including Reproduction Rights Organizations) to do the same;
- You agree to Blackwell Publishing using any images from the Article on the cover of the Journal, and in any marketing material.

You authorize Blackwell Publishing to act on your behalf to defend the copyright in the Article if anyone should infringe it, although there is no obligation on Blackwell Publishing to act in this way.

As the Author, copyright in the Article remains in your name (or your employer's name if your employer owns copyright in your work).

Blackwell Publishing undertakes that every copy of the Article published by Blackwell Publishing will include the full bibliographic reference for your Article, together with the copyright statement.

☒ **BOX A: to be completed if copyright belongs to you**

☐ **BOX B: to be completed if copyright belongs to your employer (e.g. HMSO, CSIRO)**
The copyright holder grants Blackwell Publishing an exclusive licence to publish the Article including the abstract in printed and electronic form, in all languages, and to administer subsidiary rights agreements with third parties for the full period of copyright and all renewals, extensions, revisions and revivals.

Print Name of Copyright holder: .....
This will be printed on the copyright line on each page of the Article. It is your responsibility to provide the correct information of the copyright holder.

☐ **BOX C: to be completed if the Article is in the public domain (e.g. US Federal Government employees)** You certify that the Article is in the public domain. No licence to publish is therefore necessary.

Signature (on behalf of all co-authors (if any)) [redacted] **Print name:** Philip Higuera
Date: 28 April, 2016

If your employer claims copyright in your work, this form must also be signed below by a person authorized to sign for and on behalf of your employer, as confirmation that your employer accepts the terms of this licence.

Signature (on behalf of the employer of the author (s)) **Print name:**.....

Print name of employer: .....

..... **Date:** .....

The rights conveyed in this licence will only apply upon acceptance of your Article for publication.

Data Protection: The Publisher may store your name and contact details in electronic format in order to correspond with you about the publication of your Article in the Journal. We would like to contact you from time to time with information about new Blackwell publications and services in your subject area. (For European contributors, this may involve transfer of your personal data outside the European Economic Area.) Please check the following boxes if you are happy to be contacted in this way:

☐ (conventional mailing) ☐ (via e-mail)

Production of your manuscript will begin as soon as, but not until, we have received the signed ELF form.

The signed form can be sent as a scanned pdf to: elf@oikosoffice.lu.se
Alternatively, it can be faxed to: +1 857 241 3003

If you cannot send a pdf or fax the ELF, it can be sent by regular mail to:
Ecography, Editorial Office, Lund University, Ecology Building, SE-223 62 Lund, Sweden